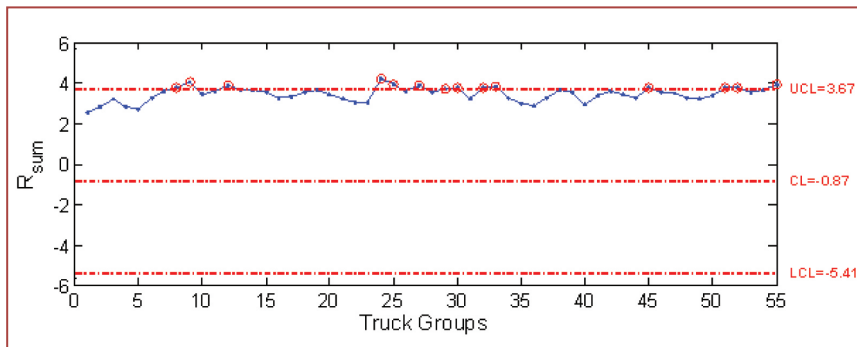


An Experimental Validation of a Statistical-Based Damage Detection Approach



Final Report
January 2011



IOWA STATE UNIVERSITY
Institute for Transportation

Sponsored by
the Iowa Department of Transportation
(InTrans Project 08-336)

About the BEC

The mission of the Bridge Engineering Center is to conduct research on bridge technologies to help bridge designers/owners design, build, and maintain long-lasting bridges.

Disclaimer Notice

The contents of this report reflect the views of the authors, who are responsible for the facts and the accuracy of the information presented herein. The opinions, findings and conclusions expressed in this publication are those of the authors and not necessarily those of the sponsors.

The sponsors assume no liability for the contents or use of the information contained in this document. This report does not constitute a standard, specification, or regulation.

The sponsors do not endorse products or manufacturers. Trademarks or manufacturers' names appear in this report only because they are considered essential to the objective of the document.

Non-Discrimination Statement

Iowa State University does not discriminate on the basis of race, color, age, religion, national origin, sexual orientation, gender identity, sex, marital status, disability, or status as a U.S. veteran. Inquiries can be directed to the Director of Equal Opportunity and Diversity, (515) 294-7612.

Iowa Department of Transportation Statements

Federal and state laws prohibit employment and/or public accommodation discrimination on the basis of age, color, creed, disability, gender identity, national origin, pregnancy, race, religion, sex, sexual orientation or veteran's status. If you believe you have been discriminated against, please contact the Iowa Civil Rights Commission at 800-457-4416 or Iowa Department of Transportation's affirmative action officer. If you need accommodations because of a disability to access the Iowa Department of Transportation's services, contact the agency's affirmative action officer at 800-262-0003.

The preparation of this (report, document, etc.) was financed in part through funds provided by the Iowa Department of Transportation through its "Agreement for the Management of Research Conducted by Iowa State University for the Iowa Department of Transportation," and its amendments.

The opinions, findings, and conclusions expressed in this publication are those of the authors and not necessarily those of the Iowa Department of Transportation.

Technical Report Documentation Page

1. Report No. InTrans Project 08-336		2. Government Accession No.		3. Recipient's Catalog No.	
4. Title and Subtitle An Experimental Validation of a Statistical-Based Damage-Detection Approach				5. Report Date January 2011	
				6. Performing Organization Code	
7. Author(s) Brent M. Phares, Terry J. Wipf, Ping Lu, Lowell Greimann, Mitchell Pohlkamp				8. Performing Organization Report No. InTrans Project 08-336	
9. Performing Organization Name and Address Institute for Transportation Iowa State University 2711 South Loop Drive, Suite 4700 Ames, IA 50010-8664				10. Work Unit No. (TRAIS)	
				11. Contract or Grant No.	
12. Sponsoring Organization Name and Address Iowa Department of Transportation Office of Bridges and Structures 800 Lincoln Way Ames, IA 50010				13. Type of Report and Period Covered	
				14. Sponsoring Agency Code	
15. Supplementary Notes Visit www.bec.iastate.edu for color PDF files of this and other research reports.					
16. Abstract <p>In this work, a previously-developed, statistical-based, damage-detection approach was validated for its ability to autonomously detect damage in bridges. The damage-detection approach uses statistical differences in the actual and predicted behavior of the bridge caused under a subset of ambient trucks. The predicted behavior is derived from a statistics-based model trained with field data from the undamaged bridge (not a finite element model). The differences between actual and predicted responses, called residuals, are then used to construct control charts, which compare undamaged and damaged structure data.</p> <p>Validation of the damage-detection approach was achieved by using sacrificial specimens that were mounted to the bridge and exposed to ambient traffic loads and which simulated actual damage-sensitive locations. Different damage types and levels were introduced to the sacrificial specimens to study the sensitivity and applicability.</p> <p>The damage-detection algorithm was able to identify damage, but it also had a high false-positive rate. An evaluation of the sub-components of the damage-detection methodology and methods was completed for the purpose of improving the approach. Several of the underlying assumptions within the algorithm were being violated, which was the source of the false-positives. Furthermore, the lack of an automatic evaluation process was thought to potentially be an impediment to widespread use. Recommendations for the improvement of the methodology were developed and preliminarily evaluated. These recommendations are believed to improve the efficacy of the damage-detection approach.</p>					
17. Key Words algorithm evaluation—bridge damage detection—damage detection methodology validation—fatigue crack—sacrificial specimens—strain response—structural health monitoring (SHM)				18. Distribution Statement No restrictions.	
19. Security Classification (of this report) Unclassified.		20. Security Classification (of this page) Unclassified.		21. No. of Pages 98	22. Price NA

AN EXPERIMENTAL VALIDATION OF A STATISTICAL-BASED DAMAGE-DETECTION APPROACH

**Final Report
January 2011**

Principal Investigator
Professor Terry J. Wipf
Director, Bridge Engineering Center
Institute for Transportation, Iowa State University

Co-Principal Investigator
Dr. Brent M. Phares
Associate Director, Bridge Engineering Center
Institute for Transportation, Iowa State University

Research Assistant
Mitchell Pohlkamp

Authors
Brent M. Phares, Terry J. Wipf, Ping Lu, Lowell Greimann, Mitchell Pohlkamp

Preparation of this report was financed in part
through funds provided by the Iowa Department of Transportation
through its research management agreement with the
Institute for Transportation
(InTrans Project 08-336)

A report from
Institute for Transportation
Iowa State University
2711 South Loop Drive, Suite 4700
Ames, IA 50010-8664
Phone: 515-294-8103
Fax: 515-294-0467
www.intrans.iastate.edu

TABLE OF CONTENTS

ACKNOWLEDGMENTS	ix
EXECUTIVE SUMMARY	xi
1 INTRODUCTION	1
1.1 General Background: Previous System Development.....	1
1.2 Scope and Objective of Research	10
1.3 Organization of the Report.....	10
2 LITERATURE REVIEW	11
2.1 SHM Systems	11
2.1.1 Wire-Based SHM Components.....	11
2.1.2 Wireless-Based SHM Components.....	13
2.2 Damage Detection.....	15
2.2.1 Damage Detection by Dynamic Response.....	15
2.2.2 Damage Detection Without Undamaged Structure.....	19
2.2.3 Statistical Based Damage Detection	19
3 EXPERIMENTAL PROCEDURE	21
3.1 Demonstration Bridge.....	21
3.1.1 General Information.....	21
3.1.2 Fatigue Sensitive Details: Girder Web-Gap	23
3.1.3 Instrumentation	24
3.2 Sacrificial Specimen	27
3.2.1 Sacrificial Specimen Description.....	27
3.2.1.1 Sacrificial Specimen 1	29
3.2.1.2 Sacrificial Specimen 2	30
3.2.2 Sacrificial Specimen Instrumentation	30
3.2.3 Sacrificial Specimen Installation	31
3.3 Data Collection and Analysis.....	34
3.3.1 Data Collection	34
3.3.2 . Data Analysis.....	34
3.4 Damage Creation Protocols	34
4 EXPERIMENTAL RESULTS.....	36
4.1 Sacrificial Specimen 1	36
4.1.1 Training prior to Damage.....	36
4.1.2 Post-Damage: Damage Detection	36
4.2 Specimen 2.....	44
4.2.1 Training prior to Damage.....	44
4.2.2 Post-Damage: Damage Detection.....	48
4.2.3 Percentage of Points outside the Control Limits.....	60
4.2.4 Corrosion Testing Results.....	61

5 ALGORITHM EVALUATION AND RECOMMENDED IMPROVEMENTS	70
5.1 Evaluation of Current Methodology	70
5.1.1 Linear Prediction Model	70
5.1.2 Normalcy of Residual and R-Sum Data.....	71
5.1.3 Quantification of Results	74
5.2 Recommended Methodology Changes	74
5.2.1 Orthogonal Regression and Orthogonal Residual.....	74
5.2.2 Damage-Detection Approach.....	76
5.2.3 Quantification of Results	80
6 SUMMARY, CONCLUSIONS, AND FUTURE WORK	81
6.1 Summary	81
6.2 Conclusions.....	83
6.3 Future Work	83
7 REFERENCES	84

LIST OF FIGURES

Figure 1.1 24 Hour Strain Record (Wipf, Phares, and Doornink 2007)	2
Figure 1.2 Zeroed, Filtered, and Event Extrema Identified Vehicular Event (Wipf, Phares, and Doornink 2007)	2
Figure 1.3 Matched Data Points from Two Sensors (Wipf, Phares, and Doornink 2007)	3
Figure 1.4 Matched Data Points with Applied Limits (Wipf, Phares, and Doornink 2007)	3
Figure 1.5 Initial Bridge Condition Daily Evaluation Histogram (Wipf, Phares, and Doornink 2007)	4
Figure 1.6 Gradually-Occurring Damage Daily Assessment Histogram (Wipf, Phares, and Doornink 2007)	4
Figure 1.7 Suddenly-Occurring Damage Daily Assessment Histogram (Wipf, Phares, and Doornink 2007)	5
Figure 1.8 Sample Scatter Plot with Different Vehicular Configurations (Vis 2007)	6
Figure 1.9 Sample Scatter Plot with Damage Effects (Vis 2007)	7
Figure 1.10 Longitudinal Strain from Sensing Point as Truck Passes (Lu 2008)	8
Figure 1.11 Truck Event Girder Bottom Strains (Lu 2008)	9
Figure 3.1 Photographs of the US 30 South Skunk Bridge (Lu 2008)	21
Figure 3.2 Plan View and Sectional Views of US 30 Bridge (Lu 2008)	22
Figure 3.3 Web-Gap Details and Out-of-Plane Bending Behavior (Lu 2008)	23
Figure 3.4 Typical Instrumented Web-Gap	24
Figure 3.5 Cross Sections of US 30 Bridge and Sensor Longitudinal Locations (Lu 2008)	25
Figure 3.6 Sensors Located at the Bridge Frame System (Lu 2008)	26
Figure 3.7 Sacrificial Specimen Geometric Details	27
Figure 3.8 Photo of Sacrificial Specimen	28
Figure 3.9 Double Curvature Bending of Sacrificial Specimen	28
Figure 3.10 Finite Element Model of Sacrificial Specimen	29
Figure 3.11 Strain Contour Plot of Sacrificial Specimen	29
Figure 3.12 Dimensions and Location of Notch	30
Figure 3.13 Sacrificial Specimen with Sensor Array Details	31
Figure 3.14 Photograph of Typical Installed Sacrificial Specimen	32
Figure 3.15 Strain Response in Web-Gaps Due to Typical Five-Axle Truck	33
Figure 3.16 Distribution of Strain in Web-Gaps Due to Typical Five-Axle Truck	33
Figure 3.17 Photographs of Rotary Shaker	35
Figure 4.1 Undamaged Sacrificial Specimen 1 Control Charts	37
Figure 4.2 Photographs of Sacrificial Specimen 1 Cracking	40
Figure 4.3 Post-Damage Sacrificial Specimen 1 Control Charts	41
Figure 4.4 Undamaged Sacrificial Specimen 2 Control Charts	45
Figure 4.5 Photographs of Sacrificial Specimen 2 Top Web Plate Cracking	49
Figure 4.6 Post-Damage Sacrificial Specimen 2 Control Charts (1.25 in. crack)	50
Figure 4.7 Post-Damage Sacrificial Specimen 2 Control Charts (1.50 in. crack)	54
Figure 4.8 Post-Damage Sacrificial Specimen 2 Control Charts (1.75 in. crack)	57
Figure 4.9 Percentage of Points Outside the Control Limits: Sacrificial Specimen 2 Cracking ..	60
Figure 4.10 Sacrificial Specimen 2 Corrosion Control Charts	62
Figure 4.11 Corrosion Simulation Area Details	65
Figure 4.12 Post-Corrosion Sacrificial Specimen 2 Control Charts	66

Figure 5.1 Sample Linear Regression.....	70
Figure 5.2 Sample Normal Distribution.....	71
Figure 5.3 Sample Distribution Comparison with 0.98 Significance Level.....	72
Figure 5.4 Sample Distribution Comparison with 0.0 Significance Level.....	73
Figure 5.5 Sample Orthogonal Regression.....	75
Figure 5.6 Sample Training Full and Reduced Model.....	77
Figure 5.7 Sample Damaged Full and Reduced Model.....	78
Figure 5.8 Flow Chart Comparison of the Two Damage-Detection Methods.....	79

LIST OF TABLES

Table 3.1 Naming Convention for Sensors Installed on the US 30 Bridge (Lu 2008).....	25
Table 4.1 Simulated Corrosion Measurement Details.....	65

ACKNOWLEDGMENTS

The authors wish to thank the Iowa Department of Transportation (DOT) for funding this work. The authors also thank the staff of the Iowa DOT Office of Bridges and Structures and, specifically, Ahmad Abu-Hawash and Bruce Brakke for their interest in and help with this developmental work. Other contributing members of the Iowa State team, whose field assistance made this work possible, are Travis Hosteng and Doug Wood.

EXECUTIVE SUMMARY

In previous projects, a structural health monitoring (SHM) system that can monitor bridges remotely and an autonomous damage-detection algorithm were developed and theoretically validated. The first-generation damage-detection system, which Wipf, Phares, and Doornink created, uses matched-event extrema to create a scatter plot relationship between target and non-target sensors. Limits were set by the user and points outside the limits are considered indications of detected damage. Refinement of the algorithm by Lu created control charts with limits automatically set by the algorithm, based on a target false-alarm rate of 0.3%.

To validate the accuracy of the previously-developed detection system, multiple field tests were completed in this project. Located on the eastbound US Highway 30 (US 30) Bridge over the South Skunk River are multiple locations sensitive to fatigue damage, called the web-gap area. It was the desire to detect damage in these areas that was the precipitous for the development of the damage-detection system. Because damage introduction into the US 30 Bridge was prohibited, a sacrificial specimen that modeled the web-gap area in the US 30 Bridge was designed and installed on the bridge. Cracking was induced by vibrating the sacrificial specimen with a rotary shaker. Thickness loss was created by removing material with a hand-held rotary grinder.

Specimen 1 was damaged with a large crack at the edge of two stress concentration locations. Damage data were then collected and plotted on previously-constructed control charts. Every post-damage statistical parameter for the three sensors closest to the damage was outside the control limits, indicating damage had been detected. Unfortunately, multiple statistical parameters were outside the control limits for sensors not near the damage, giving false-positive readings. Upon further evaluation, it was concluded that the statistical parameters for all sensors were significantly influenced by the sensors near the damage.

Sacrificial Specimen 2 was fabricated and tested similarly to Specimen 1. Specimen 2 was installed at the US 30 Bridge, training data were collected, control charts were constructed, and the sacrificial specimen was vibrated until a 1.25 in. long crack appeared in the top plate. Damage data were then collected and plotted on the control charts; this process was repeated with the crack further propagated to 1.50 in. and then 1.75 in. In all cases, all data points for the sensor closest to the damage were outside the control limits, indicating that damage had been detected. As with Specimen 1, multiple values for sensors far from the damage were outside the control limits, giving multiple false-positives.

After damaging Specimen 2 with the 1.75 in. long crack, new training data were collected and new control charts were constructed. An area of the top plate was ground off to simulate thickness loss associated with the corrosion process. Damaged data were collected and plotted on the control charts. The sensor closest to the section with the highest percentage of plate thickness ground off had numerous data points outside the control limits, indicating that thickness loss can be detected.

An evaluation of the components of the current methodology and methods for improving the approach were investigated. Several of the underlying assumptions were being violated (e.g., normalcy of response data). Furthermore, the methodology gave no easy way to automate the interpretation of the control charts. Several improvements to the methodology were investigated, evaluated, and recommended for inclusion in the methodology.

1 INTRODUCTION

The United States infrastructure continues to deteriorate and bridge inspections continue to play a crucial part in ensuring the safety of all who cross over the bridges. As visual inspections of each bridge become more difficult and costly, transportation departments are looking toward other methods of measuring the structural integrity of highway bridges, including structural health monitoring (SHM) systems. According to Chintalapudi et al., a structural health monitoring system is one that can autonomously and proactively assess the structural integrity of bridges, buildings, and aerospace vehicles. SHM systems have been in development for many years and are becoming more prominent throughout the United States.

Damage detection, with respect to SHM, is the means of determining if damage exists in the structure by changes in modal parameters, differences in strain, or other changes in behavior over time. The development of damage-detection techniques has been ongoing for about 20 years and can be as straightforward as determining that damage has occurred somewhere in the structure and as complex as determining the location and severity of the damage. It is generally thought that the use of damage-detection techniques may provide ways to increase the safety of the public traveling over the thousands of bridges currently in use.

1.1 General Background: Previous System Development

The precipitous for this work is that in 2005 the Iowa Department of Transportation (DOT) requested the development of a system that was capable of autonomously detecting damage (and specifically the development of fatigue cracks in fracture-critical, two-girder bridges). An SHM system was developed by Wipf, Phares, and Doornink, as described in “Monitoring the Structural Condition of Fracture-Critical Bridges Using Fiber Optic Technology,” using strain as the monitoring metric. The system includes a fiber-optic sensor network, data collection and management equipment, wireless communications equipment, and a novel data processing algorithm (Wipf, Phares, and Doornink 2007).

The SHM system collects data continuously, resulting in large volumes of data that would be impractical for an engineer to discretely analyze. Therefore, the system autonomously identifies and extracts only the useful sets of strain data; specifically, the quasi-static response of the bridge under ambient traffic loads (Wipf, Phares, and Doornink 2007). The raw strain data contains many unwanted elements that need to be removed to gain access to the quasi-static, live-load response. The process for reducing a continuous data set to the most useful information is described in the following paragraphs.

In a given 24-hour period, temperature variations create a cyclic strain response as is shown in Figure 1.1. The long rolling variation is the result of temperature fluctuations and the short vertical “spikes” are strains resulting from ambient traffic. It was found that if the data were split into approximately one-megabyte segments, corresponding to about 27 seconds, temperature variations do not exist. An average baseline can be determined for each 27-second data set. In a process called data zeroing, this average baseline is then subtracted from all data in the 27-second set, thereby creating a data set without temperature effects.

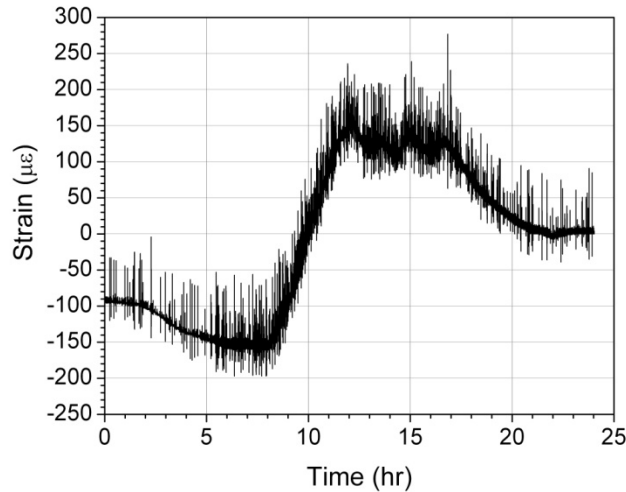


Figure 1.1 24 Hour Strain Record (Wipf, Phares, and Doornink 2007)

After data zeroing, the data set contains three components: random noise, the quasi-static vehicular response, and dynamic induced behaviors (Wipf, Phares, and Doornink 2007). A low-pass frequency filter is used to remove the noise and dynamic components from the data set, given that the frequencies of the quasi-static vehicular events are much lower than those of the dynamic responses and of the noise in the data file, leaving only the quasi-static response. After the zeroing and filtering is performed, vehicular events are identified within the strain data, based on a statistical and structural evaluation of the vehicular response relative to the location of a sensor. After event identification, maximum and minimum strain values, called event extrema, are identified for each event. An event after zeroing, filtering, and extrema identification is shown in Figure 1.2.

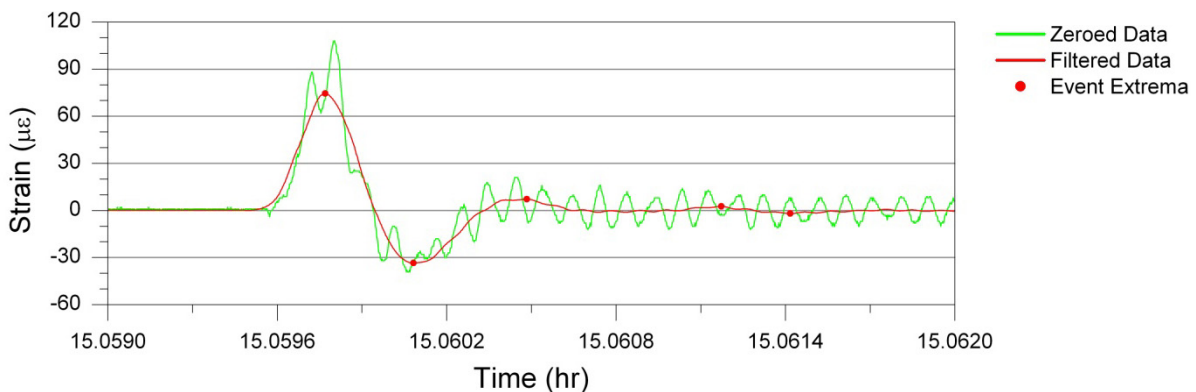


Figure 1.2 Zeroed, Filtered, and Event Extrema Identified Vehicular Event (Wipf, Phares, and Doornink 2007)

Strain sensors on the bridge are assigned one of two designations: target sensors (TSs) and non-target sensors (NTSs). In most cases, structural damaged is localized and, therefore, the TSs are those located near where damage might be expected. The NTSs are those located farther from the damage-sensitive areas and generally relate more to global structural behavior.

The event extrema from two sensors (one TS and one NTS) are matched to form x-y pairs that can be shown on a scatter plot (Figure 1.3). Initial data are collected during a “training” process, which defines the “normal” behavior. This process is completed for all applicable and desired sensor pairs. In some cases, up to four quadrants of pairs (maximum-maximum, maximum-minimum, minimum-maximum, and minimum-minimum) are present, depending on the sensitivity of the sensors to the longitudinal location of the vehicle. Once all scatter plots are created, limits for the data are manually set by an engineer. A typical scatter plot with defined limits is shown in Figure 1.4.

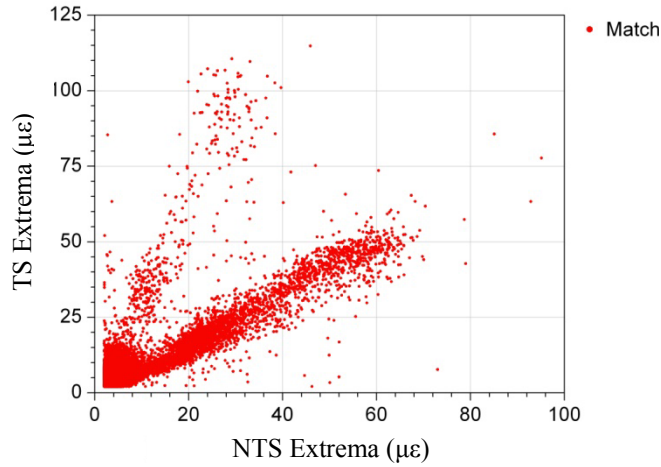


Figure 1.3 Matched Data Points from Two Sensors (Wipf, Phares, and Doornink 2007)

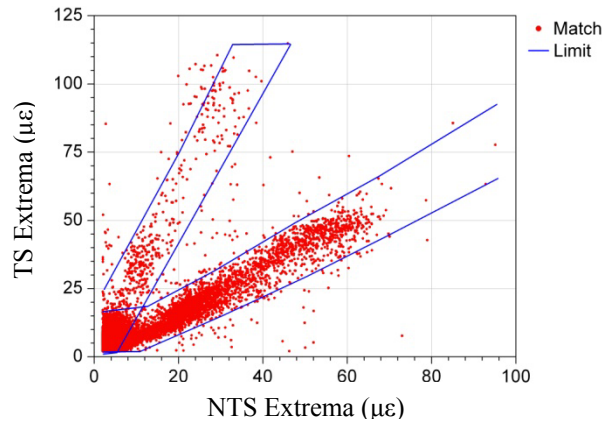


Figure 1.4 Matched Data Points with Applied Limits (Wipf, Phares, and Doornink 2007)

Following training, new data are collected from the sensors, zeroed, and filtered using the above-described methods. The event extrema are paired and compared to the previously-established limits. For data points within the set limits, a “pass” assessment is assigned, while for data points outside the set limits, a “fail” assessment is assigned. A relationship pass percentage (RPP) is computed from the data point as follows:

$$RPP (\%) = \frac{\text{Number of "pass" assessments}}{\text{Total number of assessments}} \times 100 \quad (1.1)$$

Numerous RPPs are calculated throughout the monitored time and histograms created. In the histograms from the initial bridge condition, a large grouping of assessments can be expected to have RPPs near the 100% mark as shown in Figure 1.5. If damage gradually occurs, the large grouping of RPPs can be expected to decrease from near 100% to 0% as time progresses, as illustrated in Figure 1.6. If damage occurs suddenly, the histograms can be expected to resemble Figure 1.7, where the RPP changes rapidly.

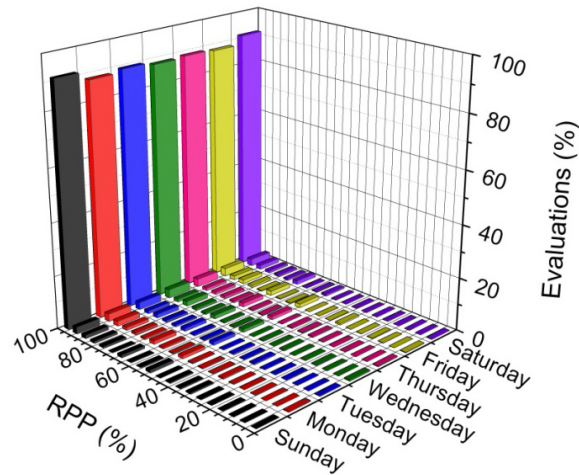


Figure 1.5 Initial Bridge Condition Daily Evaluation Histogram (Wipf, Phares, and Doornink 2007)

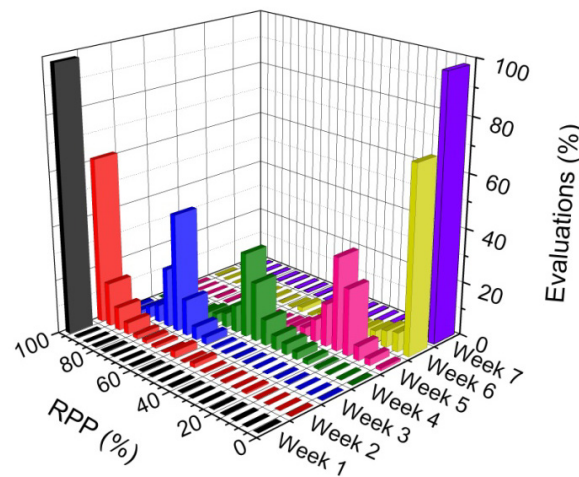


Figure 1.6 Gradually-Occurring Damage Daily Assessment Histogram (Wipf, Phares, and Doornink 2007)

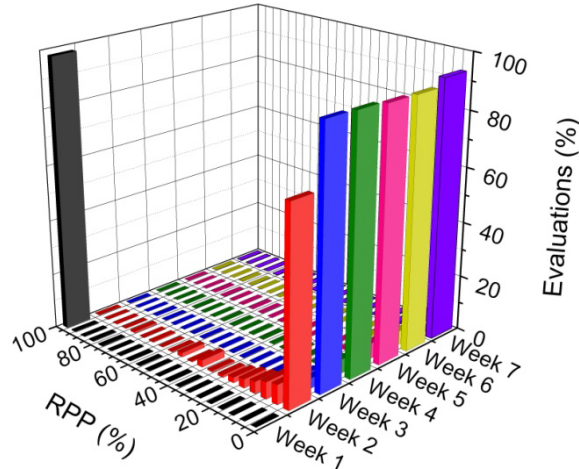


Figure 1.7 Suddenly-Ocurring Damage Daily Assessment Histogram (Wipf, Phares, and Doornink 2007)

In “Evaluation of a Structural Health Monitoring System for Steel Girder Bridges,” Vis developed a finite element (FE) model with simulated damage to analytically verify that, if damage were to occur in a damage-sensitive location near a TS, the relationships between TSs and NTSs would change significantly. An FE model of the bridge was constructed using a commercially-available FE software package. Using Shell63 four node shell elements were used to model both the structural components and the concrete deck. The damage-sensitive locations (i.e., locations with high strain concentrations) on the bridge were modeled with refined elements.

The FE model was verified using data obtained from a controlled load test conducted on the subject bridge (Vis 2007). A test truck was driven across the bridge at a crawl speed and data were collected with strain transducers. The position of the truck was recorded at 10 foot intervals so that truck position could be aligned with the collected data. Loads equivalent to the test truck were similarly applied to the FE model. The global results from the FE model closely matched the global results obtained from the load test, verifying the FE model accuracy on a global scale. The strains from damage-sensitive locations were also compared locally, but they did not agree as well as the global results did. It was, therefore, concluded that the FE model did not accurately model the damage-sensitive locations (Vis 2007). However, it was postulated that the FE model may sufficiently model changes in load behavior resulting from damage.

Using the FE model, Vis studied three variables impacting the TS-NTS relationships: transverse vehicle location, vehicle configuration, and damage in the bridge. The vehicle’s transverse location on the bridge can cause distinct groupings of data on the scatter plots, two of which are shown in Figure 1.8. These groupings of data can be represented by a straight line emanating from the origin of the scatter plot (Vis 2007). The straight lines were also used to represent different vehicular configurations. To show the effects of differing configurations, six truck configurations and loads were applied to the FE model. The lines representing the trucks on the scatter plot are shown in Figure 1.8, illustrating that vehicle configuration also has an effect on the TS-NTS relationship.

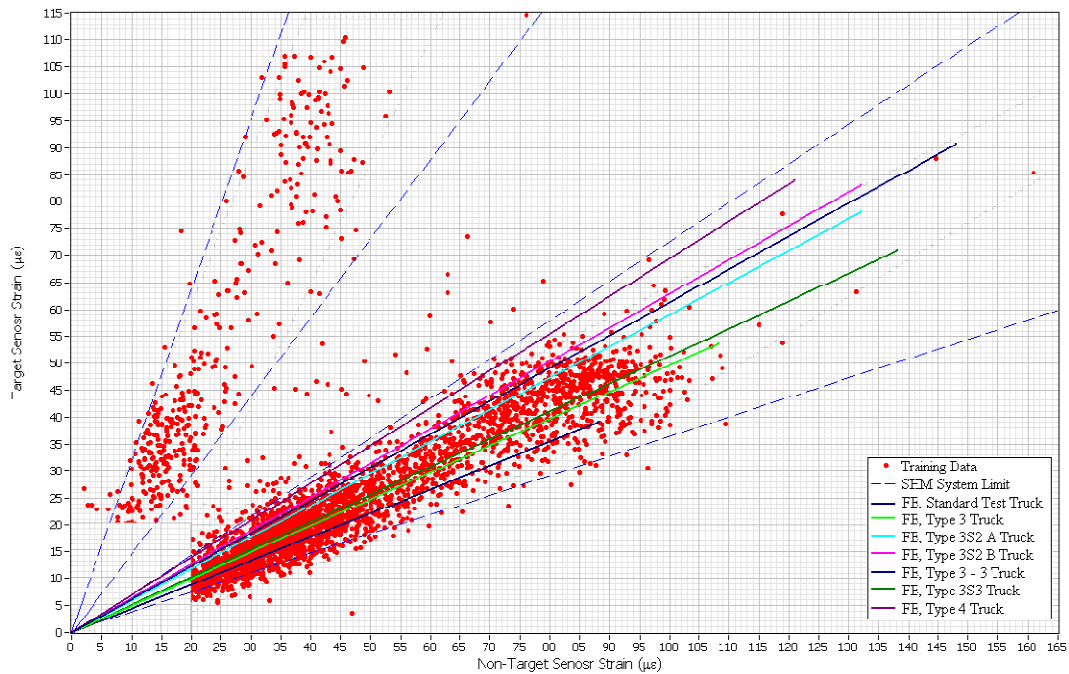


Figure 1.8 Sample Scatter Plot with Different Vehicular Configurations (Vis 2007)

Cracks of different sizes were analytically introduced at a damage-sensitive location to determine the effects of the cracks on the TS-NTS relationship. As damage was introduced, the slope (i.e., TS-NTS ratio) of the lines changed as the crack length increased as shown in Figure 1.9. To recognize a change in the TS-NTS relationship indicative of damage Vis concluded that the TS-NTS ratio must pass beyond the range of ratios associated with both transverse vehicular location and different vehicular configurations (Vis 2007). Based on these results, it was concluded that the SHM system would likely be able to identify damage once a crack 1/16 in. in size has developed if a sensor is located near the crack.

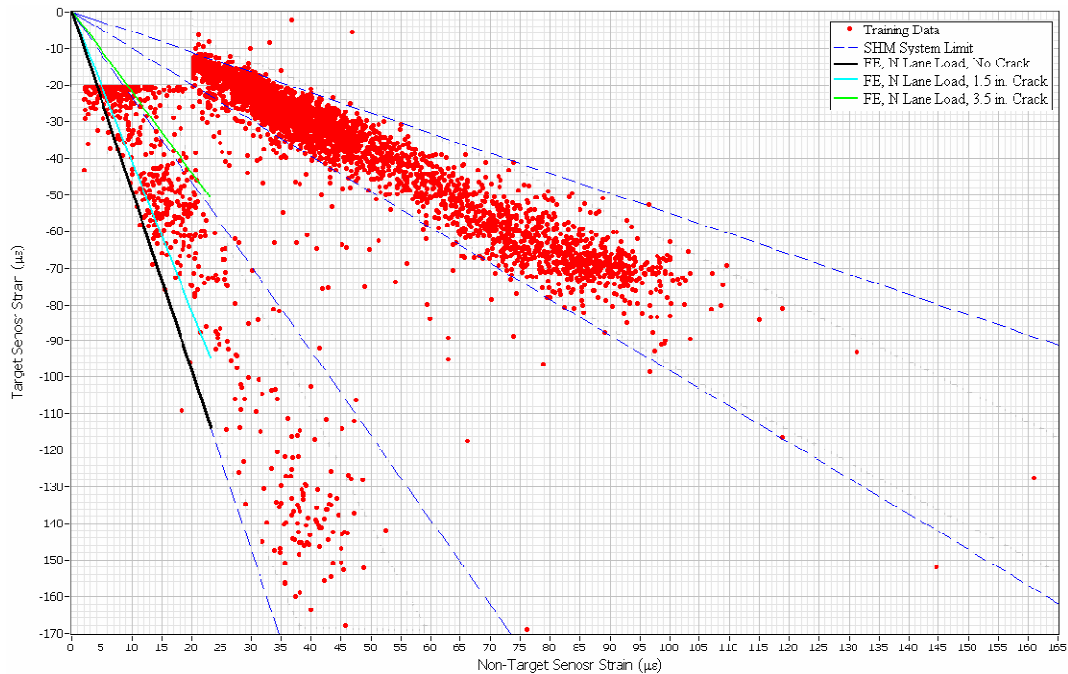


Figure 1.9 Sample Scatter Plot with Damage Effects (Vis 2007)

As it was found that is difficult to determine the differences between response changes caused by truck parameters and changes caused by structural damage, a truck parameter detection system and second-generation, damage-detection algorithm were developed by Lu, as described in “A Statistical Based Damage Detection Approach for Highway Bridge Structural Health Monitoring.” By using only specific truck types, the live load-induced variability can be reduced. Work completed by Lu extends the work previously completed by Wipf, Phares, Doornink, and Vis.

Truck parameters are characteristics of the trucks passing over the bridge and include the travel lane, number of axles, speed, axle spacing, and truck weight group. In the revised algorithm, only the strain data that are produced by select truck load conditions are utilized in damage detection (Lu 2008). To establish a truck parameter detection system, three options were considered: an existing commercial system, the use of the existing sensors on the bridge, and installing new sensors. It was found that commercially available systems were either too expensive or did not integrate into the fiber-optic sensor network and were not considered further. To determine the effectiveness of the existing sensor at detecting truck parameters, a controlled load test was completed. The results showed that existing sensors could detect tandem axle groups and the steering axle, but the differentiation of axles within a group could not be reliably achieved.

Since the existing sensors were not able to detect all the necessary truck parameters for the damage-detection algorithm, an investigation into the positions and orientation of deck bottom sensors was performed. A three-dimensional FE model was created of the bridge and trucks crossing the bridge were simulated by applying loads to the nodes of the model along the wheel lines of the truck. For example, the longitudinal strain on the deck bottom produced by a three-

axle truck is shown in Figure 1.10. The three peaks indicate there are three axles. It was determined that a good correlation between strain and truck axles existed if longitudinal strain was used and the sensing point was located within 2 feet of the truck wheel line.

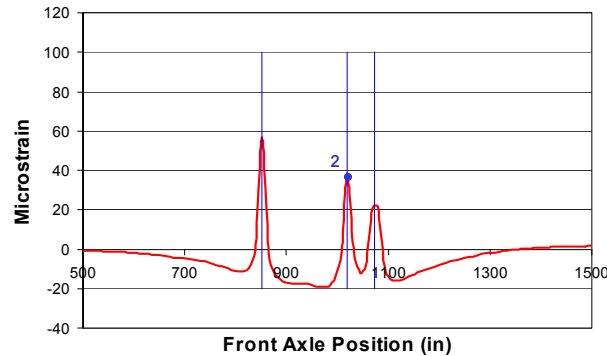


Figure 1.10 Longitudinal Strain from Sensing Point as Truck Passes (Lu 2008)

To confirm the correlation between longitudinal strain and truck axles, a second controlled load test was performed. During this test, a three-axle truck and a six-axle truck crossed the bridge at highway and crawl speeds. A total of 24 deck bottom sensors with two transverse lines of 12 sensors at different longitudinal locations, and six girder bottom sensors were used in the load test. For each truck event, a girder bottom sensor produced one large positive peak if a threshold was properly defined as shown in Figure 1.11. It was found that the sensor on the girder closest to the vehicle travel lane consistently produced a higher peak strain (above the threshold), thereby determining the truck travel lane. The deck bottom sensors nearest the left wheel line of the right lane truck and the right wheel line of the left lane truck consistently showed the best truck axle detection ability. Data acquisition frequency testing was also completed and it was found that 62.5 Hz was considered the minimum frequency required for axle detection (Lu 2008).

After verification by FE analysis and control tests, eight fiber-optic sensors (four sensors per transverse line in two different longitudinal locations) were installed on the deck bottom for integration into the long-term structural monitoring system. A good correlation existed between the strain peaks and truck axles, but in some cases, the truck axles were more difficult to detect than they were in the controlled load test. In these cases, a double checking algorithm was used to improve the axle detection capacity. By using the data from these sensors, other truck parameters, including speed and axle spacing, can be determined. It was found that the direct weight of each truck could not be calculated; however, the trucks could be sorted into two categories: heavy or light. In the work completed by Lu, only data from right-lane, five-axle heavy trucks were used in the damage-detection algorithm.

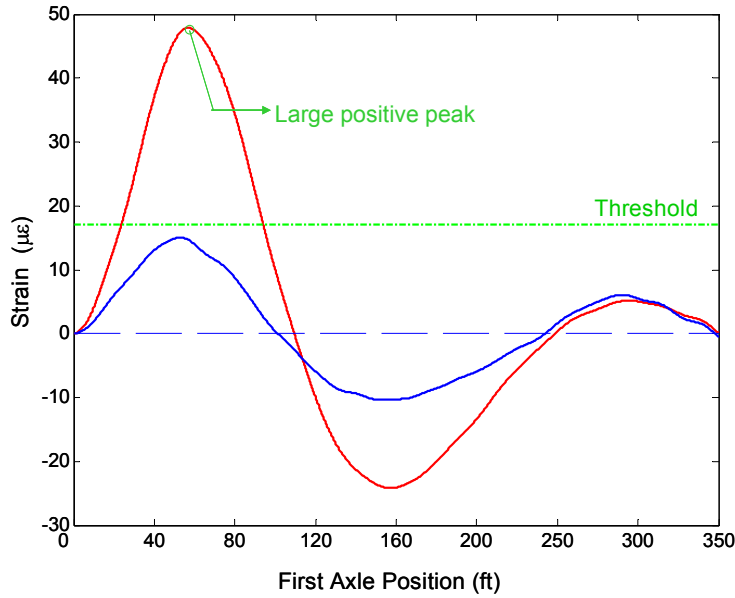


Figure 1.11 Truck Event Girder Bottom Strains (Lu 2008)

Over time, a number of issues with the deck bottom sensors have displayed themselves, including apparently incorrect or obscure data readings probably due to temperature fluctuations or poor bonding of the sensor. An investigation into different methods of attaching the deck bottom sensors was completed in the current study to address these issues.

The primary focus of the new damage-detection algorithm developed by Lu is to detect relatively small local damage in highway bridges. The algorithm utilizes event-based extreme live load strains as the input data and statistical control chart philosophies as the damage-detection tool (Lu 2008). The maximum and minimum strains produced by one truck event were used to calculate an event-based strain range (for each sensor). The strain ranges from sensor pairs are used to predict each other with linear prediction models. For a system with n sensors, n^2 prediction models can be created. Study showed that residuals defined to be the difference between the predicted data from linear prediction models and the collected strain data, were more sensitive to damage than the peak strain itself. The models are then used to calculate an $n \times n$ residual matrix for each truck event. The residual matrix is further simplified into an n -degree vector (i.e., damage indicator). Multiple matrix simplification methods were compared, after which the so called combined summation method (which is completed by subtracting the column summation of the residual matrix from the row summation of the residual matrix) was selected. The residuals were also standardized before the column and row summation calculation.

Once the damage indicator is obtained, one control chart for each sensor is constructed. A target false-alarm rate was chosen as 0.3%, following typical non-destructive evaluation practice. As the residuals were assumed to be normally distributed, the corresponding upper control limit (UCL) and a lower control limit (LCL) are set at the mean plus or minus three times the standard deviation.

As new data are collected, the residual matrix is constructed, and the residuals are plotted on the previously-constructed control charts. Any point outside the control limits is termed a damage alarm and indicates a change in the structure, which likely can be attributed to damage. As each sensor is paired with a single control chart, the control chart associated with the sensor closest to the damage will display the highest number of damage alarms.

In summary, these are the general steps in the damage-detection approach (Lu 2008):

Training Procedure:

1. Create linear prediction models from training data.
2. Calculate the residual matrix for each event.
3. Convert the residual matrix into the damage indicator.
4. Create the training stage control chart from the damage indicator.
5. Plot additional training data on the constructed control chart to test for false alarms.

Monitoring Procedure:

1. Calculate the residual matrix for each event using the linear prediction model created in the training stage.
2. Convert the residual matrix into the damage indicator.
3. Chart the damage indicator to determine the structural health state.

1.2 Scope and Objective of Research

This study is primarily an experimental validation of the damage-detection algorithm developed by Lu (Lu 2008). A number of sacrificial specimens were mounted on the eastbound US Highway 30 (US 30) Bridge crossing the South Skunk River. The bridge had been utilized in previous phases of this work with loads induced by ambient traffic. The sacrificial specimens modeled the damage-sensitive locations of the test bridge and damage was induced to the sacrificial specimens in the form of cracks and simulated corrosion. Each sacrificial specimen was connected to the existing SHM system and data were collected from the undamaged and damaged sacrificial specimens. The algorithm developed by Lu was used to detect the damage in the sacrificial specimens.

1.3 Organization of the Report

In the remainder of this report, Chapter 2 summarizes previous SHM systems and damage-detection techniques. Chapter 3 details the investigation into concrete sensor attachment methods. Chapter 4, details the experimental procedure, including the use of a sacrificial specimen to model the damage-sensitive web-gaps on the US 30 Bridge. Chapter 5 shows the results from testing the undamaged and damaged sacrificial specimen, along with the control charts, which compare the differing damage states of the sacrificial specimen. Finally, Chapter 6 summarizes the research and presents conclusions as to the validity of the statistical-based damage-detection algorithm.

2 LITERATURE REVIEW

A literature review was previously conducted by Lu and summarized in “A Statistical Based Damage Detection Approach for Highway Bridge Structural Health Monitoring.” That review summarized many of the SHM and damage-detection systems developed and tested prior to 2008. In addition, an extensive literature review was summarized in “Damage Identification and Health Monitoring of Structural and Mechanical Systems from Changes in Their Vibration Characteristics: A Literature Review” (Doebbling, et al. 1996). The Doebbling review summarizes a large array of damage-detection systems developed up to 1996. The literature summarized here is intended to “fill-the-gap” between 1996 and 2009. This review is divided into two primary areas: SHM systems and damage detection. An additional short literature review was completed on the topic of sensor attachment to concrete and is shown in the following chapter.

2.1 SHM Systems

2.1.1 Wire-Based SHM Components

A common type of SHM system is one that includes an array of wired gauges. These gauges can be located almost anywhere on the structure and the locations depend on the type of data needed. Validation and testing of these types of systems can take place either on real-world structures or in the laboratory on scale models or other similar structures. Real-world application of SHM systems has occurred on bridges ranging from short-span timber bridges to long-span suspension bridges. The subsequently described SHM systems were used to test full-scale field highway bridges. Wired SHM systems are generally used for long-term, high-speed monitoring, as one central data collection device provides power to the connecting gauges and also collects the corresponding data.

Guan, Karbhari, and Sikorsky describe a long-term SHM system in “Long-Term Structural Health Monitoring System for a FRP Composite Highway Bridge Structure.” These authors define long-term SHM as the practice of using an integrated system of sensors, data acquisition devices, data transmission and processing devices, and corresponding algorithms to continuously monitor the condition of a structure over an extended period of time (Guan, Karbhari, and Sikorsky 2007).

In this specific case, long-term SHM took place on a modular bridge in Riverside County, California that carries two lanes of traffic. The monitored bridge was the Kings Stormwater Channel Composite Bridge that consists of prefabricated, tubular, filament-wound, carbon shell girders filled, on site, with lightweight structural concrete. Supported by these tubular girders are prefabricated bridge deck panels, which are made of E-glass fiber-reinforced polymer.

The deployed SHM system consists of a combination of accelerometers, resistance strain gauges, and potentiometers. The accelerometers were set up in a 7 ft by 6 ft grid on the bottom of the deck panels. At half of the locations, two accelerometers were mounted—one oriented vertically and one oriented horizontally. The 20 strain gauges were attached to the bottom of the deck and

along the tubular girders. The positions of the strain gauges were selected to monitor high strain areas. To measure maximum deflection, four string potentiometers were placed at midspan.

As the sensors collect data, they are instantaneously sent from a wireless antenna to the University of California, San Diego, where the data are compiled and analyzed. Raw data, in the form of time-histories, are processed to generate results, which reflect the condition of the bridge (Guan, Karbhari and Sikorsky 2007). The method of damage detection was a direct mode shape comparison. A forced vibration test was conducted on the bridge shortly after construction to obtain the undamaged condition mode shapes. After the bridge was opened to traffic, data were collected on a daily basis and the daily mode shapes were compared to those of the undamaged structure. It was found, however, that variations in temperature and boundary conditions produced greater mode shape variations than damage produced.

In “Passive Structural Health Monitoring of Connecticut’s Bridge Infrastructure,” Olund and DeWolf present three SHM systems used on three types of bridges deemed critical to Connecticut’s bridge infrastructure: a steel box girder bridge, a curved cast-in-place box girder bridge, and a steel multigirder bridge. The SHM systems used are passive systems, which consist of collecting data from ambient traffic (Olund and DeWolf 2007). By using a passive SHM system, the bridges can be monitored while open to traffic and do not have to be closed to perform controlled load tests.

The Olund and DeWolf SHM system setup was basically the same for all three bridges with the main difference being where the sensors were placed. The sensors on the bridge are a combination of temperature, tilt, acceleration, and strain gauges, which are all connected to a central data acquisition system located at the bridge site. For each bridge, the smallest number of sensors that would still allow for the global characterization of the structure to be identified was used. A significant early concern related to the impact that temperature gradients would have on the natural frequencies and measured rotations. This issue was dealt with by recording temperature at the same time strain and tilts were recorded. Consideration was then given to the measured temperature when calculating the natural frequencies. To give greater flexibility in the data collection capabilities, the software was configured with three modes: the trigger approach, which collects data only if data are above or below set limits, the interval approach, which collects data at set intervals throughout a certain period of time, and manual. A modem was connected to the on-site computer; this enabled the collected data to be downloaded without having to travel to the bridge.

The first bridge monitored was a curved steel box-girder bridge with a composite concrete deck. That bridge consisted of three sets of three continuous spans. The SHM system had a total of 22 sensors: eight temperature sensors, six tiltmeters, and eight accelerometers (Olund and DeWolf 2007). The second bridge was a curved cast-in-place concrete post-tensioned box-girder bridge and the SHM system consisted of 14 temperature sensors, six tiltmeters, and 16 accelerometers. The last bridge monitored was a steel multi-girder bridge with three spans and a composite concrete deck. The monitoring system consisted of 20 uniaxial strain gauges located on one of the three spans. To track the changes in the collected data, statistical benchmarks were created from the collected data. These statistical benchmarks could be used to construct statistical

envelopes and confidence intervals with which the new collected data could then be compared and analyzed.

Betz, Staszewski, Thursby, and Culshaw explored the use fiber Bragg grating sensors for fatigue crack detection in metallic structures and for SHM. Fiber Bragg grating sensors were used, because they've been shown to be capable of sensing both the loads and ultrasonic waves (Betz et al. 2006). The structural health and usage monitoring system (HUMS) was developed to improve current inspection practices, to monitor the loads applied to the structure, and to detect possible damage. The fiber Bragg grating sensors can also be used as an ultrasonic detector to detect Lamb waves as they propagate through the structure.

To verify the use of the fiber Bragg grating sensors for damage detection, laboratory testing was conducted. Load was applied to a steel plate with multiple sensors attached to its surface. Damage, in the form of a full-depth notch, was then introduced to the plate. As cracks formed on either side of the notch, the sensors were able to detect the cracks and the size of the crack could be estimated through further analysis.

2.1.2 Wireless-Based SHM Components

An SHM system was introduced by Chintalapudi et al. in the paper "Monitoring Civil Structures with a Wireless Sensor Network." The primary motivation behind using the wireless network was the initial cost of implementing a dense network of wired sensors on large-scale structures. These coin-sized, wireless sensors consist of vibration sensors, low-power radio components, significant flash storage, and a processor. The wireless sensors are relatively easy to mount and can be organized into a dense network on the structure. Because of the relatively small size of the sensors, battery life was limited to not more than a few days. To overcome this, the sensors can operate in numerous low-power settings. The wireless sensors send the collected data to on-site hardware that can pre-process the data before sending the data to a powerful, off-site data processing computer.

The software system designed, implemented, and deployed (Chintalapudi et al. 2006) typically consists of tens of sensor nodes that send information through a series of relays to a base station, which was typically a high-end PC. The system can accommodate the entrance or exit of wireless sensors into the network at any time. A large problem encountered was the loss of data during transfer from the sensors to the base station. This problem was overcome by having individual sensors temporarily store data. When needed, the base station can send a request for a certain time-stamped data set; the sensor can then resend the missing data to the base station.

The system was deployed on two structures: a seismic test frame and the Four Seasons building located in Los Angeles, California. The seismic test frame was a model of a 28 ft x 48 ft hospital ceiling, which was designed to support 10,000 pounds and has functional electric lights, fire sprinklers, drop ceiling installations, and water pipes (Chintalapudi et al. 2006). The test ceiling can be subjected to up to 10 in. of displacement. The Four Seasons building is a four-story office building that was damaged in the 1994 Northridge earthquake and subsequently abandoned. A wireless sensor network was established on both structures, forced vibration was induced, and

data were collected. It was found that real structures are heavily damped and the response to a sudden impact lasted less than a second. Large amounts of data were collected and the fundamental rationale, flexibility and ease of deployment, was demonstrated and the experiments were considered successful. Current second- and third-generation wireless sensor systems are in development with accompanying software.

Kim et al. present the wireless health monitoring of the Golden Gate Bridge in California in the paper “Health Monitoring of Civil Infrastructures Using Wireless Sensor Networks.” The wireless sensor network used is similar to that developed by Chintalapudi et al. The main difference between the two networks is how they are implemented on the individual structures.

The Golden Gate Bridge presents a unique test bed for an SHM system because of the potential for large wind and seismic loads. The distances between the sensors in this work were limited due to the relatively-short wireless range of the sensors. In fact, the maximum separation distance of the sensors was typically limited to 100 ft and in some cases to less than 50 ft. There were 53 wireless sensors placed on the west side of the main span and three on the east side of the main span. Each of the sensors monitored two directions of acceleration and ambient temperature. Four lantern batteries were used to provide power at each sensor location, because no other power source was readily available; renewable sources of power were considered. A total of eight sensors were placed on the south tower—one at each intersection of the cross-bracing and towers.

Another SHM system based on wireless sensor networks was presented by Yin et al. in the paper “Design and Implementation of the Structure Health Monitoring System for Bridge Based on Wireless Sensor Network.” Yin et al. developed a new type of node called the S-Mote that consists of a mote (or sensor), sensor board, and batteries and collects acceleration data. As with other sensor nodes, the S-Mote can be placed in numerous locations on the structure and connected to a base station wirelessly. Once an S-Mote received the command to start collecting data, the acceleration data were temporarily stored in flash memory before being transferred wirelessly to the base station. Data loss during wireless transfer was not addressed by Yin et al.

The wireless sensor network developed by Yin et al. was tested on the Zheng Dian viaduct bridge located near Wuhan City, China. Six nodes were deployed near the middle of the bridge in a linear array (Yin et al. 2009). The S-Motes were mounted on the bridge horizontally and connected wirelessly to a base station, which was connected to a computer. The data were collected at 100Hz for 1.5 hours.

A wireless sensor network was also used to monitor the Humber Bridge in the United Kingdom. Hoult et al. developed a system to monitor the relative humidity in the anchor blocks of the Humber Bridge as described in “Wireless Structural Health Monitoring at the Humber Bridge UK.” At the anchorage, the main cable was divided into individual cable strands and tied into the foundation with no protective coating (Hoult et al. 2008). High levels of relative humidity in these areas can cause corrosion of the steel. Dehumidifiers that turn on when the relative humidity reaches a certain percentage and wired humidity gauges were located in the anchorage. The gauges can only be accessed manually.

The motes used to monitor the temperature and humidity consist of commercially-available motes from Crossbow Technology, Inc. The mote is a battery-powered central processing unit with a radio transmitter and a radio receiver (Hoult et al. 2008). As with many wireless sensor networks, power was the main issue. Four AA batteries give the motes a life of about 10 months. To conserve power and maximize the battery life, a low power mode was programmed that forces the motes to transmit data every five minutes instead of continuously. The wireless sensor network can be checked to determine if the dehumidifiers are functioning properly.

A similar but slightly more complex wireless SHM system was presented in the paper “Distributed Structural Health Monitoring System Based on Smart Wireless Sensor and Multi-Agent Technology” by Yuan et al. This SHM system was a distributed parallel concept based on the smart wireless sensor network and multi-agent system (Yuan et al. 2005). The multi-agent concept was implemented to manage the information coming from the sensors located on a large structural network. The system consists of different types of agents: sensing agents that monitor the structure, signal-processing agents that process the data from the sensing agents, fusion agents that take the data from the signal processing agents and fuse it together to form a logical sequence of information, and other agents. The collections of agents divide the larger task of data processing into smaller manageable pieces that can be combined into a network specific to a unique structure.

Another feature about the Yuan et al. SHM system was that each of the sensors was connected to mini-hubs that have microprocessors, which communicate wirelessly to a larger hub. The mini-hubs collect the data from the attached sensors, combine the data, and then communicate these data to an estimation agent. By having the smaller platforms, the data arrives at the fusion agent in a smaller number of larger packets, rather than a large number of small packets. This increases efficiency and reduces the amount of power needed. The sensors themselves can be either piezoelectric or fiber-optic; the platforms can be modified to attach to either type of sensor. After evaluation of the entire system, the sensor platform needed improvement due to speed and memory limitations. In addition, testing was limited to small-scale applications; testing on large-scale structures would need to be completed to verify the usefulness of the distributed parallel SHM system.

2.2 Damage Detection

Almost all SHM systems are said to have a damage-detection process. Damage detection ranges from the analysis of direct readings to complex algorithms that analyze dynamic characteristics to detect structural damage. All of these detection systems have one main aspect in common: they use measured data from the bridge and try to detect damage.

2.2.1 Damage Detection by Dynamic Response

Damage detection by dynamic response is usually accomplished by exposing the structure to a dynamic load and recording data as the structure responds. In many cases, this data set is compared to a data set from the original undamaged structure; this comparison of data sets is completed in differing ways, a few of which are described below.

A method of structural damage detection is called the Local Damage Factor (LDF) and it was reportedly able to detect the location and severity of damage. LDF takes two random vibration signals, one from the local structure and the other from the entire structure, and finds the correlation between them through a process known as auto-correlation. From these correlations, the auto-spectral densities are found using a Fourier transform. The auto-spectral densities are used to find the generalized coherence function, which in turn indicates the severity of the nonlinearity between the local structure and the entire structure. Damage in the structure usually reduces the stiffness of the local structure, where the damage occurs, and it purportedly increases the nonlinear severity between the local structure and the entire structure (Wang, Ren, and Qiao 2006). From the coherence function, the LDF can be found; a change, or damage, in the structure will change the LDF.

A modified LDF (MLDF) was subsequently introduced that does not need the data and dynamic characteristics of the undamaged structure. This method was beneficial because in many cases the undamaged structure is not attainable and undamaged data cannot be recorded.

In the case of Wang, Ren, and Qiao, LDF and MLDF were evaluated with a 3-D steel frame to determine if damage could be detected using both methods. Baseline data were collected and a crack was then introduced into one of the frame legs. The authors report that both methods effectively determined the severity and location of the damage in this case and provide a simple and straightforward approach to local damage detection (Wang, Ren, and Qiao 2006).

Ng and Veidt present a damage-detection technique that uses Lamb waves to locate and estimate the severity of the damage. The Lamb-wave technique uses an array of piezoelectric transducers that transmit and receive an excitation frequency that can then be analyzed. The structure can then be reconstructed using superposition.

Numerical studies were conducted to investigate the Lamb-wave technique. The studies utilized finite element models to predict the Lamb-wave propagation through the material and the simulated damage detection. A simple laboratory test of a carbon-fiber-reinforced composite plate was conducted. In this test transducers were located at four corners around the simulated damage area. The composite laminate was excited using Lamb waves and data collected using the transducers. The data were then compared to data from finite element models. Through the numerical and experimental studies, the Lamb-wave-based technique for damage detection has been verified to detect and locate different stages of damage in composite laminate structures.

A method of damage detection presented by Guan, Karbhari, and Sikorsky compares the mode shape curvatures of the undamaged and damaged structure. It has been found that mode shape curvature was more sensitive to local changes of stiffness and was shown to be particularly suitable for damage localization in beam-like structures (Guan, Karbhari, and Sikorsky 2007). The mode shape curvature of the undamaged structure was considered the “baseline” and all other mode shape curvatures computed from the potentially damaged structure were compared to this “baseline.” The general trends of the differing mode shape curvatures were found to be similar, but that they differed in distinct places leading to the classification and location of the damage.

In the paper titled “Nondestructive Crack Detection Algorithm for Full-Scale Bridges,” Kim and Stubbs present a method to determine crack location, size, and shape. These descriptors of the crack are determined by the change in modal characteristics (e.g., natural frequencies and mode shapes) of the structure. A data set was collected for the undamaged structure and then compared to data from the damaged structure. Specifically, changes in modal shapes and natural frequencies are used to identify the presence of damage. The crack detection algorithm can then use the collected data to locate and determine the qualities of the damage.

To experimentally verify the crack-detection algorithm, a full-scale test bridge was located and initial modal tests were performed to obtain a set of baseline undamaged data. Once initial data collection was complete, four levels of damage were introduced to the bridge by means of torch-cutting flanges and webs at certain distances. The first damage case damaged a central portion of the web, the second damaged the lower half of the web, the third damaged the lower half of the web plus the lower flange tips, and the fourth damaged the entire bottom half of the I-beam cross-section. After each level of damage was established, modal tests were performed and data were collected to compare to the undamaged data set.

The data collected were analyzed using the crack-detection algorithm and the algorithm was found to reasonably predict the size and location of the damage. False alarms were triggered during some parts of the analysis, but the authors are working on further refining the nondestructive crack-detection algorithm.

Galvanetto, Surace, and Tassotti present a new structural damage-detection method, based on proper orthogonal decomposition, in the paper “Structural Damage Detection Based on Proper Orthogonal Decomposition: Experimental Verification.” This damage-detection technique uses proper orthogonal modes (POM) and the variance between the orthogonal modes of an undamaged structure and a damaged structure to detect the level of damage for the structure. This damage-detection approach does not require the creation of a mathematical model.

The first step was to collect data and construct a POM for the undamaged structure. This was accomplished by placing many accelerometers on the structure and recording data. The data are then used to create the POM. This undamaged POM will be used to compare to all of the additional POMs created from the potentially-damaged structure.

To verify the proper orthogonal decomposition damage-detection method and to ensure its accuracy, a cantilever beam (20 x 20 x 520 mm) was constructed and accelerometers were attached to the undamaged structure. A shaker was used in two different locations and vibrated at three different frequencies to obtain undamaged structure data. Saw cuts were then introduced into the cantilever at increasing depths and the structure was shaken at two different locations and at three different frequencies. The first saw cut was 1 x 20 x 0.5 mm and the second cut was 1 x 20 x 2 mm. From the collected data, POMs were created and it was found that the damage was accurately located.

Another approach to structural damage detection was presented in the paper “Vibration Based Damage Detection in a Uniform Strength Beam Using Genetic Algorithm” by Panigrahi,

Chakraverty, and Mishra. In this damage-detection procedure, a Genetic Algorithm (GA) was used to solve an optimization procedure specified by a residual force vector (Panigrahi, Chakraverty, and Mishra 2009). After the objective function has been solved, it could then be related back to the physical properties of the structure. These physical properties are directly related to the structural stiffness. The underlying approach assumes that the stiffness of a structure decreases when there is damage to the structure. Two cases were investigated in the validation of the damage-detection algorithm: the first being a uniform strength beam with a slope function integrated into the width of the beam (0.08 x 0.01 m to 0 x 0.01 m with a length of 0.8 m), and the second being a uniform strength beam with a slope function integrated into the width and depth of the beam (0.08 x 0.015 m to 0 x 0 m with a length of 0.8 m). Data were collected from the undamaged states of the beams along with different stages of damage. Throughout this process, the modes of the damaged structures were found to be lower than those of the undamaged structure. For both cases, the GA identified damage for both uniform strength beams.

In the paper “Experimental Validation of Structural Health Monitoring for Flexible Bridge Structures,” Caicedo and Dyke present a health monitoring system specifically validated on a model of a cable-stayed bridge that uses changes in a structure’s dynamic characteristics (e.g., natural frequencies, mode shapes) to detect and locate damage. There are five steps to implementation of the technique: development of an identification model, sensor placement, data acquisition, modal identification, and parameter identification (Caicedo and Dyke 2005). Data are obtained from both the undamaged and potentially-damaged structures to make a direct comparison between the two.

The identification model was created using finite element software and the model must be complex enough to accurately model the behavior of the structure, but not too complex as to have very large quantities of data. The primary purpose for creating the model was to find the critical locations to place the accelerometers. Once the locations are identified, accelerometers are then placed on the bridge and data acquisition can begin. The dynamic excitation of the bridge can either be known or unknown (the eigensystem realization algorithm can calculate the natural frequencies and mode shapes with either). The differences in the natural frequencies and mode shapes was what determined if there was damage and where the damage was located on the structure.

Numerous experimental tests were conducted on the cable-stayed bridge model. The model has a total length of 2 m and a width of 19 cm with the h-shaped tower being 50 cm tall, 29 cm wide at the base, and 18.41 cm wide at the top. A total of 60 cables were used to support the deck with connections at 1.27 cm increments (Caicedo and Dyke 2005). A finite element model was constructed and accelerometers were placed on the test model to coincide with critical locations identified on the finite element model. The undamaged structure was dynamically excited and data were collected and analyzed. Damage was introduced into the structure by randomly choosing a small deck section and replacing it with a smaller “damaged” element. The damaged structure was also dynamically excited and data were collected. By comparing the natural frequencies and mode shapes of the undamaged and damaged structures using the algorithm, the damage could be detected and located.

2.2.2 Damage Detection Without Undamaged Structure

A unique feature about a few damage-detection systems is the fact that the undamaged structure is not needed to detect future damage of the structure. Each method has a different way of accomplishing this, but, in general, a theoretical model is constructed and data collected from the bridge are compared to the model in some fashion. Summarized below are two such approaches.

In a paper by Kim and Melham titled “Damage Detection of Structures by Wavelet Analysis,” a relatively new method was presented for damage detection and SHM that includes the utilization of dynamic characteristics of the structure that does not need an analysis of the structure to detect and locate damage on the structure. Typical modal-based methods encounter various difficulties, including obtaining correct material properties and the need to measure vibration responses of structures before damage occurs. These difficulties are reportedly able to be eliminated by using wavelet analysis.

Wavelet analysis is a mathematical and signal-processing tool that takes raw vibration data and analyzes the decomposition and irregularities of the signal. It is a time-frequency analysis that provides more-detailed information about non-stationary signals, which traditional Fourier analyses miss (Kim and Melhem 2004). Using wavelet analysis, the damage can be detected and reported to the agency or department monitoring the structure.

Saadat et al. present an intelligent parameter-varying technique (IPV) for damage detection in structures that behave non-linearly under seismic conditions in the paper “Structural Health Monitoring and Damage Detection Using an Intelligent Parameter Varying (IPV) Technique.” The IPV technique combines features of non-parametric and parametric simplified structural models to recognize the non-linear behavior portions of the response during seismic loading and uses this to identify areas on or within the structure where damage may be located. Rather than comparing this non-linear behavior of the damaged structure to the behavior of the non-damaged structure, the IPV technique identifies structural forces that mathematically return the structure back to its original shape, called restoring forces, to detect the differing levels of damage. Case studies and simulations were investigated to determine if the IPV technique recognizes the structural restoring forces of the damaged structure that can be related to the damage that took place.

2.2.3 Statistical Based Damage Detection

Another general damage-detection approach is one that only uses statistics to analyze data collected from the bridge. Worden and Manson present a study on a statistical approach to damage detection in their paper “Damage Detection Using Outlier Analysis.” Outlier analysis detects when a machine or structure deviates from the normal condition responses; the analysis detects when data points occur outside of the normal behavior range. The outliers can arise on either side of the data set, signaling that the performance of the machine or structure is out of the ordinary.

For more complicated sets of data, a discordancy test called Mahalanobis squared distance was used to analyze the outliers. The Mahalanobis squared distance approach, which is a function for calculating distances between two seemingly related points, was used in case studies presented in the paper and was successfully demonstrated on numerous large data sets. As with most data analyses, assumptions were made to simplify the outlier analysis damage-detection procedure.

3 EXPERIMENTAL PROCEDURE

This chapter describes the processes and tools used to experimentally validate the damage-detection algorithm developed by Lu in “A Statistical Based Damage Detection Approach for Highway Bridge Structural Health Monitoring.” A description of the dimensions and instrumentation of the demonstration bridge, an introduction and purpose of the sacrificial specimen, and an explanation of the types of damaged induced to the sacrificial specimen are included in the following sections.

3.1 Demonstration Bridge

For the experimental validation, a two-girder, fracture-critical demonstration bridge that was previously instrumented with fiber-optic sensors was utilized. The demonstration bridge has numerous fatigue-sensitive locations, which were closely monitored and, ultimately, has the need for the SHM system. The following sections provide general information, describe the fatigue-sensitive locations on the bridge, and describe the instrumentation on the demonstration bridge.

3.1.1 General Information

As with the related work preceding what’s described in this report, the bridge used for this project was the eastbound US 30 Bridge crossing the South Skunk River near Ames, Iowa (Figure 3.1). The US 30 Bridge has three spans with two equal outer spans (97.5 ft) and a longer middle span (125 ft), a width of 30 ft, and a skew of 20 degrees.

The superstructure consists of two continuous welded steel plate girders, 19 floor beams, and two stringers that support a 7.25 in. thick cast-in-place concrete deck. The bridge supports are pinned at the west pier and are roller-type supports at the east pier and at each of the abutments. The abutments are stub reinforced concrete and the piers are monolithic concrete (Lu 2008). The general bridge framing plan, along with general member dimensions, are shown in Figure 3.2.

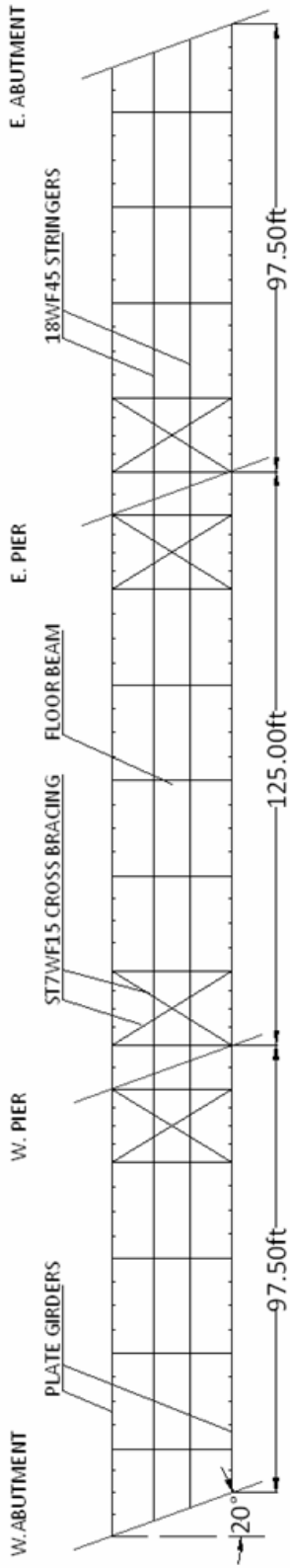


a. Side View

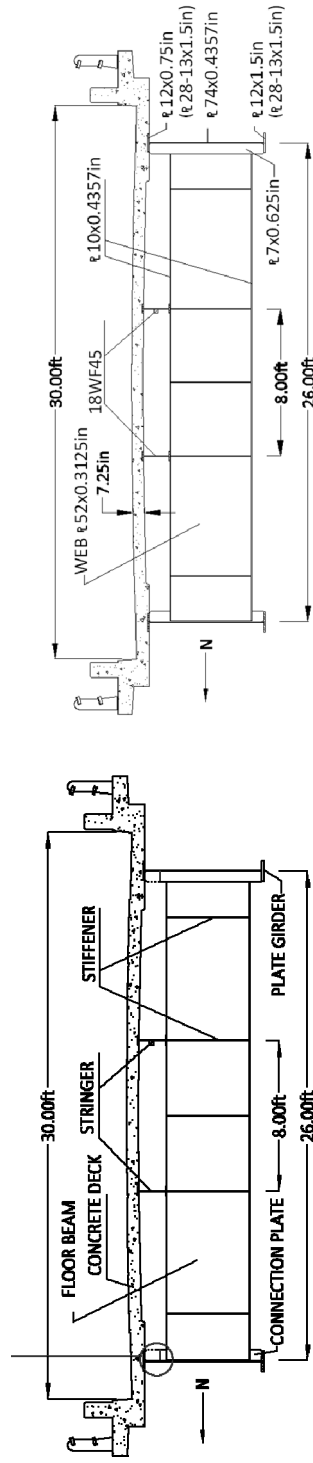


b. Bottom View

Figure 3.1 Photographs of the US 30 South Skunk Bridge (Lu 2008)



a. Plan view



b. Typical cross section

c. Sizes of structural components

Figure 3.2 Plan View and Sectional Views of US 30 Bridge (Lu 2008)

3.1.2 Fatigue Sensitive Details: Girder Web-Gap

In previous research by Wipf et al., several fatigue-sensitive locations of the US 30 Bridge were instrumented with fiber-optic strain gauges. These locations are generally located at the connection between the floor beams and the web of the welded plate girders, as shown in Figure 3.3a.

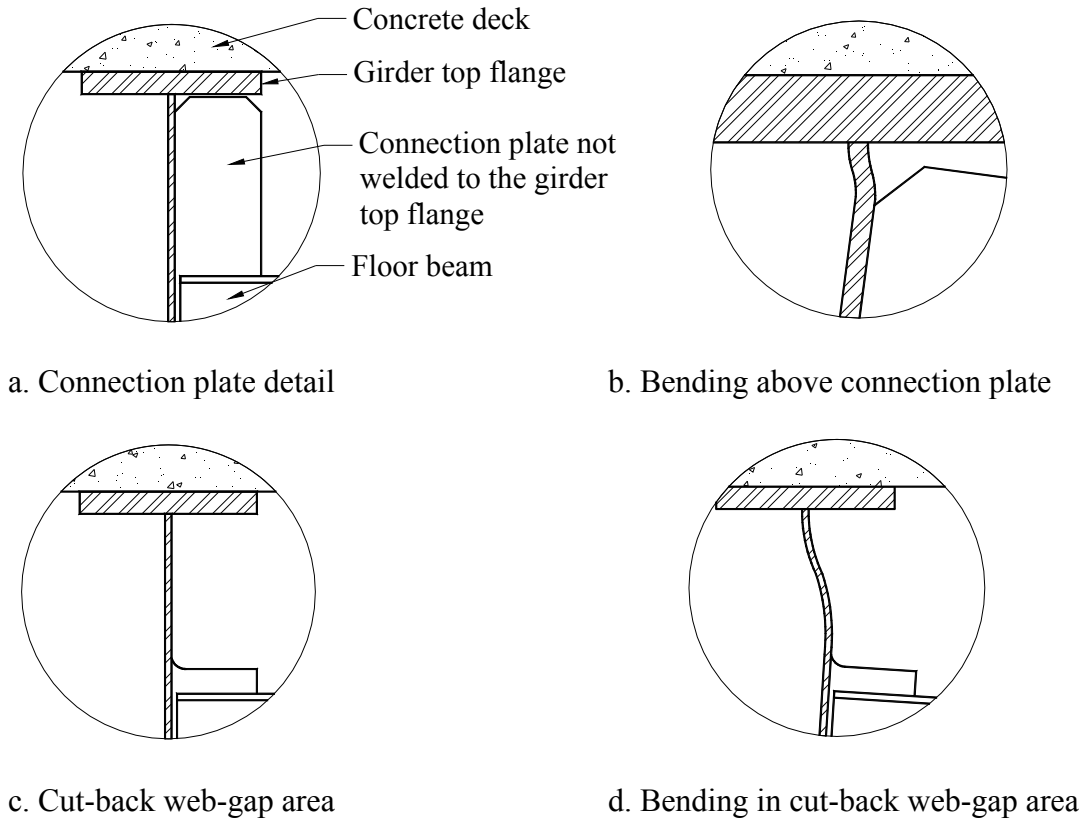


Figure 3.3 Web-Gap Details and Out-of-Plane Bending Behavior (Lu 2008)

During initial construction of the bridge, the connection plate welded to the web of the plate girder extended to directly under, but not welded to, the top flange of the plate girder. As vehicles cross the bridge, the deflection of each of the girders differs due to the skew of the bridge; this causes a rotation of the floor beam, which is especially pronounced near the piers (Lu 2008).

Due to its large stiffness, the composite concrete deck restrains rotation of the plate girder top flange. Therefore, as the floor beam rotates, double curvature bending of the plate girder web (between the top flange and the top of the floor beam connection plate) occurs. This phenomenon can schematically be seen in Figure 3.3b. This double curvature creates high levels of stress and has been linked to the formation of fatigue cracks. Cutting back the floor beam connection plate, as illustrated in Figure 3.3c, allows the double curvature to act over a longer length (Figure 3.3d).

This reduces the stress concentration/levels and, therefore, reduces the susceptibility to fatigue cracking. Although this repair reduces the fatigue damage, it does not completely eliminate it. In some cases fatigue cracks have continued to develop in these regions. Autonomous detection of crack formation in these areas was the precipitous for this and preceding work.

3.1.3 Instrumentation

During previous work, 48 fiber-optic strain gauges were installed on the bridge. Numerous fiber-optic strain gauges were placed in the web cut-back regions to monitor the strain caused by live loads. Figure 3.4 shows the location of the five-sensor array at Section C, on the north girder, cut-back region (C-NG-CB), which is geometrically similar to all web gaps. Note that the sensor numbers shown in Figure 3.4 will be used elsewhere in this report.

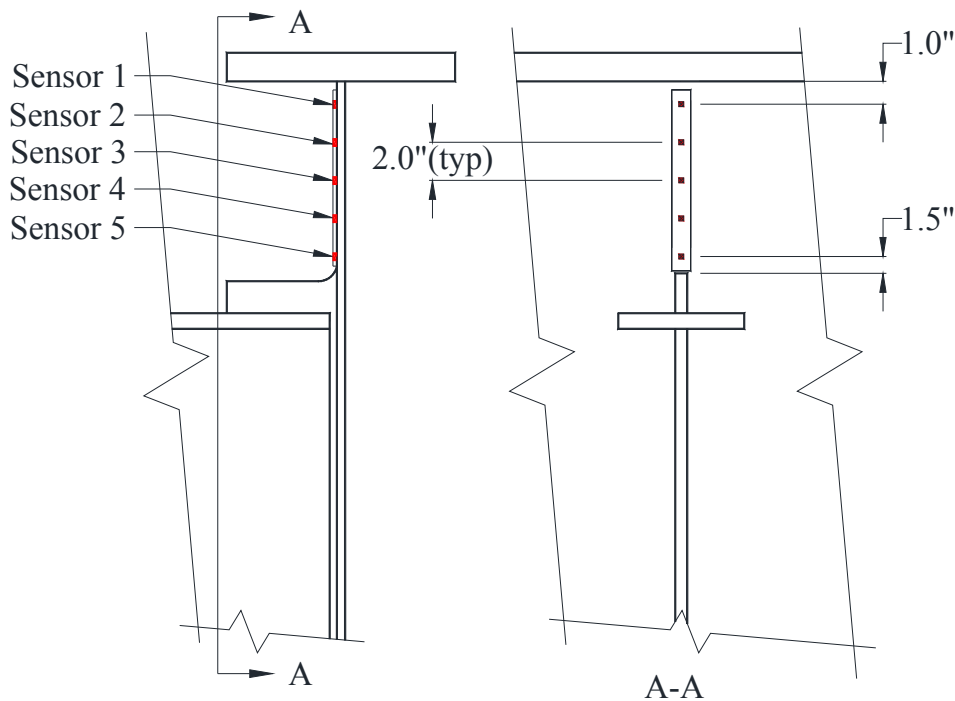


Figure 3.4 Typical Instrumented Web-Gap

Sensors were also placed at numerous other locations on the US 30 Bridge. These sensors were distributed across six cross-sections (Figure 3.5) and are aligned in two orientations: vertical or horizontal. Sensors were installed on the bottom flanges of the two plate girders, the bottom flanges of multiple floor beams, the bottom flanges and webs of the stringers, and on the deck bottom. The distribution of the sensors across the different cross-sections (Sections A through F and Lines 1 and 2) is summarized in Figure 3.6.

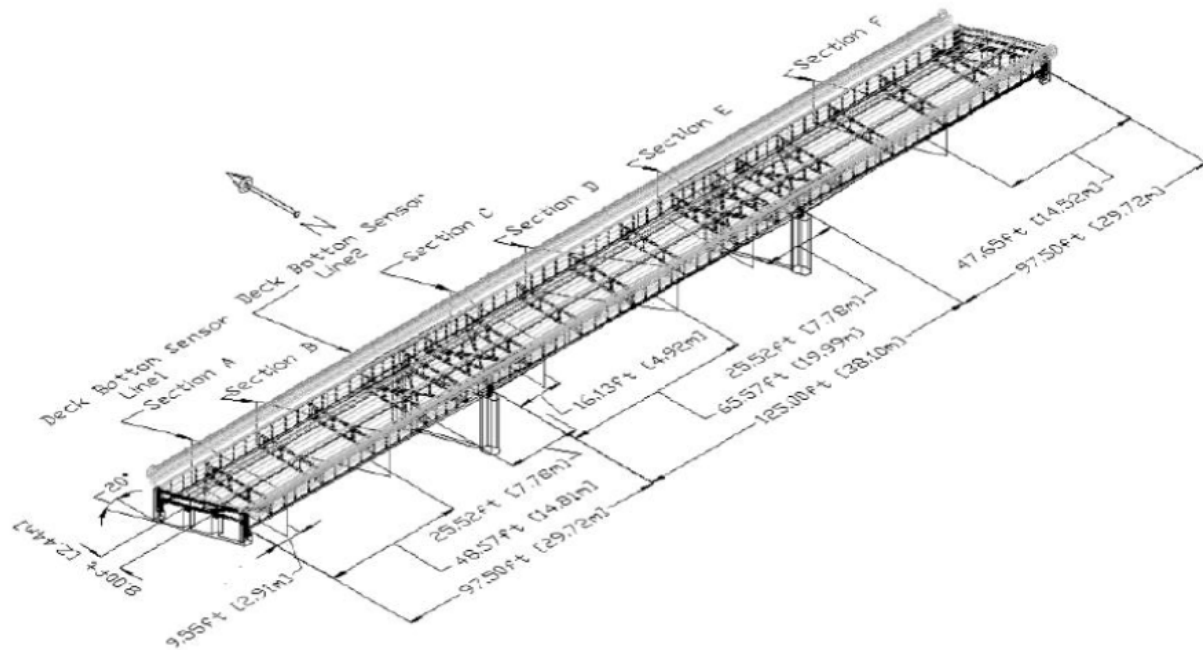


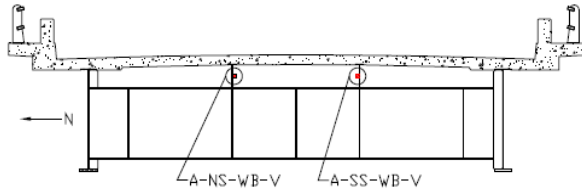
Figure 3.5 Cross Sections of US 30 Bridge and Sensor Longitudinal Locations (Lu 2008)

A naming convention for the sensors based on their location and orientation was inherited from previous work with descriptions shown in **Error! Reference source not found..**

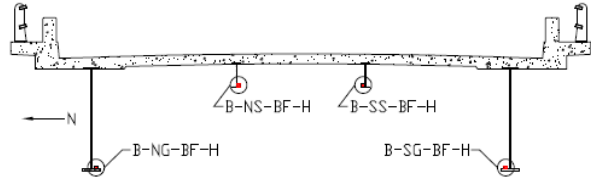
Table 3.1 Naming Convention for Sensors Installed on the US 30 Bridge (Lu 2008)

Member	Description
NG	North Girder
SG	South Girder
NS	North Stringer
SS	South Stringer
FB	Floor Beam
DB	Deck Bottom
Part	Description
BF	Bottom flange
CB	Cut-back region
WB	Web
Orientation	Description
H	Horizontal
V	Vertical

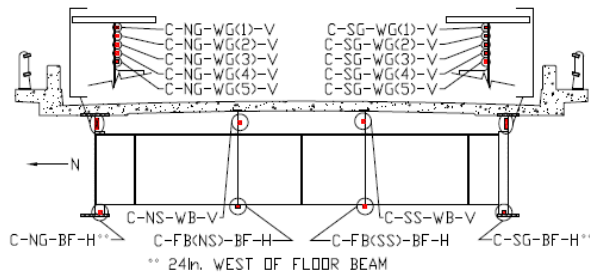
For example, a sensor designated B-NG-BF-H means the sensor is at Section B, on the north girder, on the bottom flange, and in the horizontal orientation. More information on the complete monitoring system can be found in “Damage Detection in Bridges through Fiber Optic Structural Health Monitoring” (Doornink 2006) and “A Statistical Based Damage Detection Approach for Highway Bridge Structural Health Monitoring” (Lu 2008).



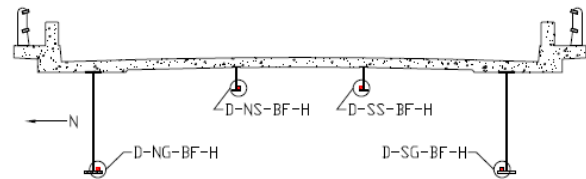
a. Cross section A



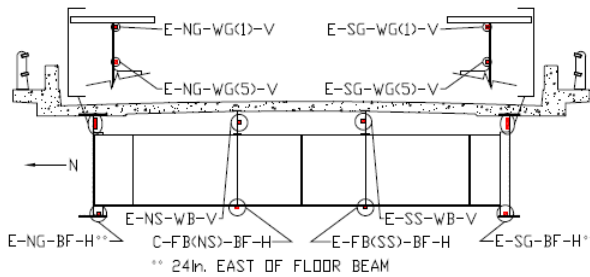
b. Cross section B



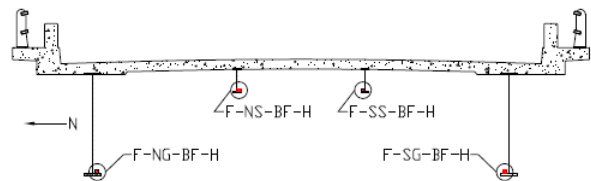
c. Cross section C



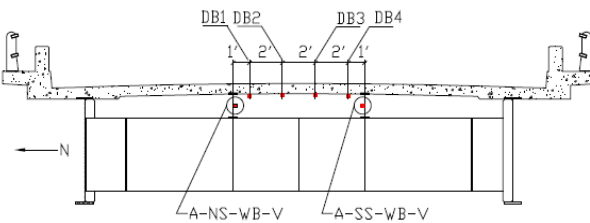
d. Cross section D



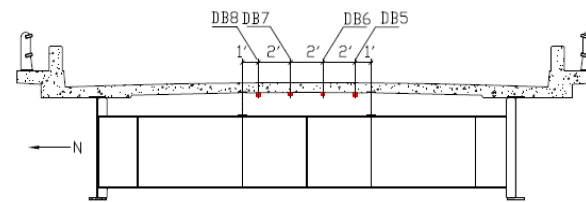
e. Cross section E



f. Cross section F



e. Line of deck-bottom sensors at Section A



f. Line of deck-bottom sensors above fifth floor beam

Figure 3.6 Sensors Located at the Bridge Frame System (Lu 2008)

3.2 Sacrificial Specimen

As the goal of this work was to validate the damage-detection algorithms developed in previous work, and in light of the fact that the Iowa DOT prohibited the introduction of damage into a public bridge, a sacrificial specimen was designed, installed at the US 30 Bridge, and forced to accumulate damage. The design and configuration of the sacrificial specimen focused on simulating the double curvature bending occurring within the web-gap regions.

3.2.1 Sacrificial Specimen Description

The sacrificial specimen details are shown in Figure 3.7 and a photograph is shown in Figure 3.8. To encourage similar strain levels and behaviors, the sacrificial specimen plate thicknesses and welds were designed to match those found on the US 30 Bridge.

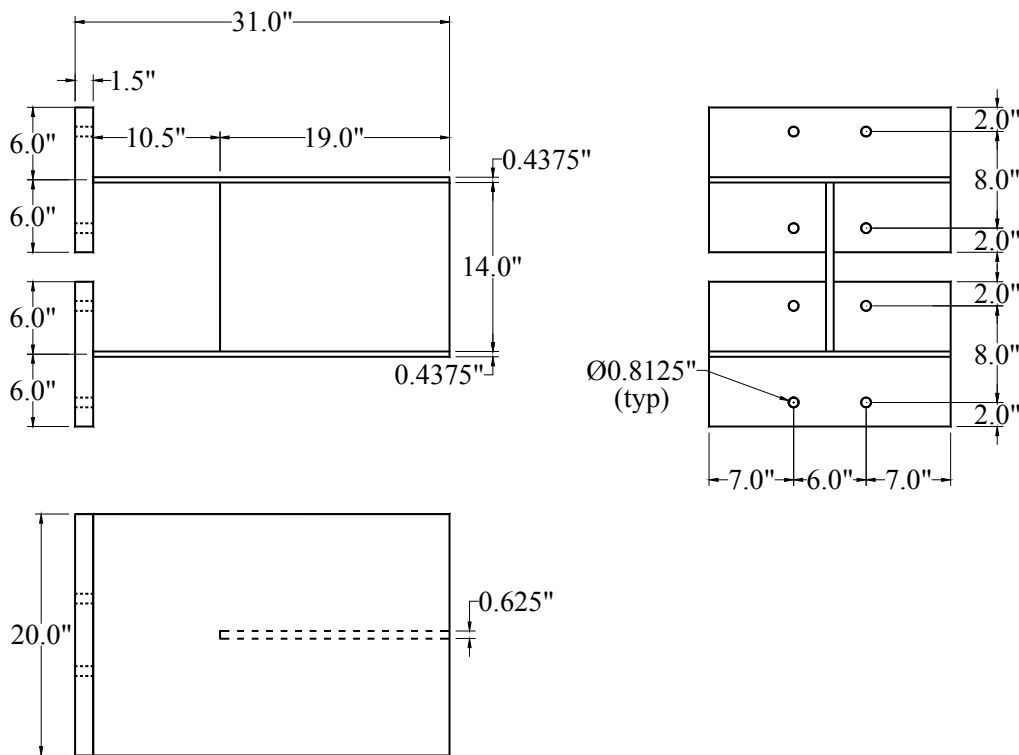


Figure 3.7 Sacrificial Specimen Geometric Details

The sacrificial specimen consists of two web-gaps connected by a steel plate (simulating the floor-beam connection plate). In this configuration each of the two web gaps undergoes double curvature bending similar to the actual bridge (Figure 3.9).

A finite element model (FEM) of the sacrificial specimen was constructed before fabrication to study the behavior. The FEM is shown in Figure 3.10 and the strain contour plot from a point load placed at the end of the sacrificial specimen can be seen in Figure 3.11. The high strain locations from the FEM of the sacrificial specimen (e.g. the dark blue and yellow areas in Figure

3.11) coincide with the expected high strain locations caused by double curvature bending. A simpler beam-type analysis also confirmed the general behavior. In total two sacrificial specimens were fabricated and tested.



Figure 3.8 Photo of Sacrificial Specimen

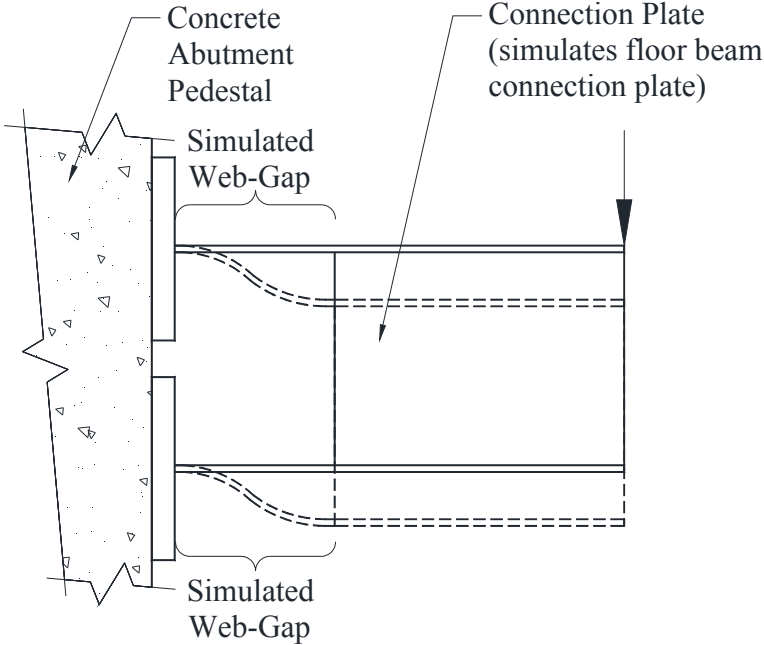


Figure 3.9 Double Curvature Bending of Sacrificial Specimen

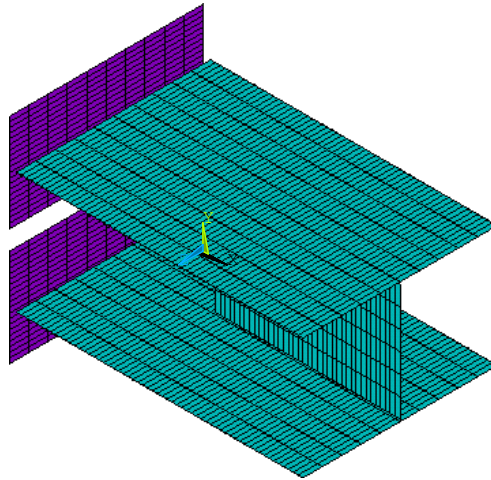


Figure 3.10 Finite Element Model of Sacrificial Specimen

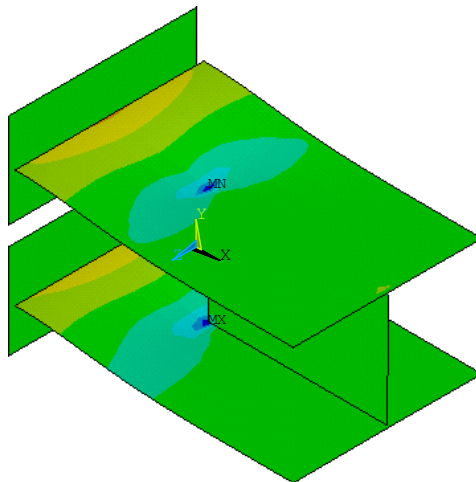


Figure 3.11 Strain Contour Plot of Sacrificial Specimen

3.2.1.1 Sacrificial Specimen 1

Sacrificial Specimen 1 was fabricated with a small Electrical Discharge Machining (EDM) notch through the thickness of the top plate (i.e., the plate directly connected to the steel strut) near an anticipated high strain area (Figure 3.11) as illustrated in Figure 3.12.

Sacrificial Specimen 1 modeled two web-gap areas connected together by a simulated connection plate, which in turn helps to transform the ambient traffic loads into double curvature bending of the simulated web-gaps. When subjected to high strains and a large number of cycles, a crack was expected to initiate at the EDM notch. Different damage levels were introduced in sacrificial Specimen 1 and are discussed in later paragraphs.

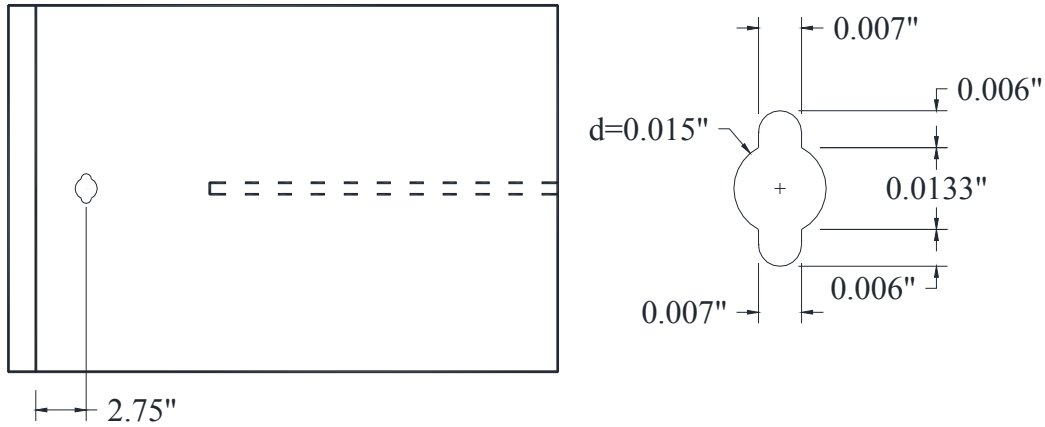


Figure 3.12 Dimensions and Location of Notch

3.2.1.2 Sacrificial Specimen 2

Sacrificial Specimen 2 was constructed as shown in Figure 3.7 and instrumented as shown in

Figure 3.13. The EDM notch through the thickness of the top plate was not fabricated on sacrificial Specimen 2 due to the cracking that did not occur through the EDM notch in sacrificial Specimen 1 as expected. When the location of the EDM notch was determined on sacrificial Specimen 1, the second high-strain location was not considered as a possibility for a crack location.

3.2.2 Sacrificial Specimen Instrumentation

An array of four fiber-optic sensors arranged in-line was installed in one web-gap of each sacrificial specimen as shown in

Figure 3.13. Carbon fiber reinforced polymer was used to hold the sensors in place and to attach the sensors to the steel. A grating length (i.e., sensor length) of each of the sensors was chosen as 5 mm to ensure the accurate recording of peak strains. The array was chosen to closely match the sensor arrays placed on the web-gaps of the US 30 Bridge (Figure 3.4). The area of steel on which the sensors were attached using Loctite H4500 epoxy was sanded down and pressure was applied to ensure proper bonding of the carbon fiber package and the accuracy of the strain readings. This process was completed for both sacrificial specimens.

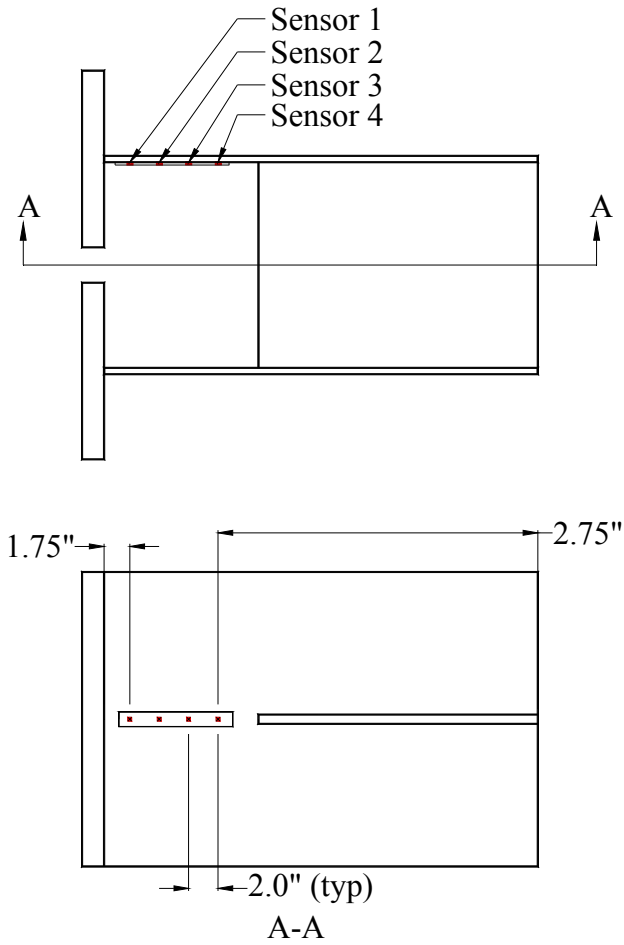


Figure 3.13 Sacrificial Specimen with Sensor Array Details

3.2.3 Sacrificial Specimen Installation

Each sacrificial specimen was installed in a horizontal orientation with the plates simulating the girder top flanges secured to a west abutment pedestal using anchor bolts, as shown in Figure 3.14. A steel strut attached to the sacrificial specimen and a stringer were used to transfer the load from the bridge to the sacrificial specimen.

Typical strain vs. time curves for both the bridge and the sacrificial specimen web-gaps are shown in Figure 3.15. These data were produced by a single, five-axle truck driving across the bridge. Note that the strains for the sacrificial specimen web gap were collected using a four-sensor array, whereas strains in the bridge web gap were collected using a five-sensor array. As a result, the gauges were not measuring strain at exactly the same location in the web-gap.

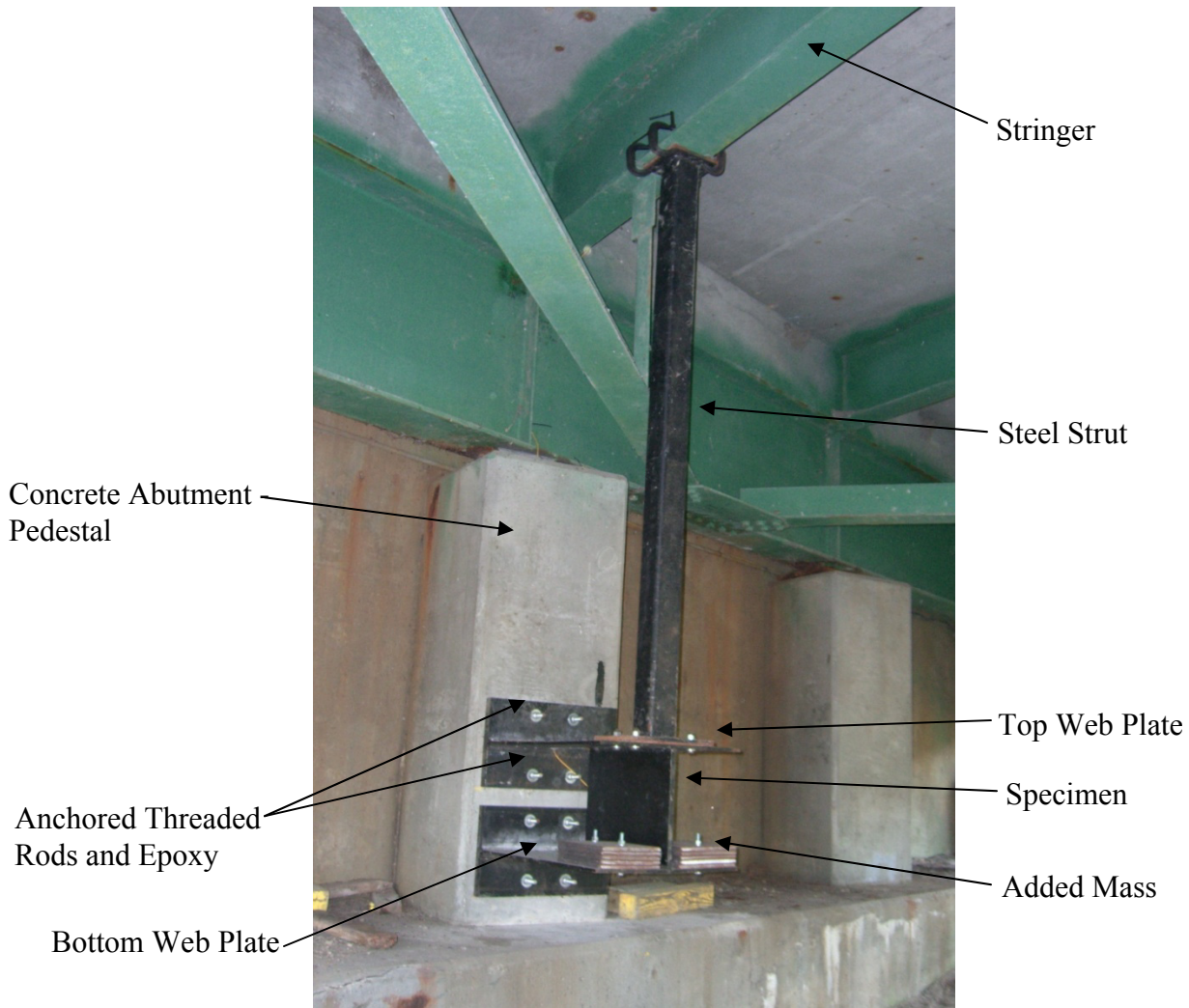


Figure 3.14 Photograph of Typical Installed Sacrificial Specimen

As can be seen in Figure 3.15, the shape of the strain curve from the sacrificial specimen generally matches the shape of the strain curve from the US 30 Bridge. However, the strain range in the sacrificial specimen was consistently observed to be less than that in the bridge. The results of this lead to two conclusions. First, the sacrificial specimen was unlikely to develop a fatigue crack in a “reasonable” time period. Second, it was felt that if damage could be detected in this lower strain range environment, the sensitivity in the bridge should be even higher.

The strain distribution in the web-gap at a single point in time was further evaluated, as shown in Figure 3.16. The distribution in the sacrificial specimen again matches the shape of that from the US 30 Bridge. The approximate linear strain variation from negative to positive shows that double curvature bending occurs in both web-gaps.

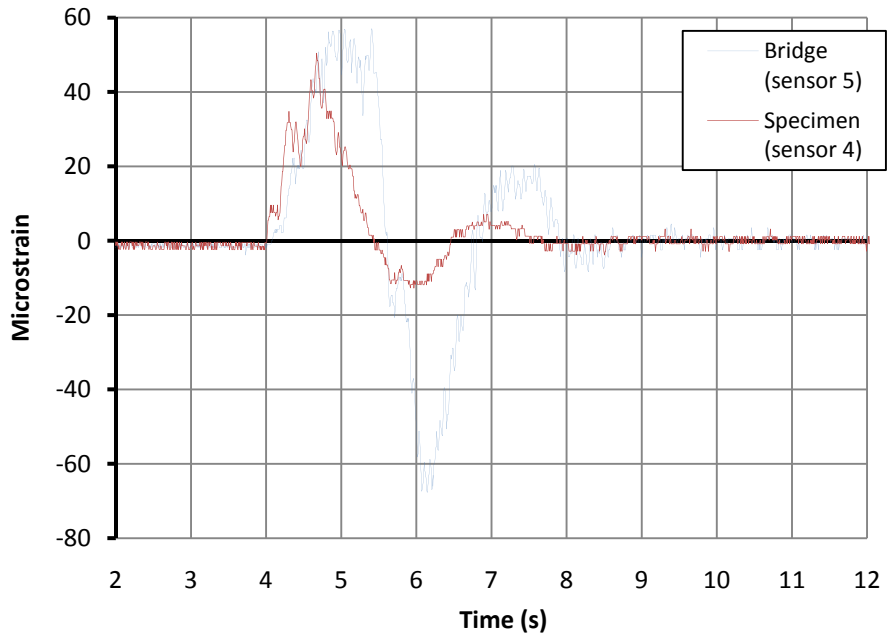


Figure 3.15 Strain Response in Web-Gaps Due to Typical Five-Axle Truck

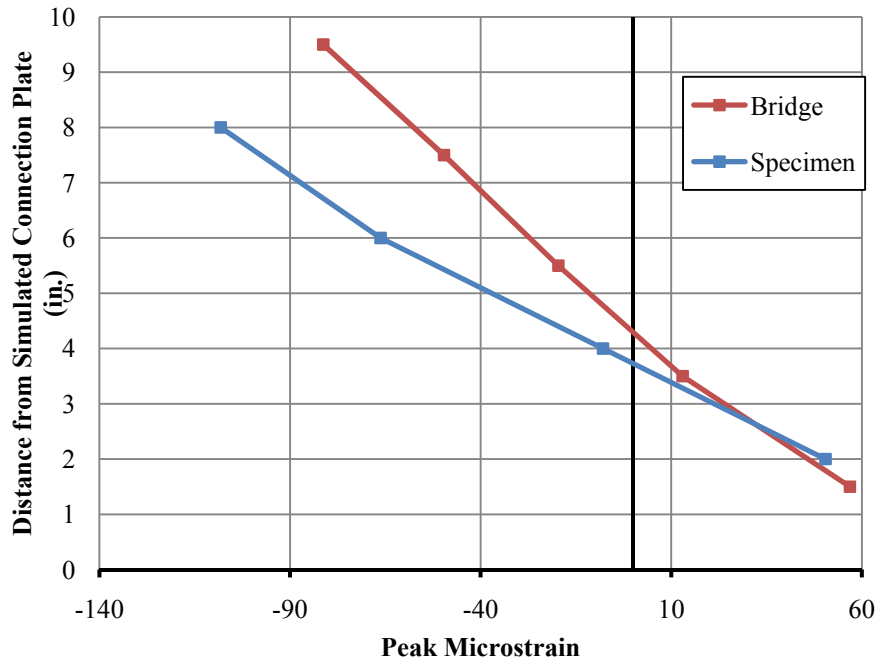


Figure 3.16 Distribution of Strain in Web-Gaps Due to Typical Five-Axle Truck

3.3 Data Collection and Analysis

For the damage-detection algorithm to detect damage, data from both the undamaged and damaged structures must be collected. For this experimental verification of the algorithm, damage must be introduced to the sacrificial specimen and not to the US 30 Bridge. This section details the data collection and the data analysis process.

3.3.1 Data Collection

Baseline data for each undamaged sacrificial specimen and bridge (i.e., training data) were collected for about one month. The process for collecting and processing the training data is described in detail in “A Statistical Based Damage Detection Approach for Highway Bridge Structural Health Monitoring” (Lu 2008) and summarized in section 1.1 of this report. After training data were collected, the sacrificial specimen was damaged by either creating a fatigue crack or by simulating thickness loss caused by corrosion

3.3.2 . Data Analysis

Once the training data collection is complete, the process of creating prediction models begins. Prediction models plot a best-fit line through peak strain values of all combinations of sensor pairs. Additional data are plotted on the prediction models and the vertical distance from the data to the best-fit line is calculated and called the residual.

The residuals are compiled for each sensor pair in matrices and simplified, so each sensor has one vector. These vectors are then used to create control charts, as previously described. The control charts have upper control limits (UCLs) and lower control limits (LCLs) set by adding and subtracting three times the standard deviation of the data to and from the mean, respectively. In all cases, points outside the control limits are possible indicators of damage. The control charts must be visually analyzed to determine the location and severity of the occurring damage.

3.4 Damage Creation Protocols

The first type of damage induced was fatigue cracking. Accelerated fatigue damage was created by subjecting the sacrificial specimen to many cycles of loading using the rotary shaker shown in Figure 3.17.

The rotary shaker is a motor with eccentric weights, which rotate at a user-specified frequency up to 100 Hz. The rotary shaker may be “dialed in” to the resonant frequency of the attached object to create very large strain values and number of cycles. To accumulate damage quickly, the shaker was bolted to the free end of the sacrificial specimen and then operated near the natural frequency of the sacrificial specimen. This induced high levels of strain at the high rate needed to create fatigue cracks in a relatively short time.



a. Side View



b. Top View

Figure 3.17 Photographs of Rotary Shaker

Mass was added to the sacrificial specimen as shown in Figure 3.14 to reduce the resonant frequency to within the operable range of the shaker. In general, the rotary shaker was operated in the range of 60 Hz to 70 Hz.

The second type of damage investigated was thickness loss that might result from corrosion. This damage was simulated by removing steel in a discrete area with a hand-held rotary grinder.

4 EXPERIMENTAL RESULTS

In this chapter, results and discussions related to the training and post-damaged evaluation are presented. A brief statistical analysis of the data for Specimen 2 is also presented and discussed.

4.1 Sacrificial Specimen 1

Sacrificial Specimen 1 was installed at the US 30 Bridge as shown in Figure 3.14 and undamaged data, called training data, were collected from May 10, 2009 to June 3, 2009. The SHM system being validated in this work only uses heavy, right-lane, five-axle trucks and, among the 5,105 right-lane five-axle trucks, 2,009 are classified as heavy trucks.

4.1.1 Training prior to Damage

Select control charts for the sensors on the undamaged sacrificial Specimen 1 and for other sensors on the US 30 Bridge are shown in Figure 4.1. The control charts are generally representative for the sensors throughout the bridge.

More specifically, the control charts for sensors B-NG-BF-H and D-SG-BF-H shown in Figure 4.1e and Figure 4.1f, respectively, are representative of all girder bottom-flange sensors on the bridge. Likewise, the control charts for sensors B-SS-BF-H and D-NS-BF-H shown in Figure 4.1g and Figure 4.1h, respectively, are representative of all stringer bottom-flange sensors on the bridge. Finally, the control charts for sensors C-SG-CB(1)-V, C-SG-CB(5)-V, E-SG-CB(1)-V, and E-SG-CB(5) shown in Figure 4.1i, j, k, and l, respectively, are representative of all sensors in the cut-back areas of the bridge.

These sensors will be used throughout the remaining sections of this chapter to provide a means with which to compare the control charts for the specimens. R-sum values (i.e., the difference between predicted and actual strain values, also called residuals) are plotted on the control charts versus Truck Group number. In this work, a truck group size of 10 was used.

The upper and lower dash-dot lines in Figure 4.1 and all similar figures represent the upper control limit (UCL) and lower control limit (LCL), respectively. As described previously, the UCL and LCL are the average of the training truck groups plus or minus, respectively, three standard deviations of the training data. The fundamental assumption, then, is that points above the UCL or below the LCL are considered damage indicators. To test the control limits, 400 heavy truck events were withheld from the training data and used as testing data. The resulting data are similarly shown in Figure 4.1. As can be seen, nearly all points lie between the LCL and UCL indicating that the LCL and UCL have been properly set.

4.1.2 Post-Damage: Damage Detection

After a cumulative time of about one hour of vibrating sacrificial Specimen 1 at resonance (as

discussed previously) a large crack was observed near the simulated connection plate of the web-gap of both the top and bottom web plates (Figure 4.2). The cracks were not detected earlier, because they did not occur through the fabricated EDM notch and they formed quickly. The top plate crack was about 7 in. long and the bottom plate crack was about 6.5 in. long.

Data were collected from the damaged sacrificial Specimen 1 from August 25, 2009 to September 4, 2009. A total of 2,415 right-lane five-axle trucks were detected and, among them, 860 of the 2,415 were classified as heavy trucks. R-sum values for each sensor were calculated (using a truck group size of 10) and then plotted on the previously-constructed control charts (Figure 4.3).

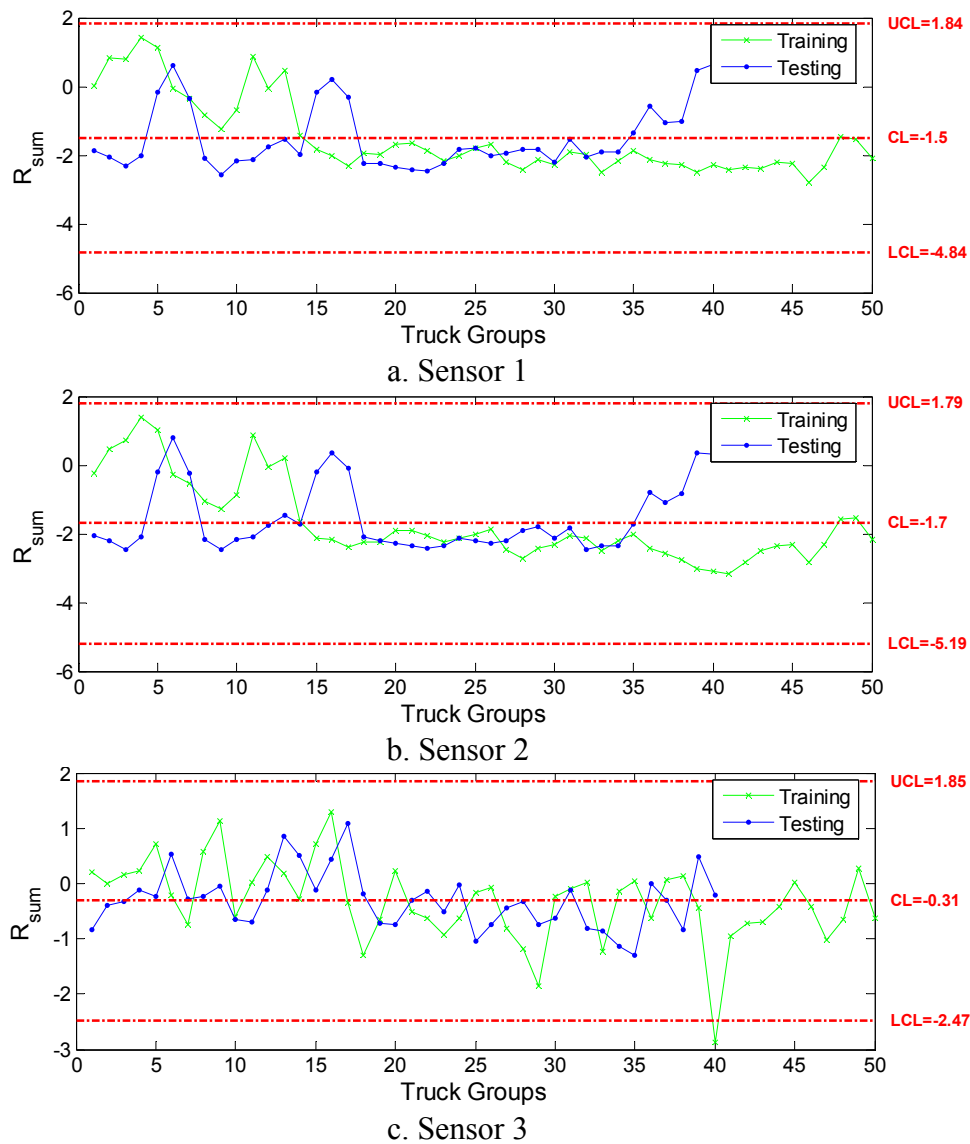
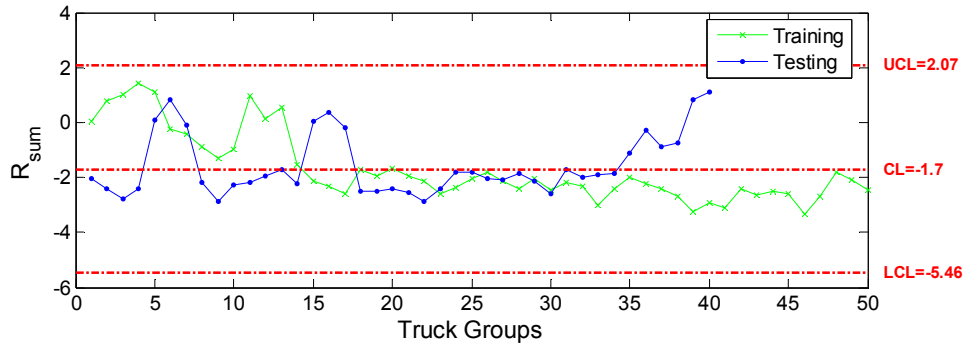
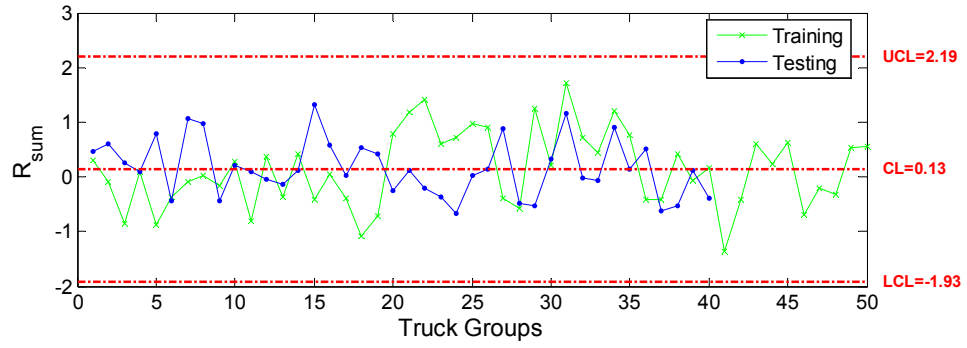


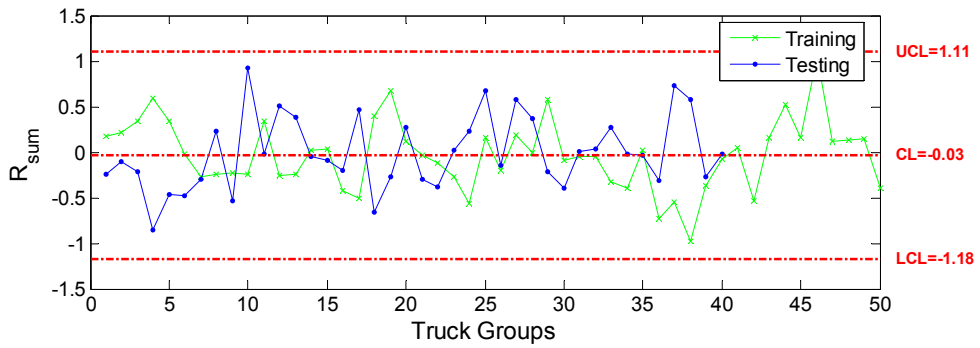
Figure 4.1 Undamaged Sacrificial Specimen 1 Control Charts



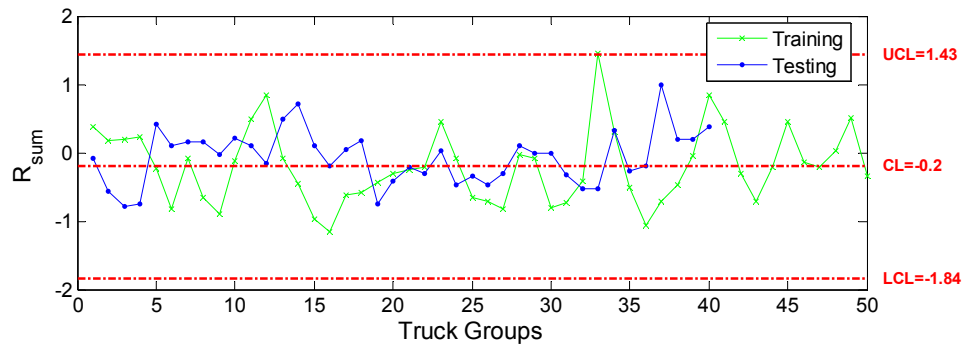
d. Sensor 4



e. B-HG-BF-H



f. D-SG-BF-H



g. B-SS-BF-H

Figure 4.1 continued Undamaged Sacrificial Specimen 1 Control Charts

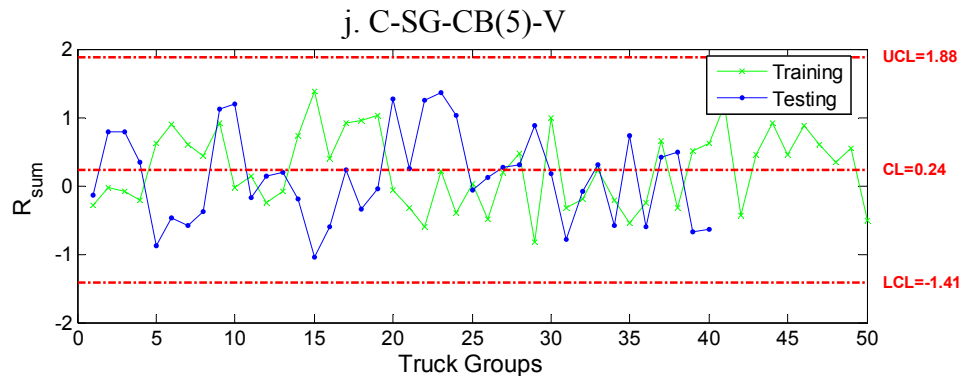
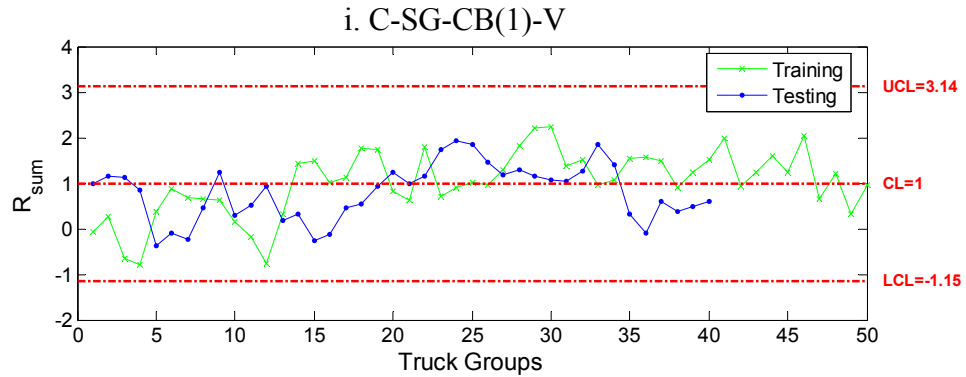
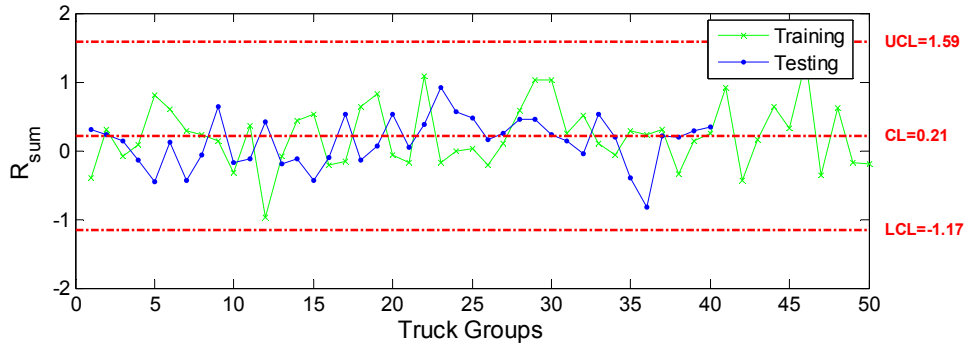
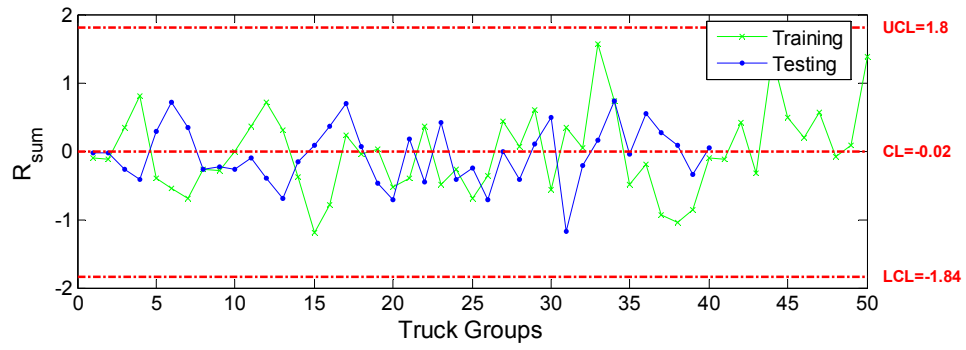
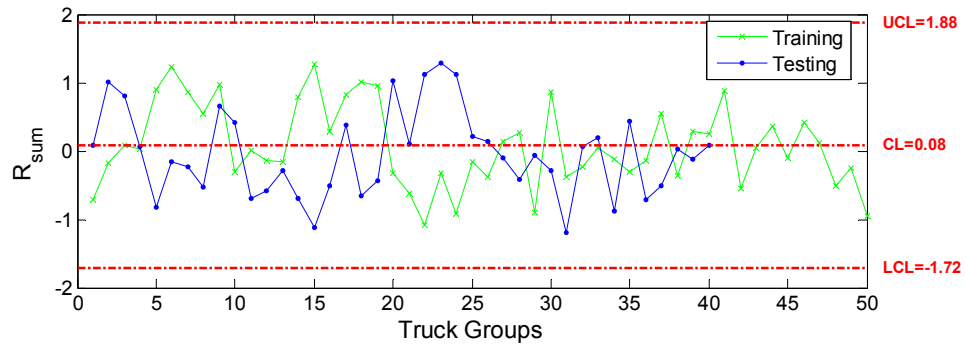


Figure 4.1 continued Undamaged Sacrificial Specimen 1 Control Charts



1. E-SG-CB(5)-V

Figure 4.1 continued Undamaged Sacrificial Specimen 1 Control Charts



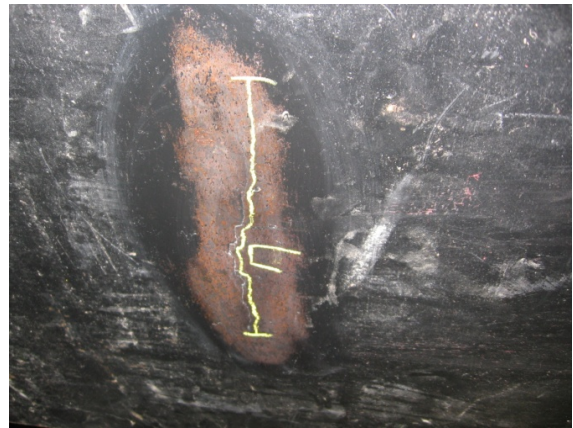
a. Top web plate cracking



b. Close-up of top web plate cracking



c. Bottom web plate cracking



d. Underside of bottom web plate cracking

Figure 4.2 Photographs of Sacrificial Specimen 1 Cracking

The control limits in each of the charts shown in Figure 4.3 match the control limits shown on the corresponding charts in Figure 4.1. For Sensors 2, 3, and 4, all of the R-sum values are outside of the control limits, indicating damage was detected. Because the damage is located closest to Sensor 4, it was expected that a large number of points would be outside the control limits; indeed, in Figure 4.3d all point are outside the control limits. Sensors 2 and 3, shown in Figure 4.3b and Figure 4.3c, respectively, also have every point outside the control limits. This fact may be an indication that the damage that occurred near Sensor 4 was quite severe (i.e., the farther away damage is detected from the source, the more severe the damage).

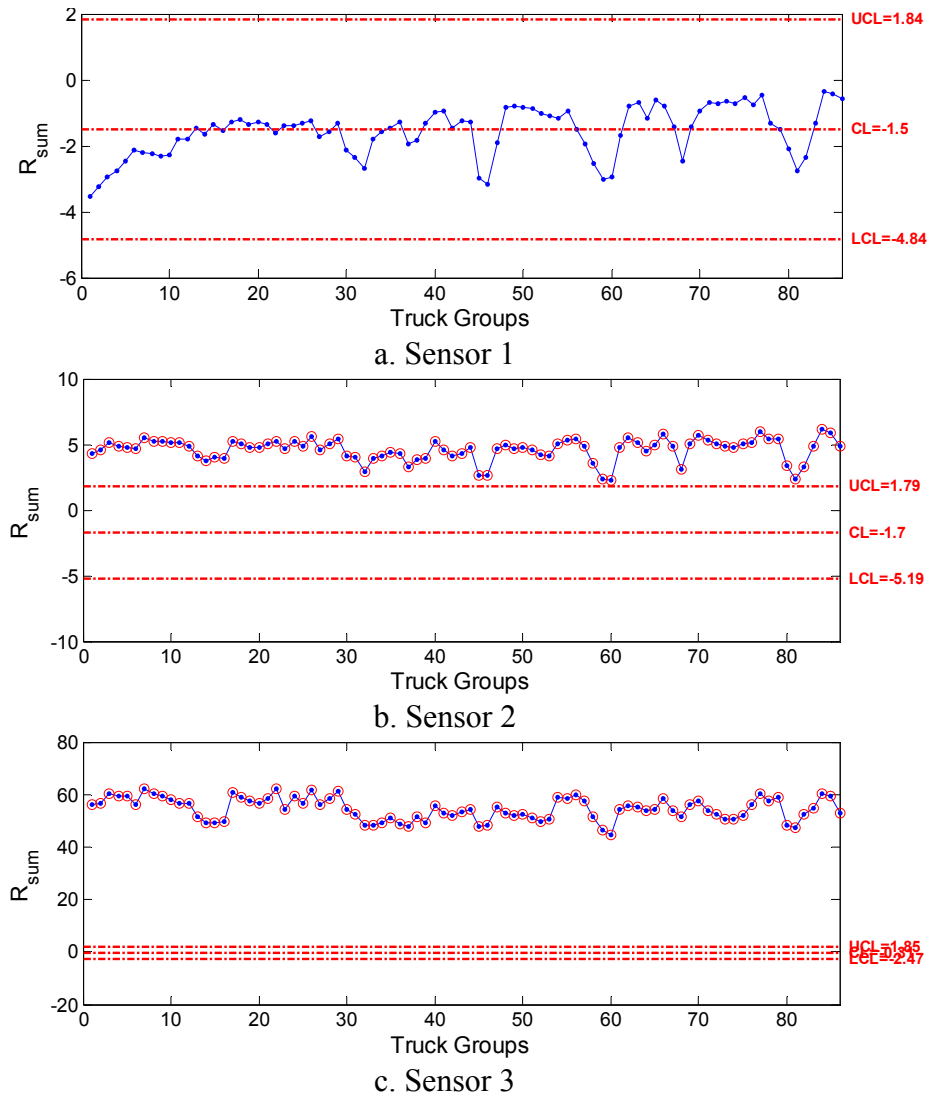
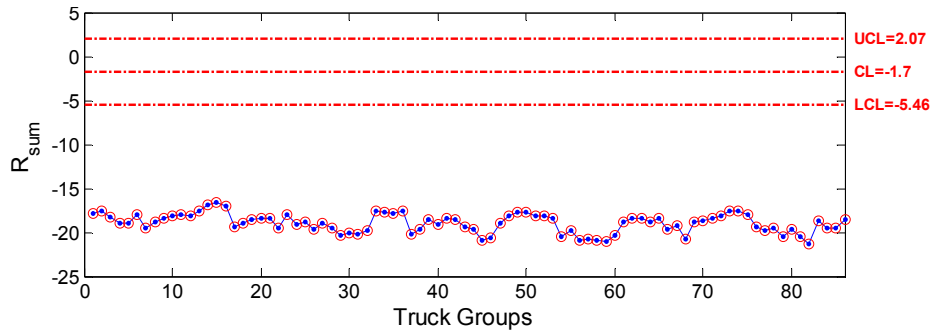
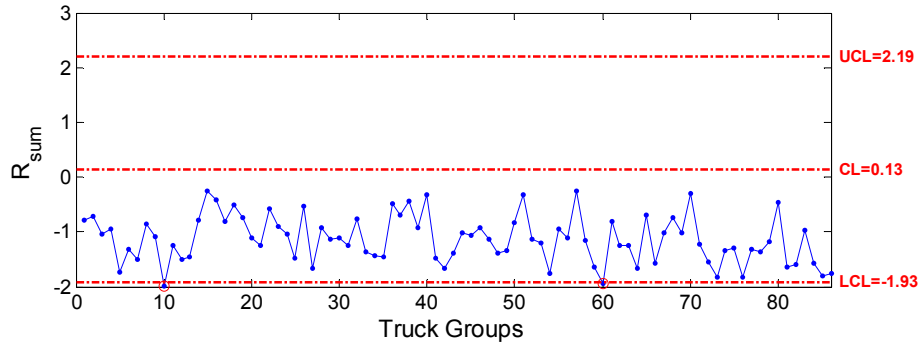


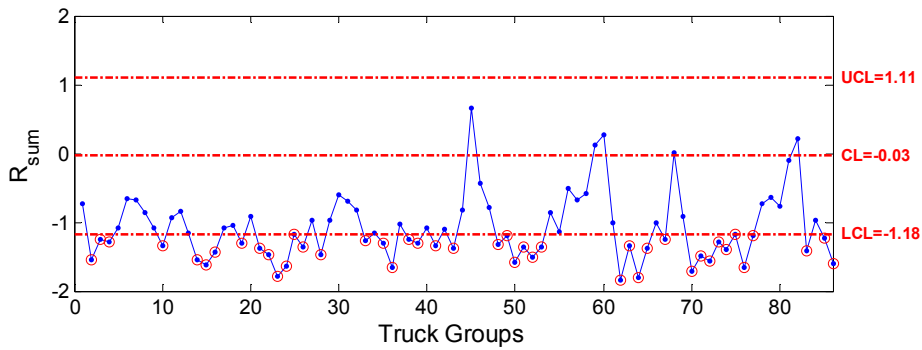
Figure 4.3 Post-Damage Sacrificial Specimen 1 Control Charts



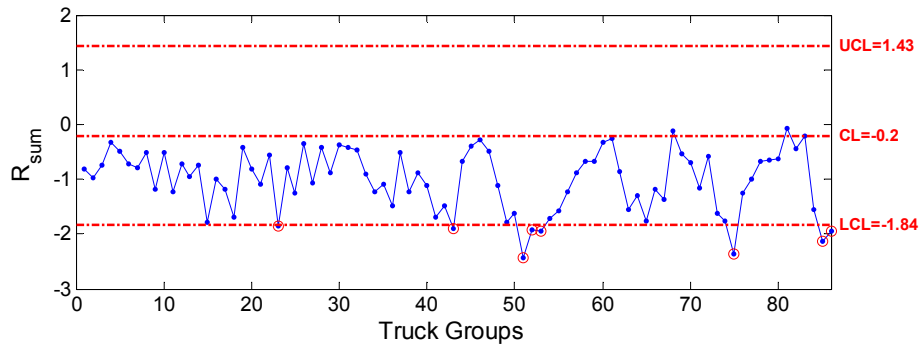
d. Sensor 4



e. B-NG-BF-H

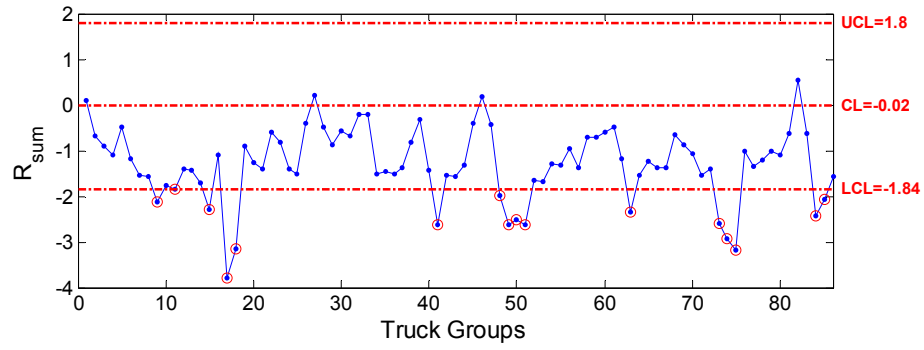


f. D-SG-BF-H

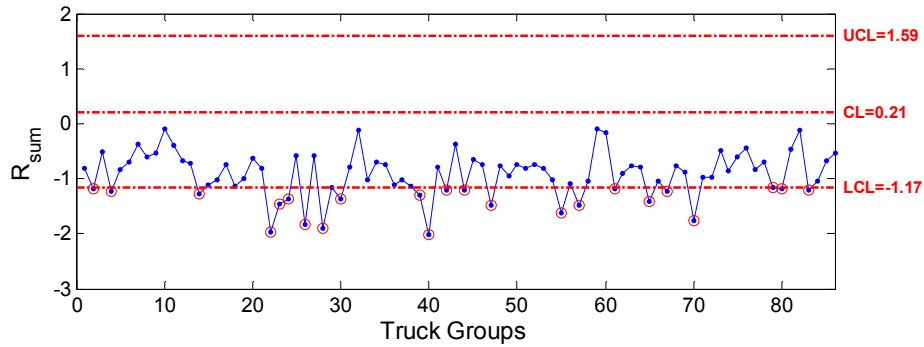


g. B-SS-BF-H

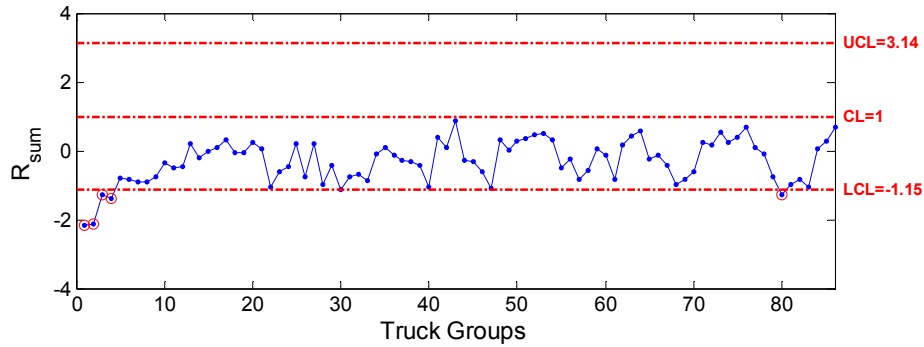
Figure 4.3 continued Post-Damage Sacrificial Specimen 1 Control Charts



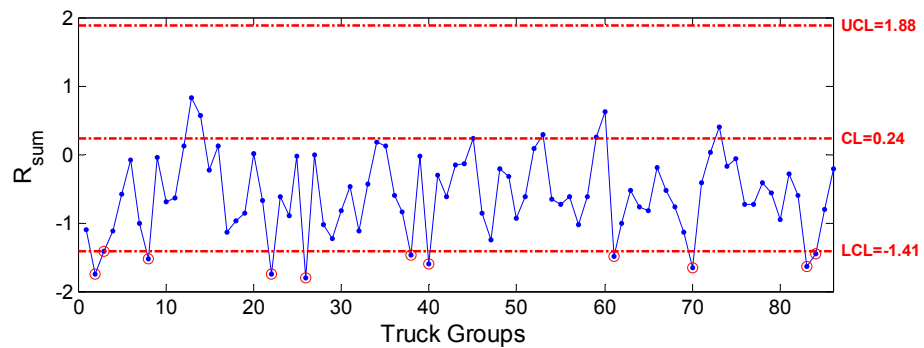
h. D-NS-BF-H



i. C-SG-CB(1)-V



j. C-SG-CB(5)-V



k. E-SG-CB(1)-V

Figure 4.3 continued Post-Damage Sacrificial Specimen 1 Control Charts

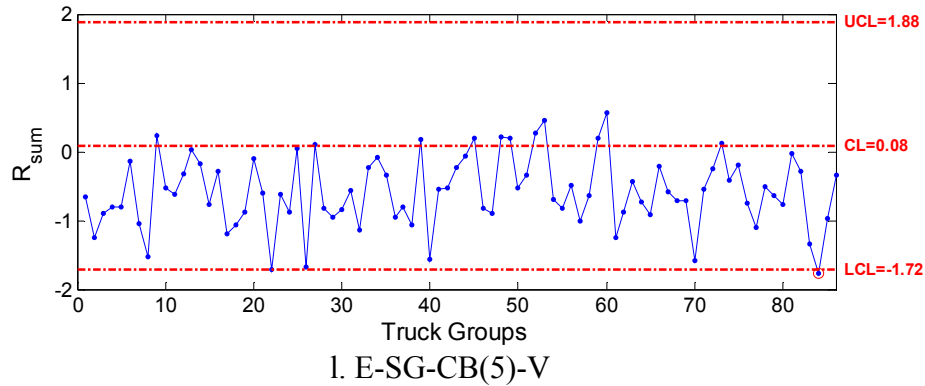


Figure 4.3 continued Post-Damage Sacrificial Specimen 1 Control Charts

In the control charts for the sensors not on Specimen 1 (Figure 4.3e through Figure 4.3i), all have at least one point outside the control limits and four (Figure 4.3f, h, i, and k) have a large percentage of points (greater than 10%) outside the control limits. Although this may be an indication of damage near these sensor locations, it was determined through analysis of the data that the control chart results for other sensors on the bridge are influenced by the large indications of damage from the sensors on Specimen 1.

Specifically, during the row- and column-sum calculations needed to create a single control chart for each sensor, the largely-skewed values from the sensors on Specimen 1 contribute a larger percentage to the column- and row-sum values compared to the values contributed by the other sensors. The contribution of the large values may shift a large percentage of R-sum values outside the control limits, as can be seen in Figure 4.3f, h, i, and k. Therefore, it was concluded that there was no damage at these locations, but rather the R-sum values were skewed due to the contribution of the large R-sum values from the sensor on Specimen 1.

A possible damage severity indicator is the distance the damaged points are away from the average of the training data. For example, in Figure 4.3d, the R-sum average of the damaged data is roughly negative 17, a large distance away from the training data R-sum average of approximately negative 2. This large difference in the average also occurs in Figure 4.3c and is to be expected.

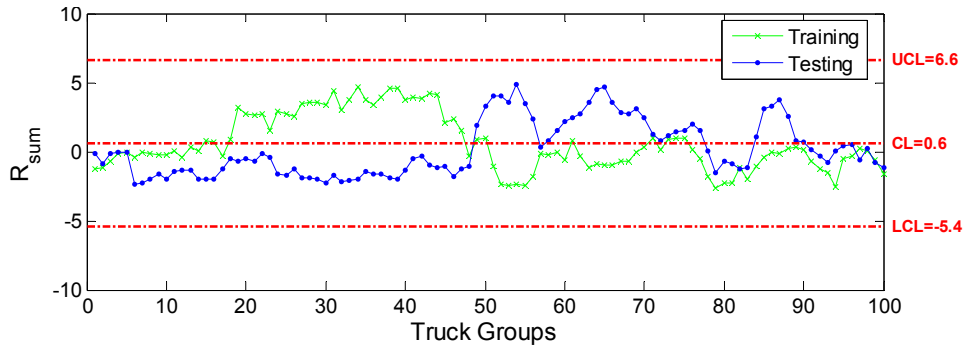
4.2 Specimen 2

Sacrificial Specimen 2 was installed at the US 30 Bridge and training data were collected from December 11, 2009 to January 31, 2010. From the collected training data, 3,653 heavy right-lane five-axle trucks were detected and used in the control chart construction and false-alarm testing.

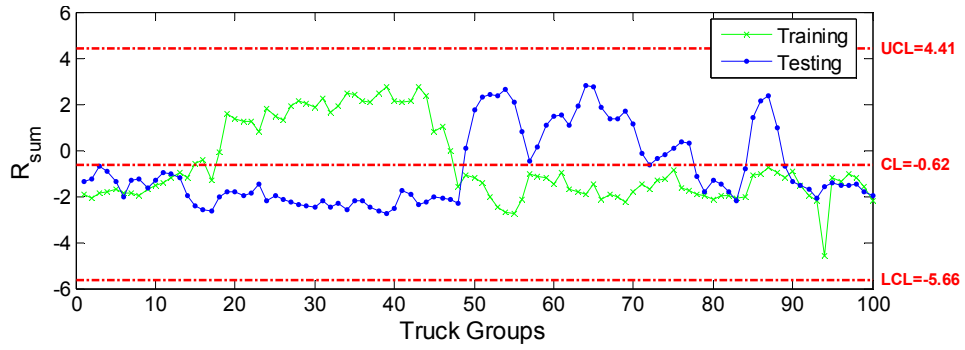
4.2.1 Training prior to Damage

Control charts for the collected training data from sacrificial Specimen 2 were constructed from 3,653 heavy, right-lane, five-axle trucks, following the same procedure outlined in section 4.1.1,

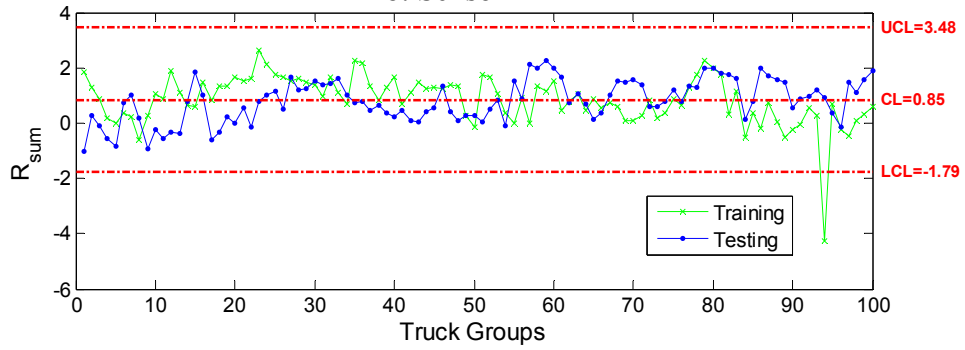
and the control charts are shown in Figure 4.4.



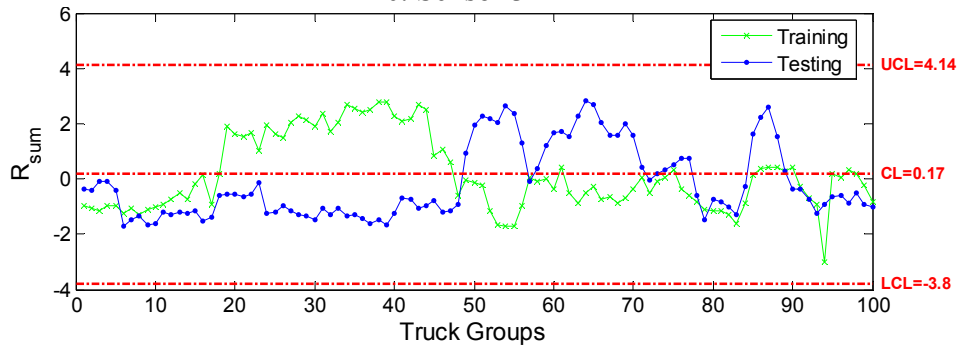
a. Sensor 1



b. Sensor 2

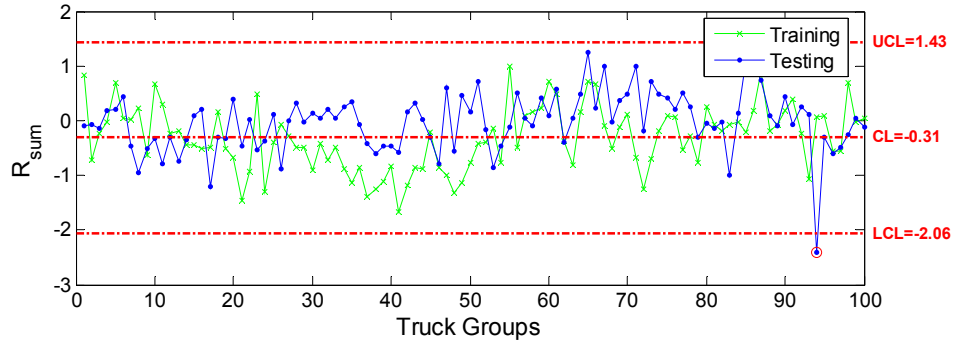


c. Sensor 3

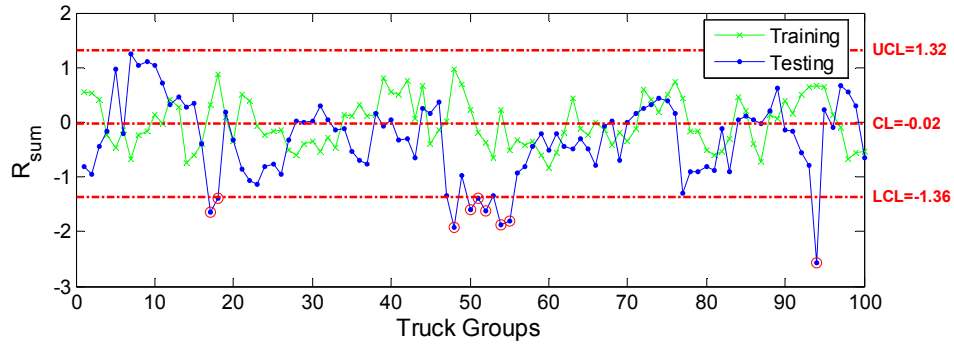


d. Sensor 4

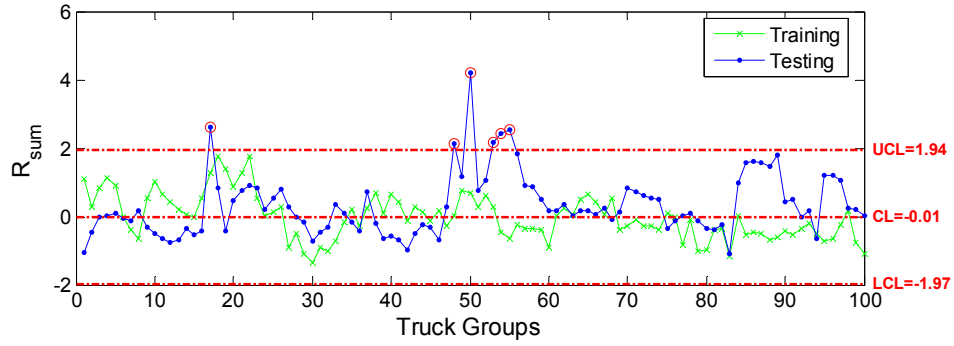
Figure 4.4 Undamaged Sacrificial Specimen 2 Control Charts



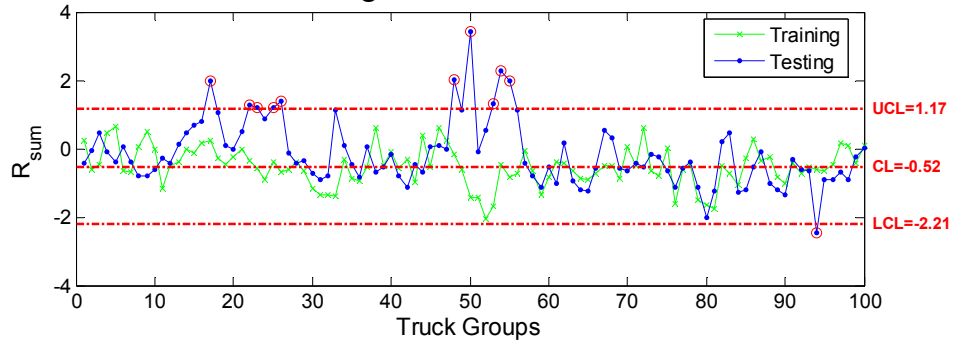
e. B-NG-BF-H



f. D-SG-BF-H

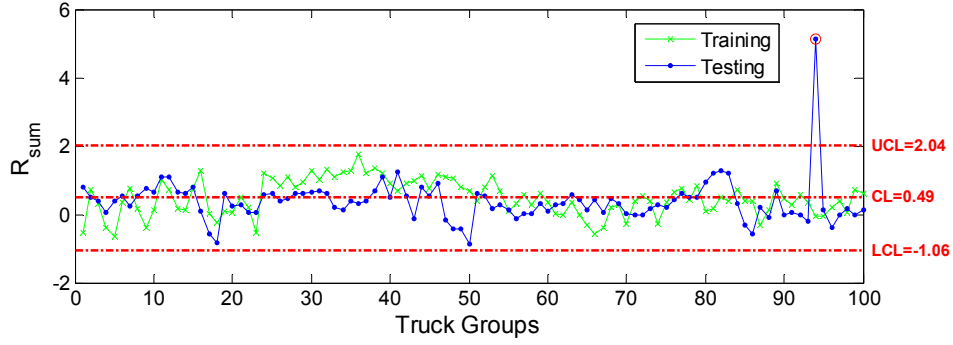


g. B-SS-BF-H

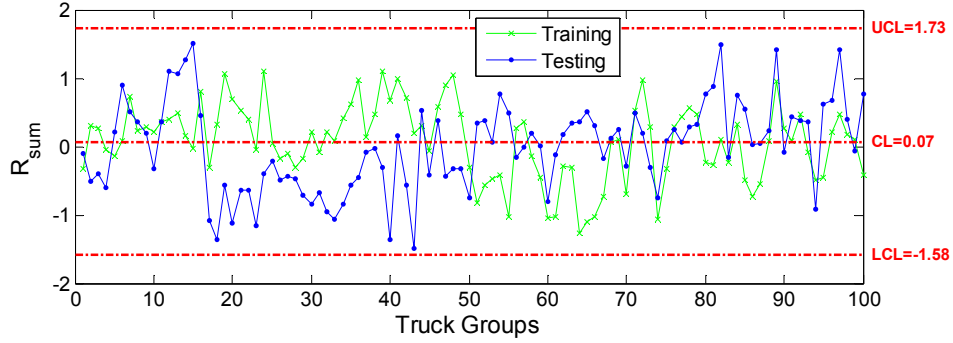


h. D-NS-BF-H

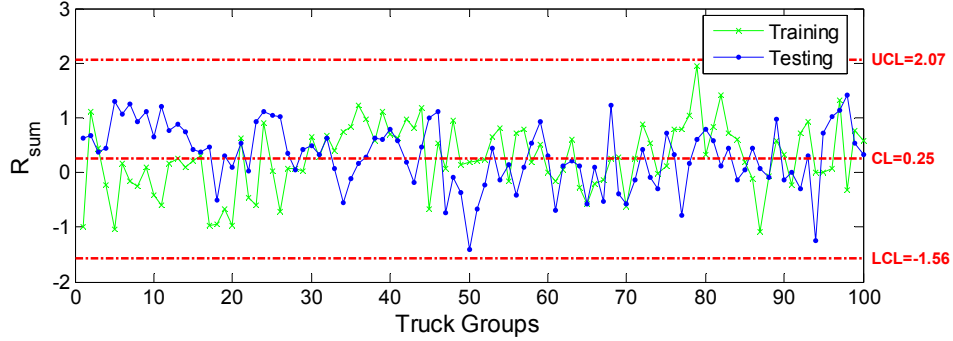
Figure 4.4 continued Undamaged Sacrificial Specimen 2 Control Charts



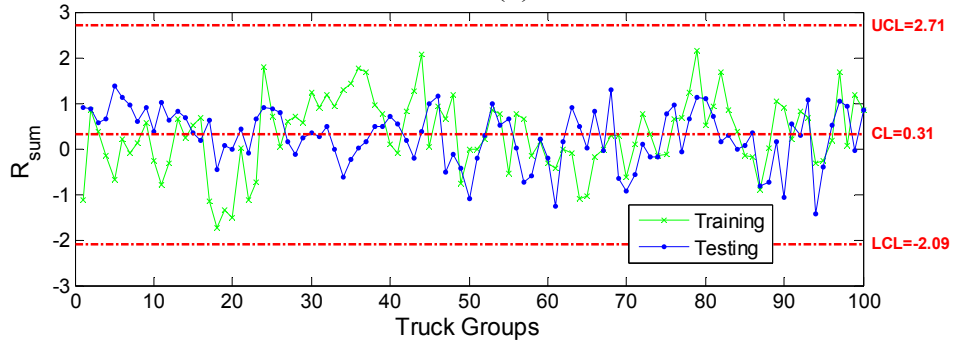
i. C-SG-CB(1)-V



j. C-SG-CB(5)-V



k. E-SG-CB(1)-V



l. E-SG-CB(5)-V

Figure 4.4 continued Undamaged Sacrificial Specimen 2 Control Charts

For testing data, 1,000 truck events were withheld from the training data and are shown on the control charts as the blue lines. If the control charts were constructed correctly, very few, if any, points should fall outside the control limits for the undamaged structure (e.g., no more than 1%). As can be seen, multiple points are below the LCL in Figure 4.4c, f, g, and h and may be due to natural variability in the data, an overweight or unusual truck passing over the bridge, or be an indicator of unknown damage, a false-positive, or may represent a flaw in the methodology. All of the testing data follow the average established by the training data and display the characteristics of an undamaged structure.

4.2.2 Post-Damage: Damage Detection

To study different levels of damage occurring in the web-gap area, different crack sizes were produced in specimen 2. After each propagation of the crack to a larger size, damage data were collected and control charts produced. The procedure and results pertaining to each crack size are described in the paragraphs below.

On February 16, 2010, sacrificial Specimen 2 was vibrated at an average resonant frequency of 66 Hz for about 18 minutes (71,000 cycles) before a crack occurred. The crack was about 1.25 in. long and occurred in Region 4 of the top web plate (similar to the cracking of sacrificial Specimen 1). The cracking is shown in Figure 4.5.

Data were then collected from the damaged sacrificial Specimen 2 from February 16, 2010 to February 23, 2010 and a total of 627 heavy, right-lane, five-axle trucks were detected. The control charts for sacrificial Specimen 2 with the 1.25 in. crack are shown in Figure 4.6. The control limits for each sensor in Figure 4.6 match the control limits for each sensor in Figure 4.4.

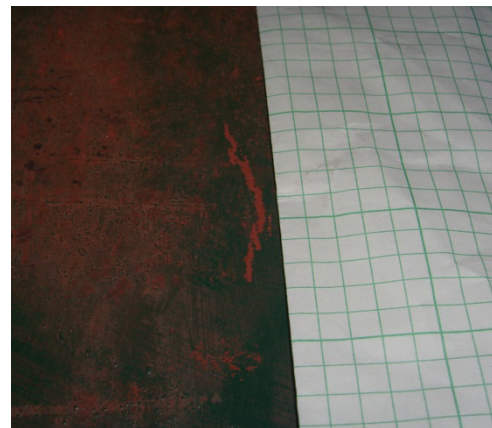
The R-sum data for Sensor 4 (i.e., the sensor closest to the crack) are below the LCL, indicating damage detection. In Figure 4.6a, b, and c there, no R-sum data fall outside the control limits, which is an indication that the damage that occurred closest to Sensor 4 is not severe enough to cause a change in behavior at these locations. Note, however, for Sensors 1, 2, and 3, the R-sum data moved slightly downward, following the trend shown in Figure 4.6d. As the damage becomes more severe, it is thought that these R-sum data will continue to shift until all data points are out of the control limits.



a. Overview of Top Web-Plate Cracking



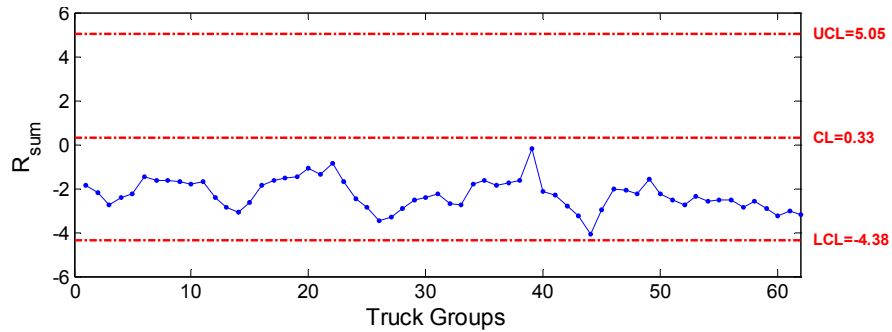
b. Top Web-Plate Cracking



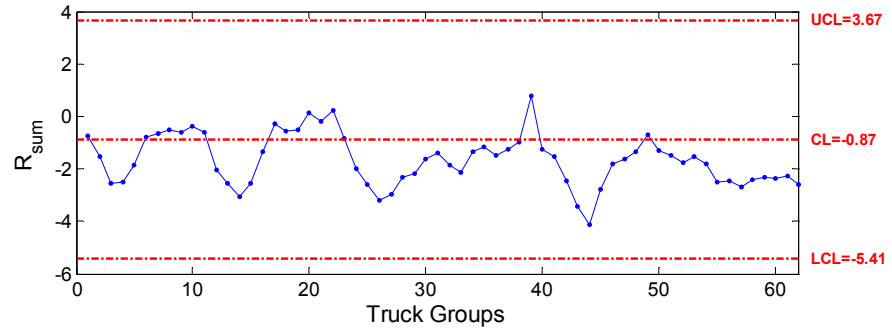
c. Close-Up of Crack

Figure 4.5 Photographs of Sacrificial Specimen 2 Top Web Plate Cracking

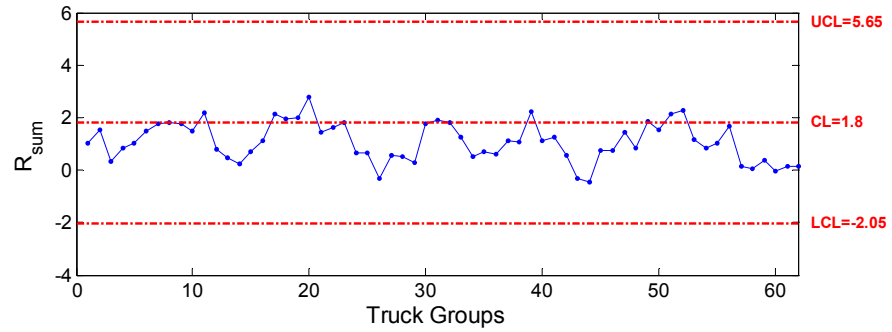
Also noticeable in Figure 4.6f and Figure 4.6h are the higher percentage of R-sum values outside of the control limits. In Figure 4.6f, 14.5% of the R-sum values are outside the control limits and in Figure 4.6h, 8.1% of the R-sum values are outside the control limits. As discussed earlier, this may be due to the large values provided by the sensors on Specimen 2, which may shift multiple R-sum values outside the control limits, even though damage may not be present at those other locations. The typical unidirectional shift in R-sum values was not observed for sensor D-SG-BF-H in Figure 4.6f. This figure shows multiple R-sum values outside both the upper and lower control limits. Even though a distinct shift in the R-sum values is not present, the cause of the R-sum values outside of the control limits may still be the inclusion of the larger-than-average Specimen 2 sensor residuals in the column- and row-sum calculations.



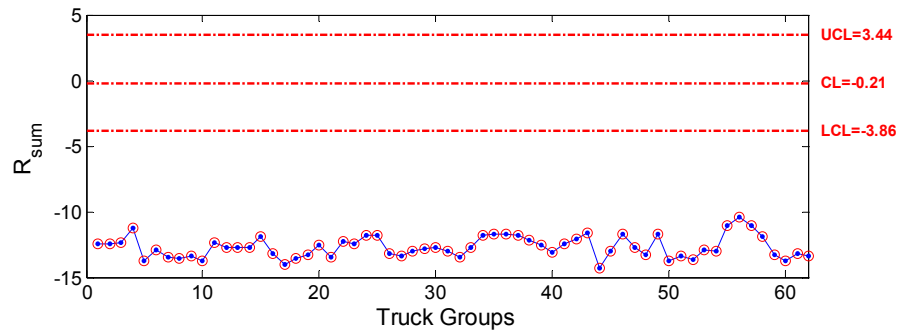
a. Sensor 1



b. Sensor 2

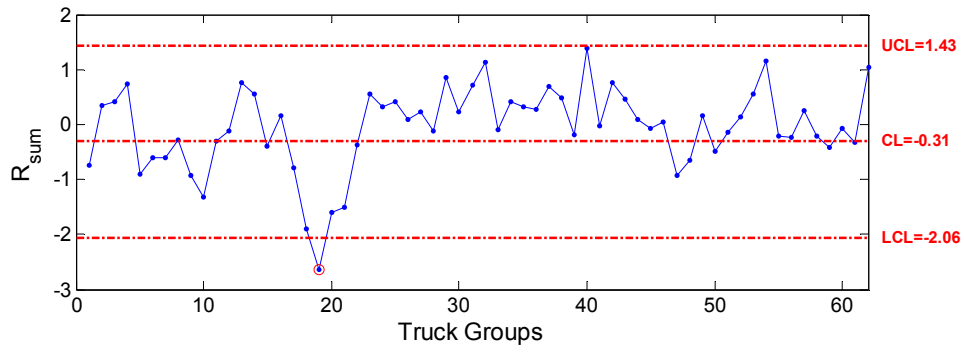


c. Sensor 3

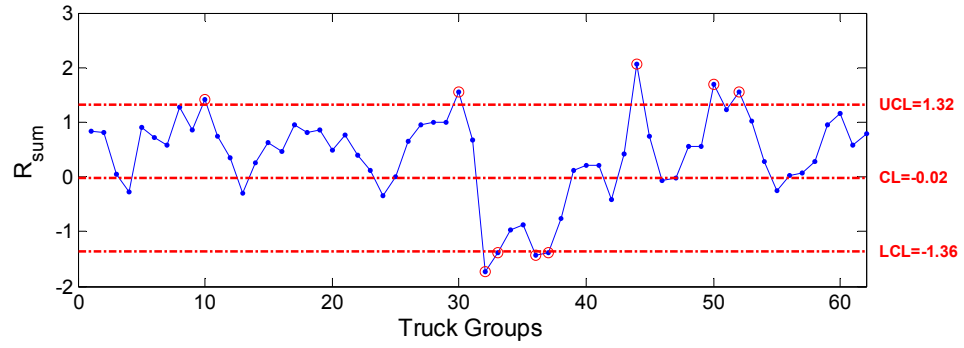


d. Sensor 4

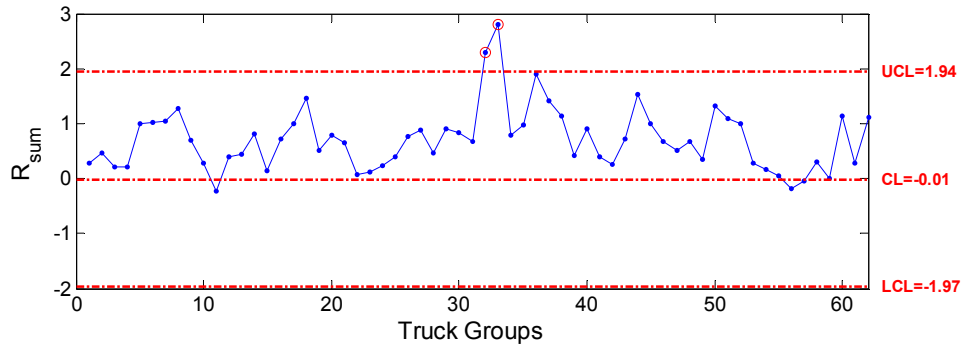
Figure 4.6 Post-Damage Sacrificial Specimen 2 Control Charts (1.25 in. crack)



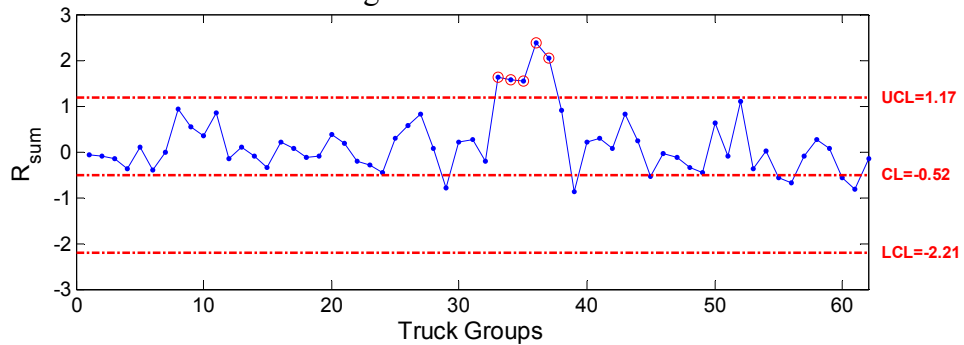
e. B-NG-BF-H



f. D-SG-BF-H

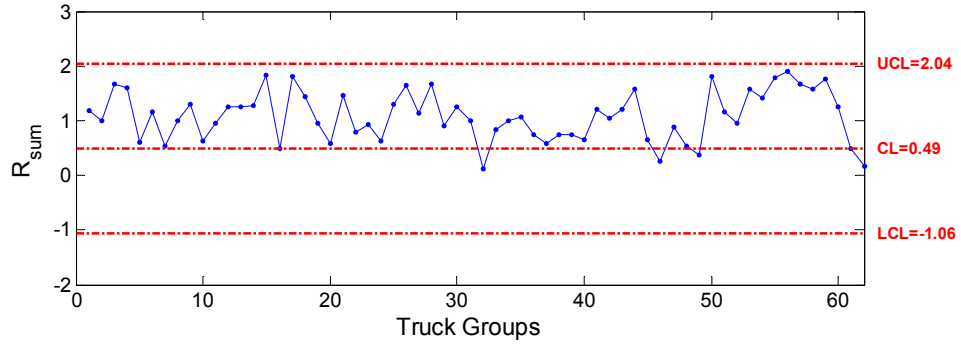


g. B-SS-BF-H

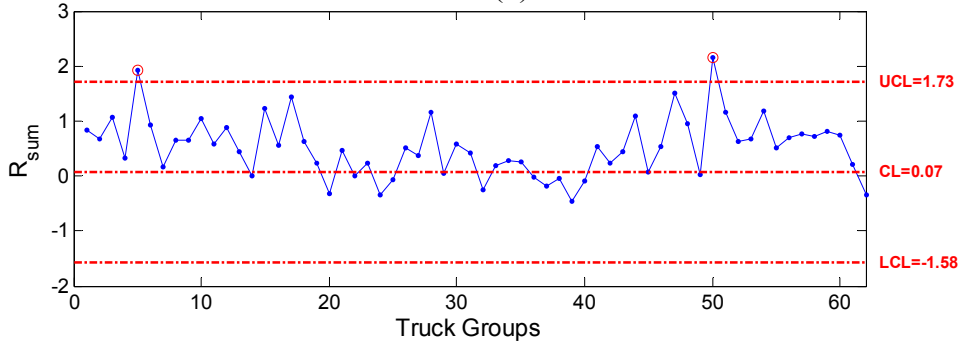


h. D-NS-BF-H

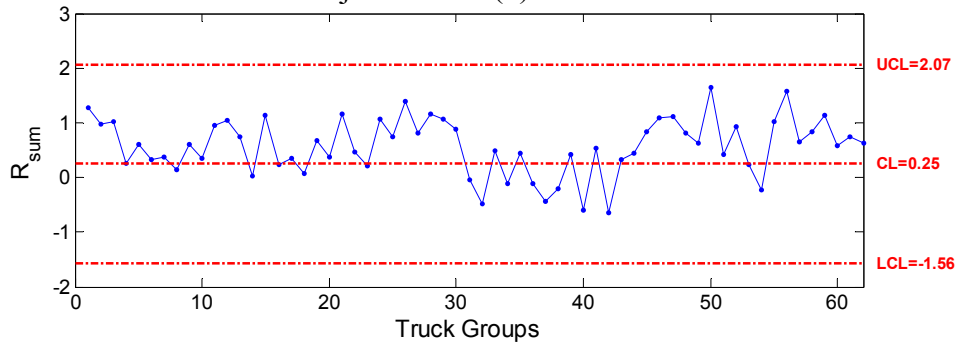
Figure 4.6 continued Post-Damage Sacrificial Specimen 2 Control Charts (1.25 in. crack)



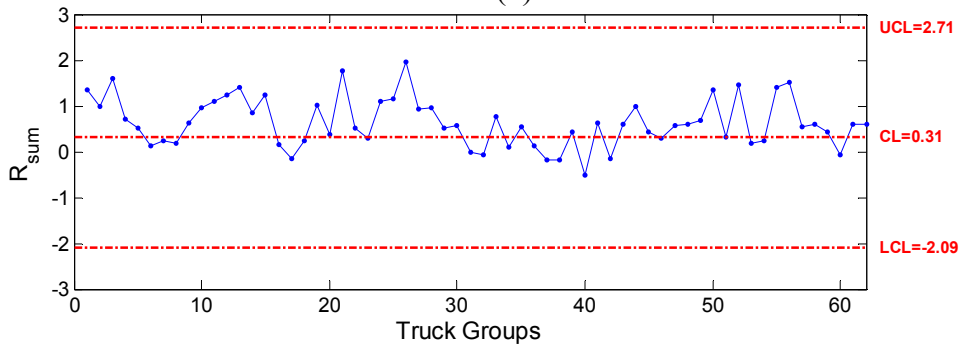
i. C-SG-CB(1)-V



j. C-SG-CB(5)-V



k. E-SG-CB(1)-V



l. E-SG-CB(5)-V

Figure 4.6 continued Post-Damage Sacrificial Specimen 2 Control Charts (1.25 in. crack)

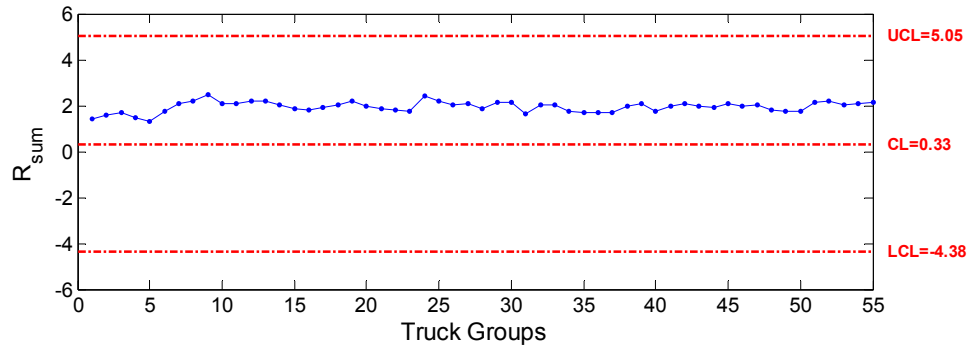
On March 5, 2010, sacrificial Specimen 2 was vibrated at an average resonant frequency of 63 Hz for about 2 minutes (6,600 cycles) to extend the crack from 1.25 in. to 1.50 in. long. Data were then collected from March 6, 2010 to March 12, 2010 and a 551 heavy, five-axle, right-lane trucks were detected.

For comparison to the undamaged state, the control limits in Figure 4.7 match the control limits in Figure 4.4. As with the 1.25 in. crack condition, the data points for Sensor 4 are again below the LCL, indicating damage. A few R-sum data from Sensors 2 and 3, as shown in Figure 4.7b and Figure 4.7c, are above the UCL. This suggests that with increasing damage severity, the damage can be detected with sensors located farther away. It is not fully understood why in Figure 4.6 the trend for Sensors 2 and 3 was toward the LCL and in Figure 4.7 the trend is toward the UCL. It is speculated that experimental procedures may be the source. The control charts for the additional sensors in Figure 4.7e through Figure 4.7l show very few R-sum values outside the control limits indicating that no damage has occurred near these sensor locations. The control chart for sensor B-NG-BF-H (Figure 4.7e) shows five R-sum values above the control limits (9.1%). This may again be due to the skewed values of the column- and row-sum calculations discussed previously.

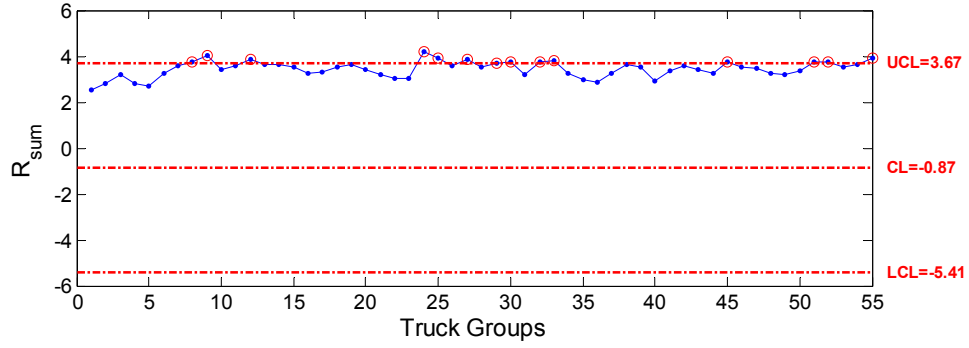
On April 1, 2010, sacrificial Specimen 2 was vibrated at an average resonant frequency of 73 Hz for about 3.25 minutes (14,400 cycles) to extend the crack from 1.50 in. to 1.75 in. long. Data were collected from April 2, 2010 to April 16, 2010 and 952 five-axle, heavy, right-lane trucks were detected.

The control charts corresponding to the 1.75 in. crack are shown in Figure 4.8. All of the data points for Sensors 3 and 4 are below their respective LCLs, again indicating damage detection. The data point trends for Sensors 1 and 2 (Figure 4.8a and Figure 4.8b) both shifted down opposite of the results from the 1.50 in. crack, but similar to those for the 1.25 in. crack. This shift could be due to slightly differing loading conditions, from placing the load transferring vertical strut in a different location than it was previously, but it doesn't have any adverse effects on the damage-identifying capabilities of the control charts.

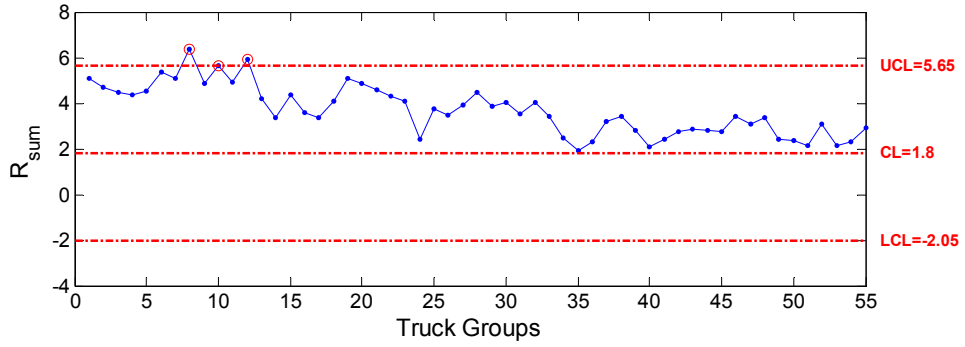
The control charts for the sensors not on Specimen 2 are shown in Figure 4.8e through Figure 4.8l. All of these control charts show an acceptable number of R-sum values outside the control limits except for sensors B-NG-BF-H and C-SG-CB(5)-V in Figure 4.8e and Figure 4.8i, respectively. Figure 4.8e shows a high percentage (33.7%) of R-sum values above the UCL and also shows an upward shift of the entire set of R-sum values. Figure 4.8i also shows a large percentage (60%) of R-sum values below the LCL, as well as a downward moving shift of the R-sum values. Again, the data in both of these cases were influenced by the residual values from the sensors on Specimen 2 in the column- and row-sum calculations. Further modifications to the damage-detection algorithm are needed to address the high false-positive rate.



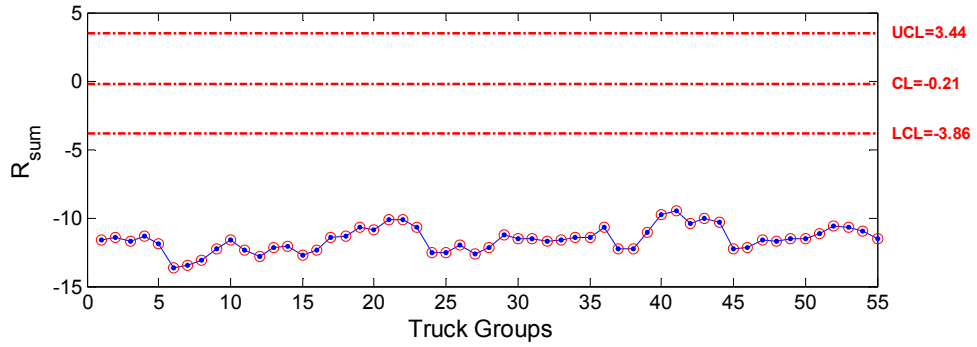
a. Sensor 1



b. Sensor 2

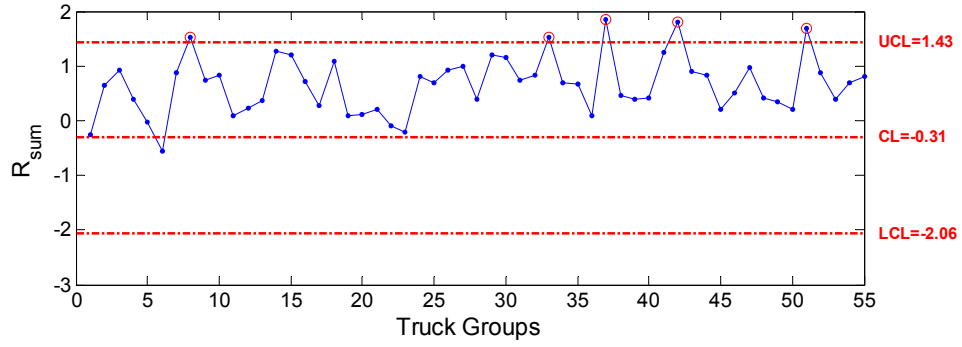


c. Sensor 3

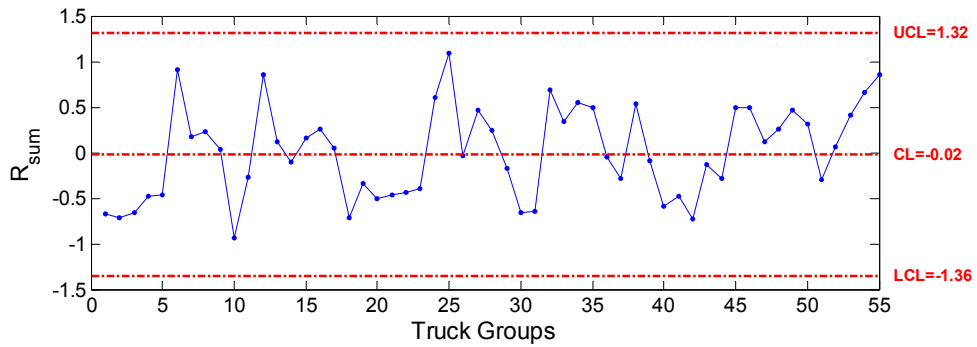


d. Sensor 4

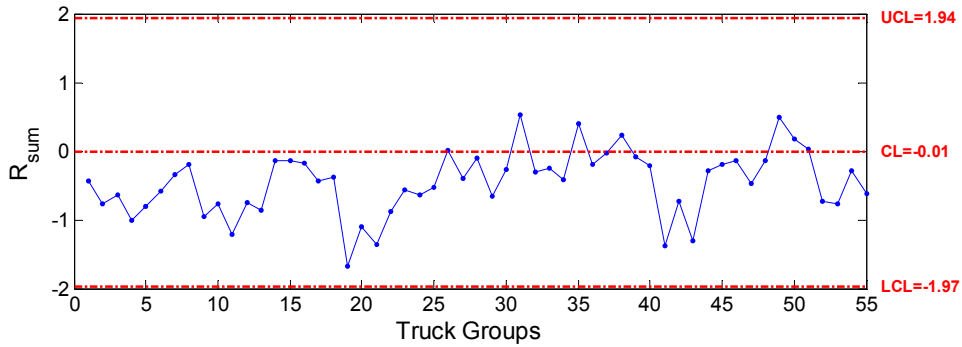
Figure 4.7 Post-Damage Sacrificial Specimen 2 Control Charts (1.50 in. crack)



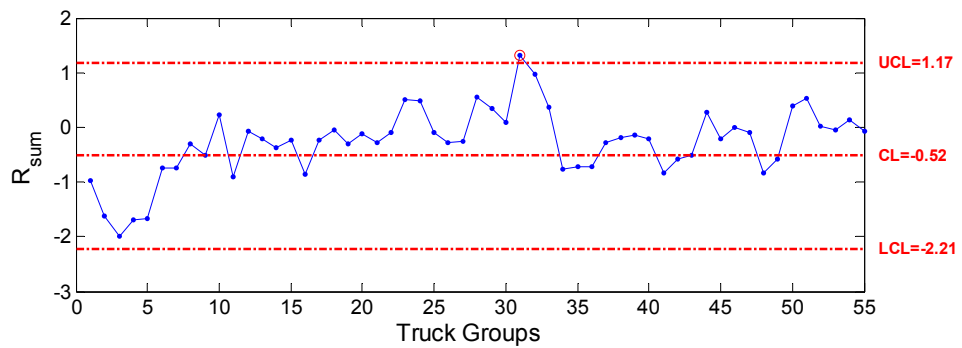
e. B-NG-BF-H



f. D-SG-BF-H

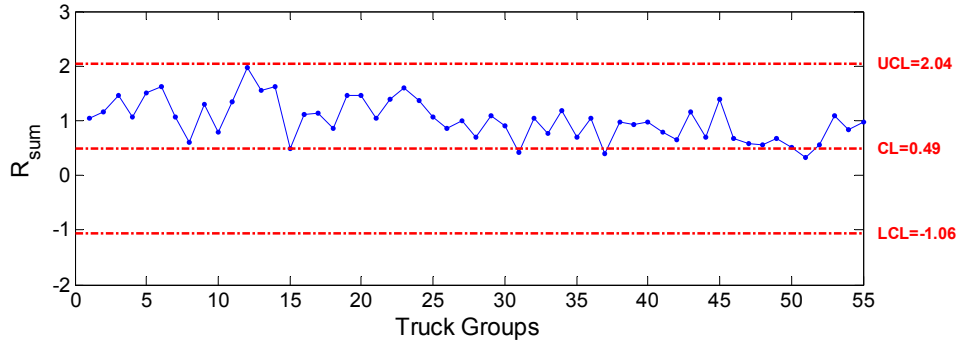


g. B-SS-BF-H

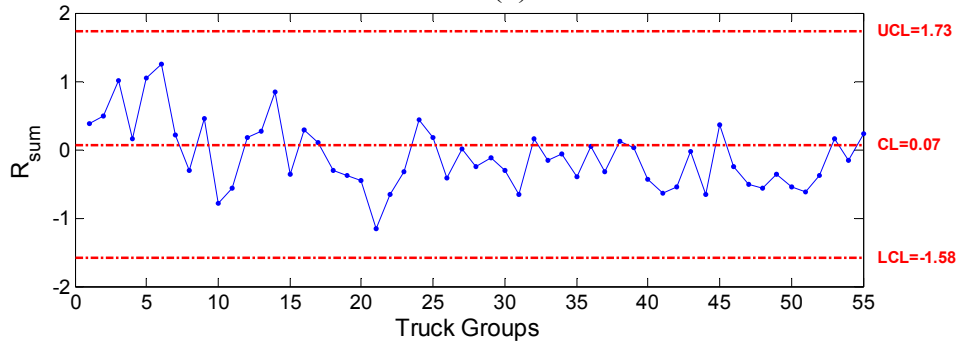


h. D-NS-BF-H

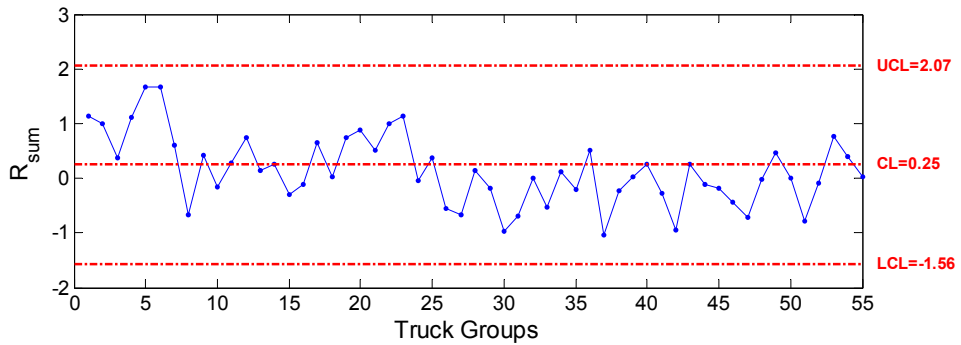
Figure 4.7 continued Post-Damage Sacrificial Specimen 2 Control Charts (1.50 in. crack)



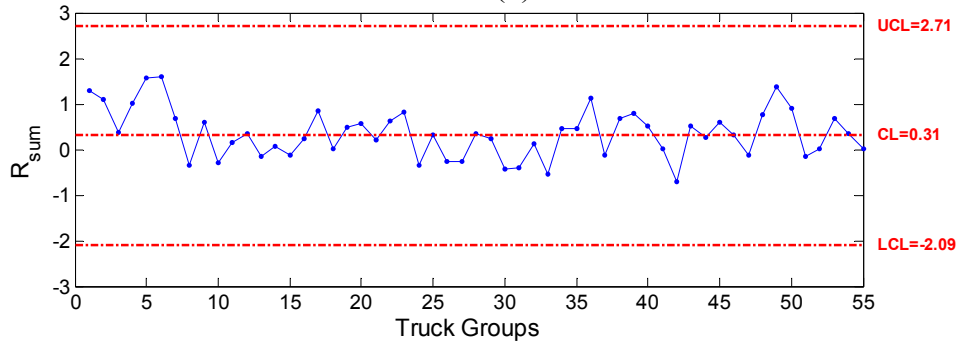
i. C-SG-CB(1)-V



j. C-SG-CB(5)-V



k. E-SG-CB(1)-V



l. E-SG-CB(5)-V

Figure 4.7 continued Post-Damage Sacrificial Specimen 2 Control Charts (1.50 in. crack)

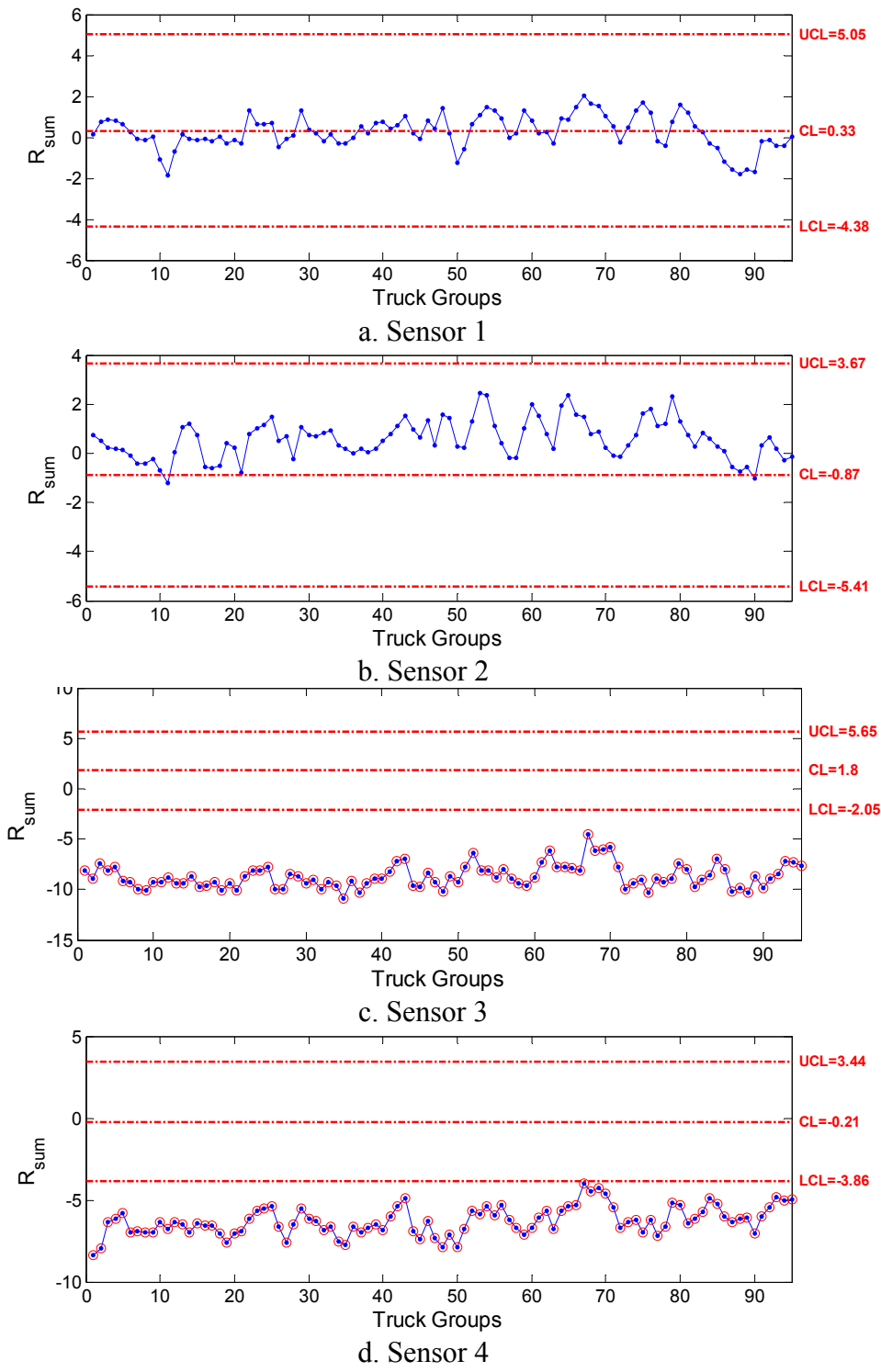
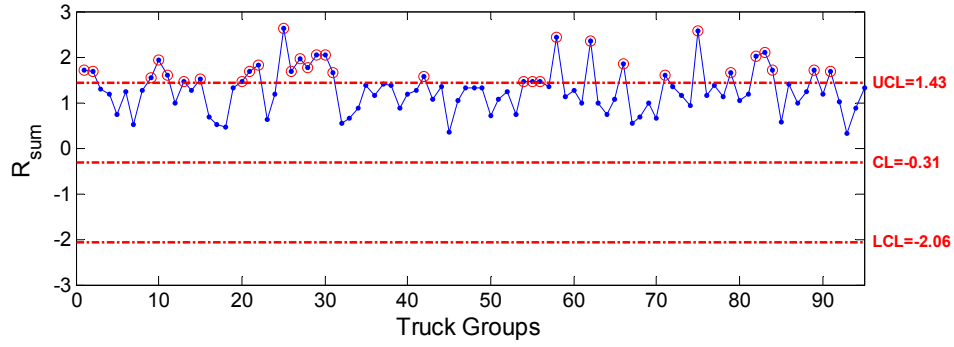
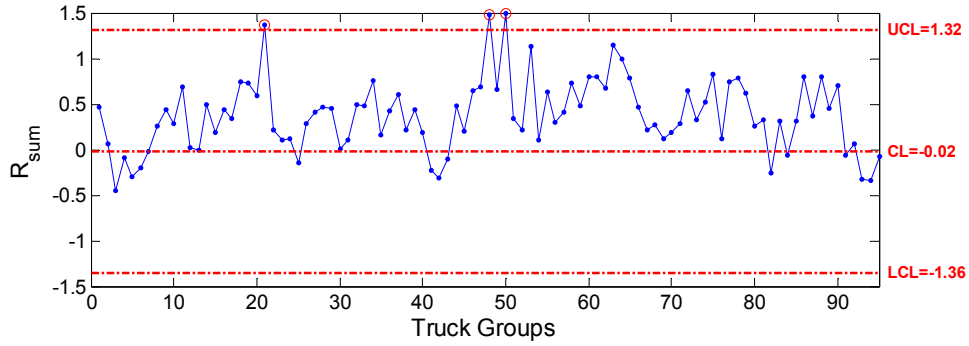


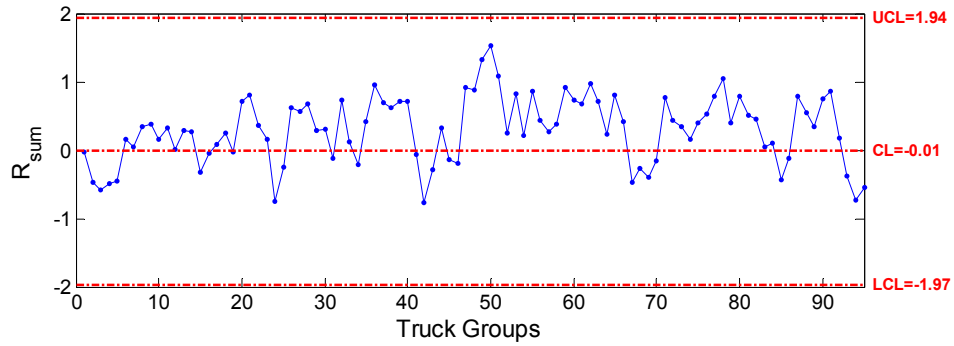
Figure 4.8 Post-Damage Sacrificial Specimen 2 Control Charts (1.75 in. crack)



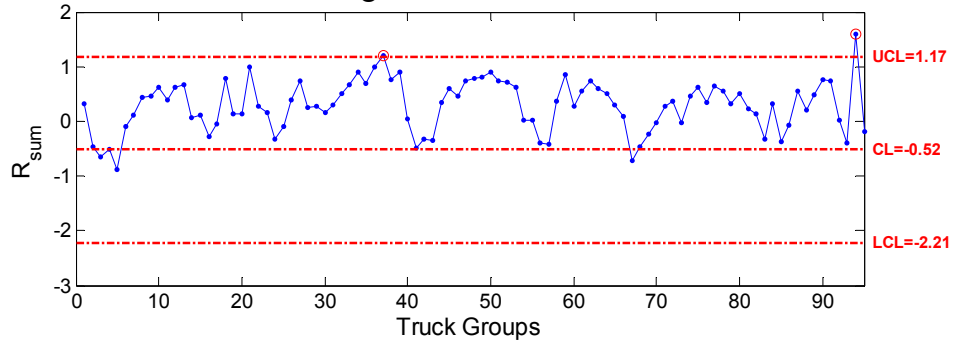
e. B-NG-BF-H



f. D-SG-BF-H

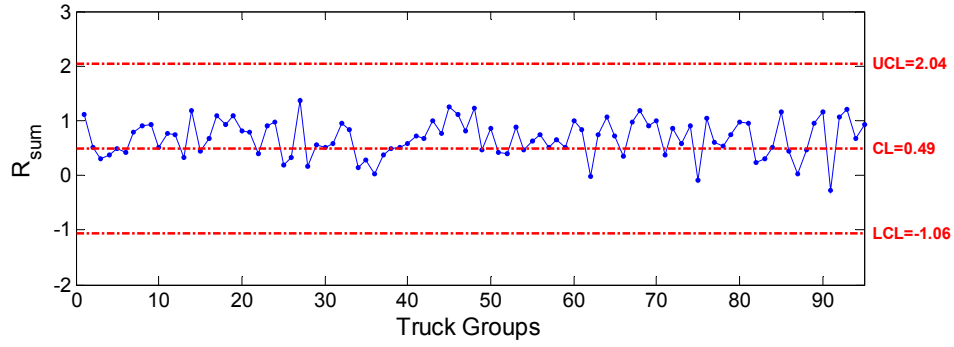


g. B-SS-BF-H

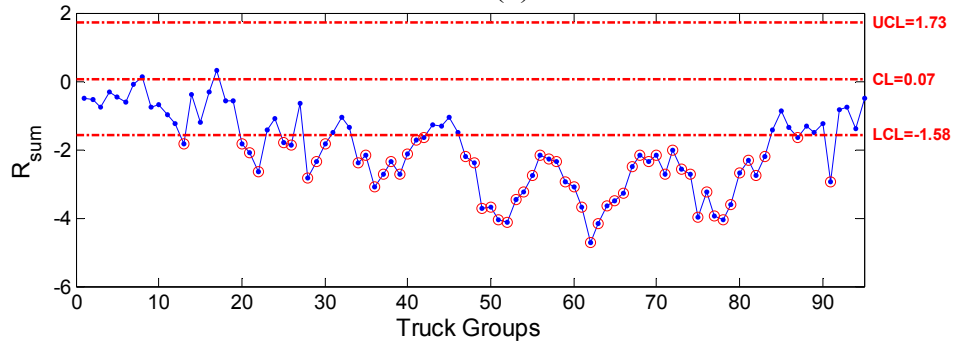


h. D-NS-BF-H

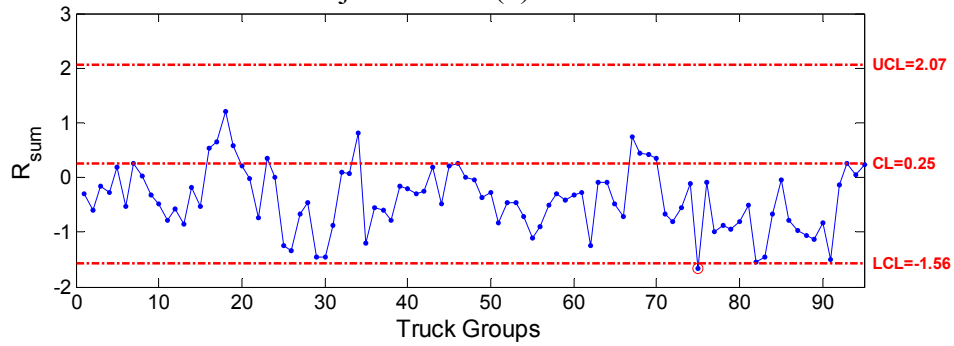
Figure 4.8 continued Post-Damage Sacrificial Specimen 2 Control Charts (1.75 in. crack)



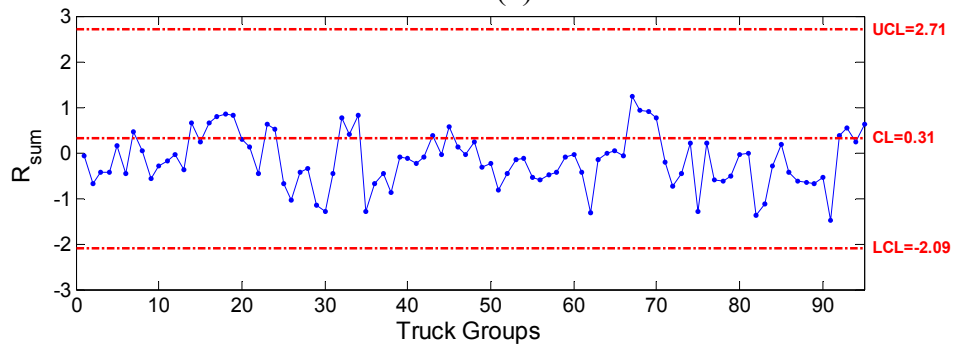
i. C-SG-CG(1)-V



j. C-SG-CG(5)-V



k. E-SG-CB(1)-V



l. E-SG-CB(5)-V

Figure 4.8 continued Post-Damage Sacrificial Specimen 2 Control Charts (1.75 in. crack)

4.2.3 Percentage of Points outside the Control Limits

To aid in studying the relationship between data, the control limits, and the severity of the damage that occurred, a bar chart was constructed that displays the percentage of points outside the control limits for the sensors on Specimen 2 (Figure 4.9). This chart presents a summary of the 12 control charts for each of the three previous figures (Figure 4.6, Figure 4.7, and Figure 4.8).

The chart indicates the location of the damage with the tallest bars being closest to the damage. For example, by investigating the 1.25 in. crack condition, the sensor with the largest percentage of points outside the control limits is Sensor 4, suggesting that the damage occurs near Sensor 4. The 1.25 in. crack occurred near Sensor 4, so the conclusion is correct. The suggested crack location may also be found for Sensors 2, 3, and 4 following a similar procedure.

The cracking in sacrificial Specimen 2 occurred nearest to Sensor 4 and is displayed in Figure 4.9 as the bars nearing 100% of the points outside the control limits. As the size of the crack increases to 1.75 in., the percentage of points outside the control limits of Sensor 3 also starts to increase, as was expected. This increase in points outside of the control limits of Sensor 3 for the 1.75 in. crack again confirms that more severe damage can be detected by sensors farther away from the damage. The location of the damage, though, may be more difficult to detect as it becomes more severe.

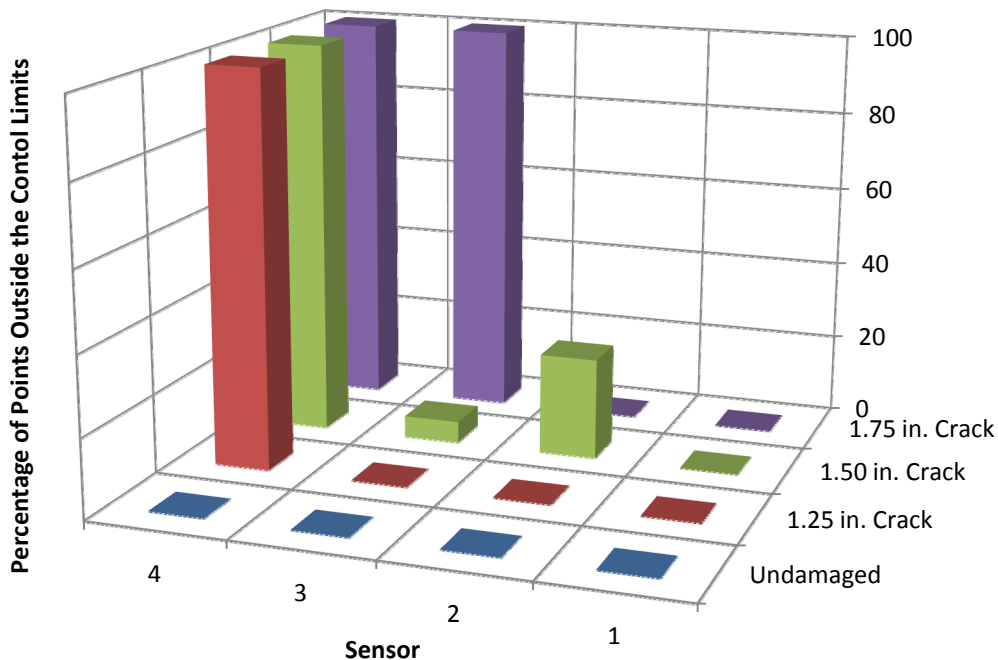


Figure 4.9 Percentage of Points Outside the Control Limits: Sacrificial Specimen 2 Cracking

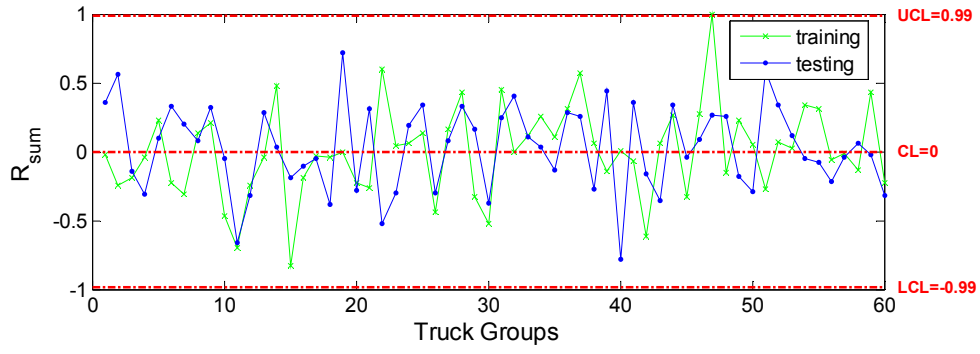
For example, in the case of the 1.50 in. crack, one can determine that that damage occurs near Sensor 4, because the bar is the tallest for that sensor (i.e., 100% of points fall outside the control limits). But, in examining the 1.75 in. crack case, the damage may be located near either Sensor 3 or Sensor 4.

4.2.4 Corrosion Testing Results

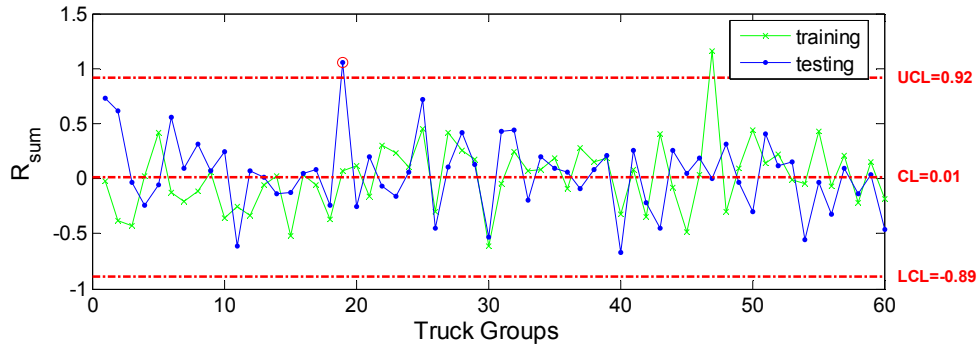
After fatigue cracking sacrificial Specimen 2 to a crack size of 1.75 in., new training data for the corrosion damage testing were collected from April 15, 2010 to April 29, 2010. A total of 2,544 heavy, right-lane, five-axle trucks were detected and used for control chart construction and false-alarm testing. The resulting control charts are shown in Figure 4.10.

Only one of the points (1.67%) for either the training or testing data fell outside the control limits (Figure 4.10b, k and l). Unlike previous undamaged control chart construction, there appears to be a large amount of variation of the residuals. Although the reasons for this could be quite varied, the likely explanations include influence from previous fatigue crack damage, unusual variability in truck traffic configuration, or environmental influences.

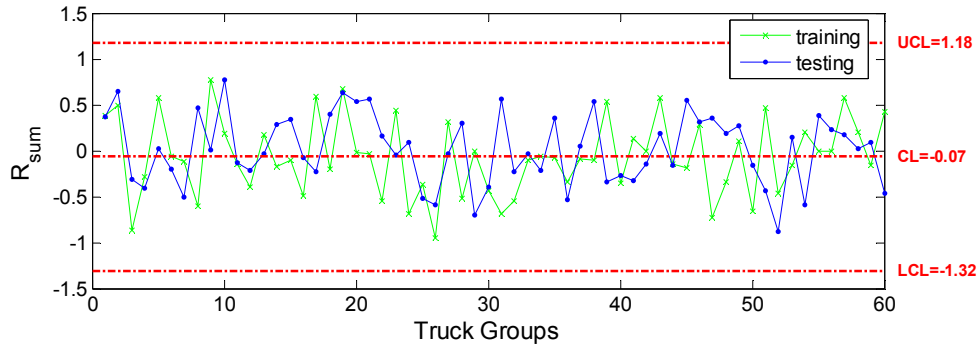
Following the collection of the training data, roughly 5% of the total plate thickness in a 1 in. by 3 in. section centered over Sensor 1 was removed. The location was centered over Sensor 1 to determine the effects of the corrosion when directly over a sensor and when in close proximity to other sensors. The locations of the simulated corrosion area and measurement points are shown in Figure 4.11. To measure the decrease in plate thickness, an additional steel plate was placed over each point and the distance from the top to the top plate was recorded. After grinding, this process was repeated and the percent decrease was calculated for each measurement point, as shown in Table 4.1



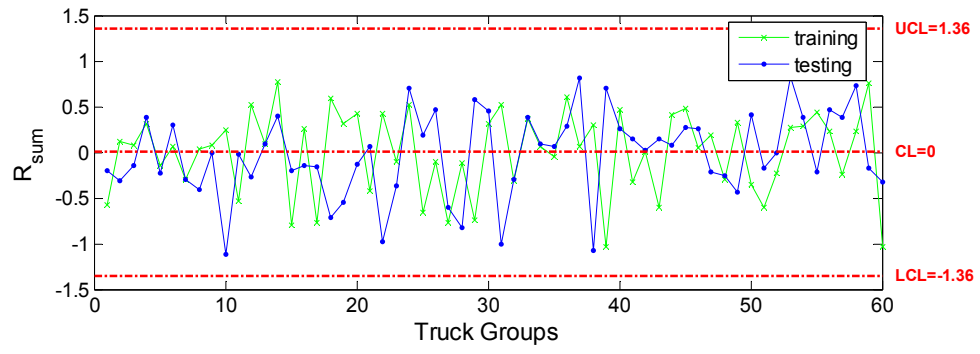
a. Sensor 1



b. Sensor 3

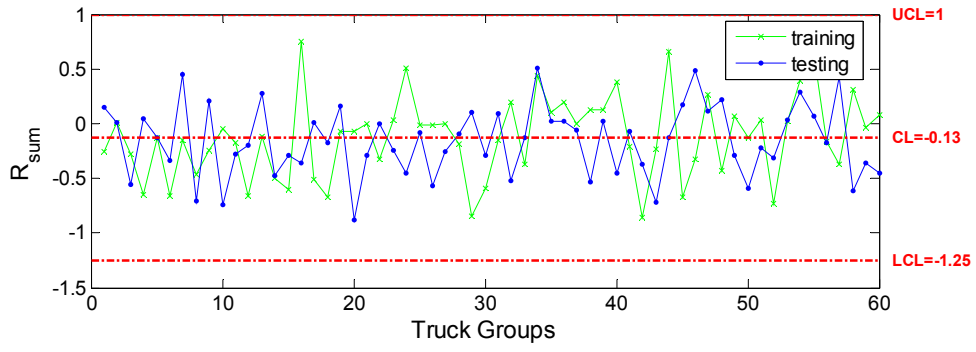


c. Sensor 3

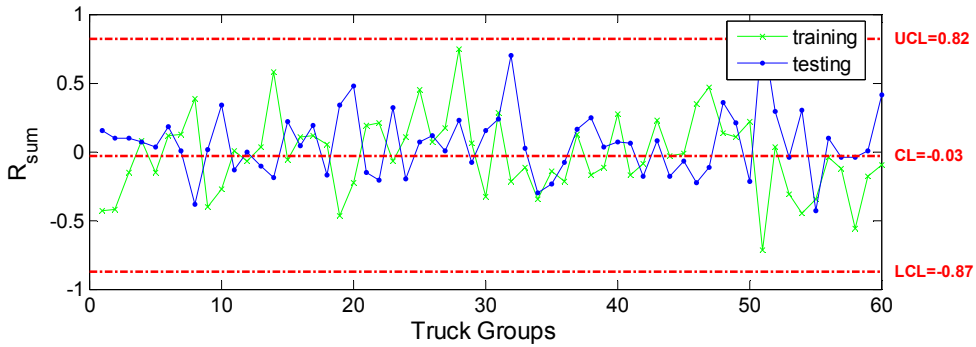


d. Sensor 4

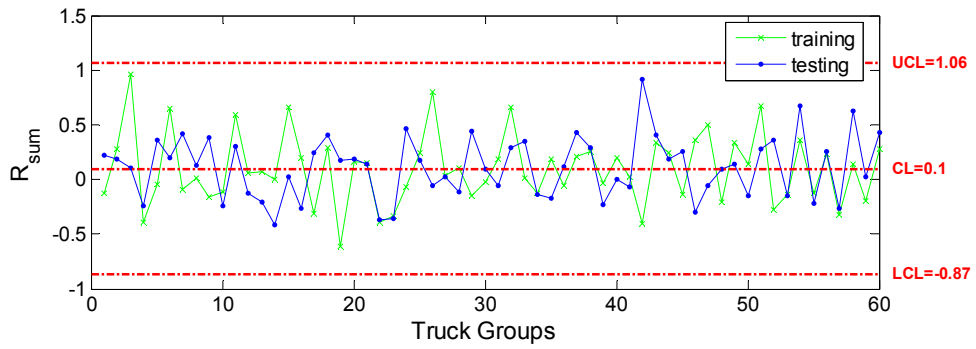
Figure 4.10 Sacrificial Specimen 2 Corrosion Control Charts



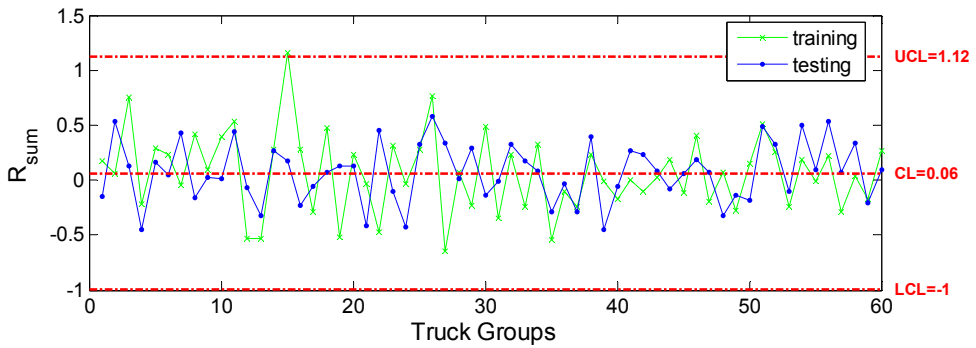
e. B-NG-BF-H



f. D-SG-BF-H

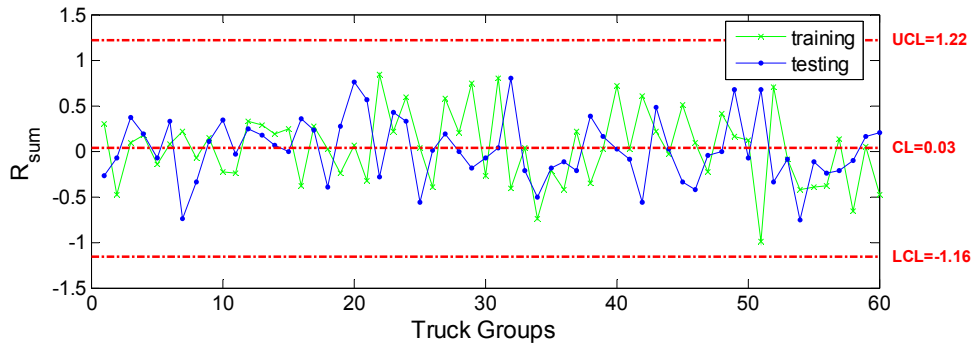


g. B-SS-BF-H

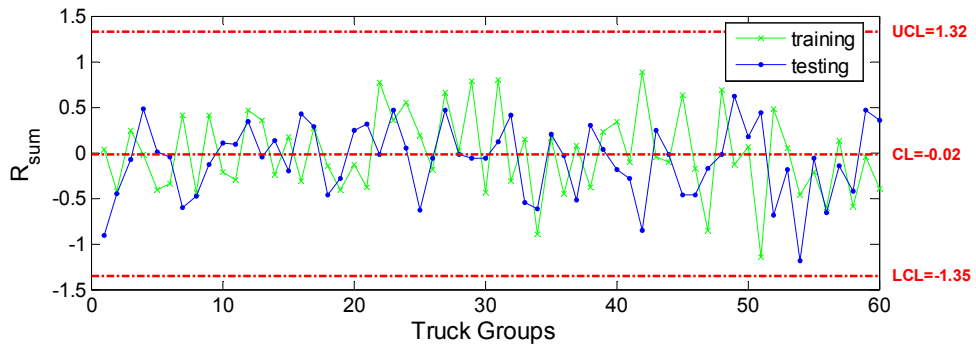


h. D-NS-BF-H

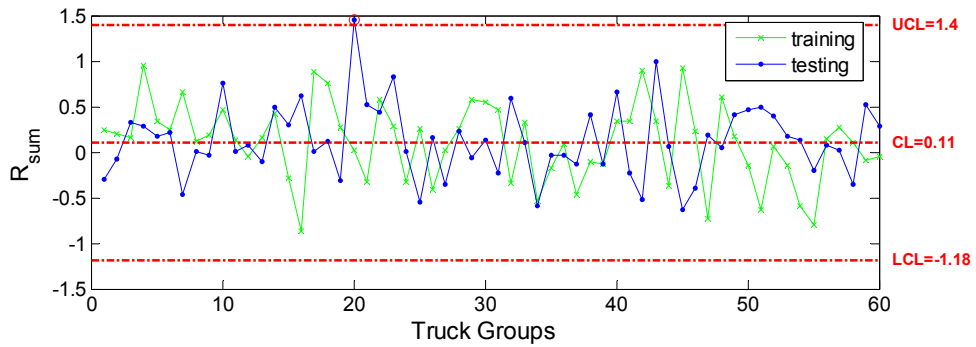
Figure 4.10 continued Sacrificial Specimen 2 Corrosion Control Charts



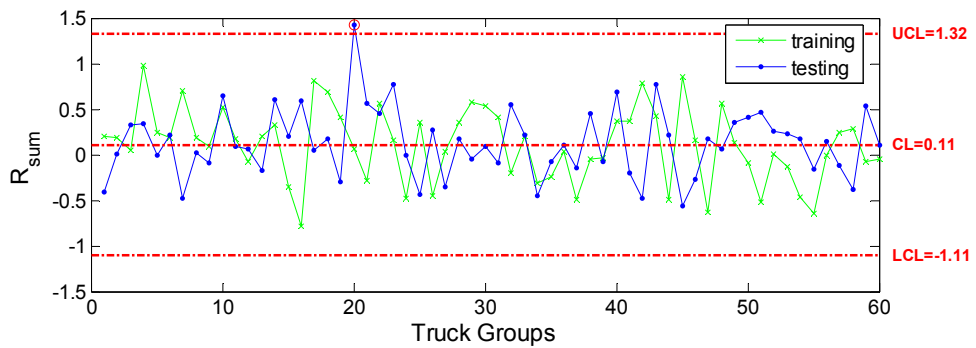
i. C-SG-CB(1)-V



j. C-SG-CB(5)-V



k. E-SG-CB(1)-V



l. E-SG-CB(5)-V

Figure 4.10 continued Sacrificial Specimen 2 Corrosion Control Charts

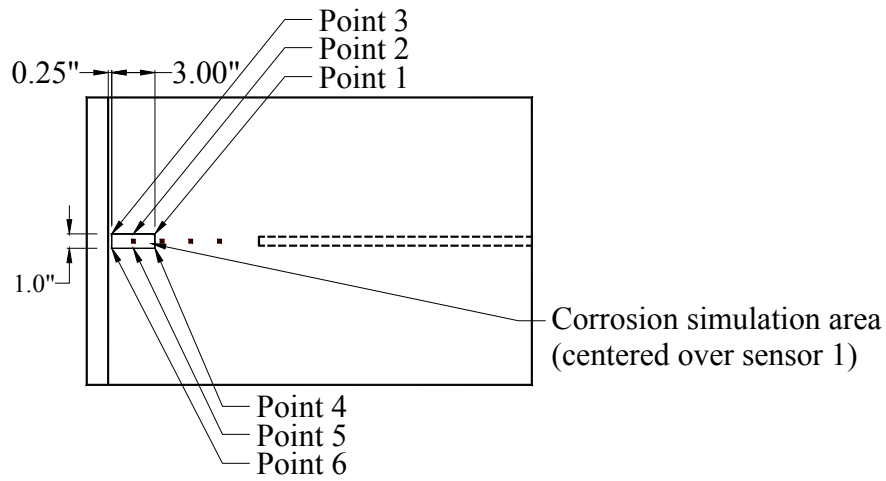


Figure 4.11 Corrosion Simulation Area Details

Table 4.1 Simulated Corrosion Measurement Details

Measurement Point	Start (in.)	Finish (in.)	Difference (in.)	% Difference of Plate Thickness
1	0.396	0.438	0.042	9.6
2	0.396	0.412	0.016	3.7
3	0.395	0.418	0.023	5.3
4	0.393	0.429	0.036	8.2
5	0.390	0.412	0.022	5.0
6	0.396	0.420	0.024	5.5

Damage data were then collected from the corrosion simulated sacrificial Specimen 2 from May 1, 2010 to May 8, 2010. From the collected data, 497 heavy, five-axle, right-lane trucks were detected with the resulting control charts shown in Figure 4.12.

Multiple points (42.9%) are below the LCL for Sensor 2, indicating damage detection near Sensor 2. Recall that the damage simulation area was centered over Sensor 1. However, Sensor 2 seemed to be more sensitive to the damage due to the higher percentage of material removed as shown in Table 4.1.

The damaged control charts from Sensors 1 and 3 remained similar relative to the undamaged control charts; there is a large amount of variation of the residuals within the control limits, but very few points are outside of the control limits. The damaged control chart for Sensor 4 differs from its undamaged control chart. Specifically, the mean of the damaged data is shifted up and is close to the UCL. This shift could be caused by the effects of the double curvature on the damage near Sensor 2. Further damage may place more data points for Sensor 4 outside the UCL, giving a false reading on where the damage occurred.

The control charts for sensors not on Specimen 2 are shown in Figure 4.12e through Figure 4.12i and show very few R-sum values outside of the control limits. Because the damage to Specimen 2 was small in this case, there are no large adverse effects to the R-sum values in the control charts for the sensors not on Specimen 2, as previously discussed.

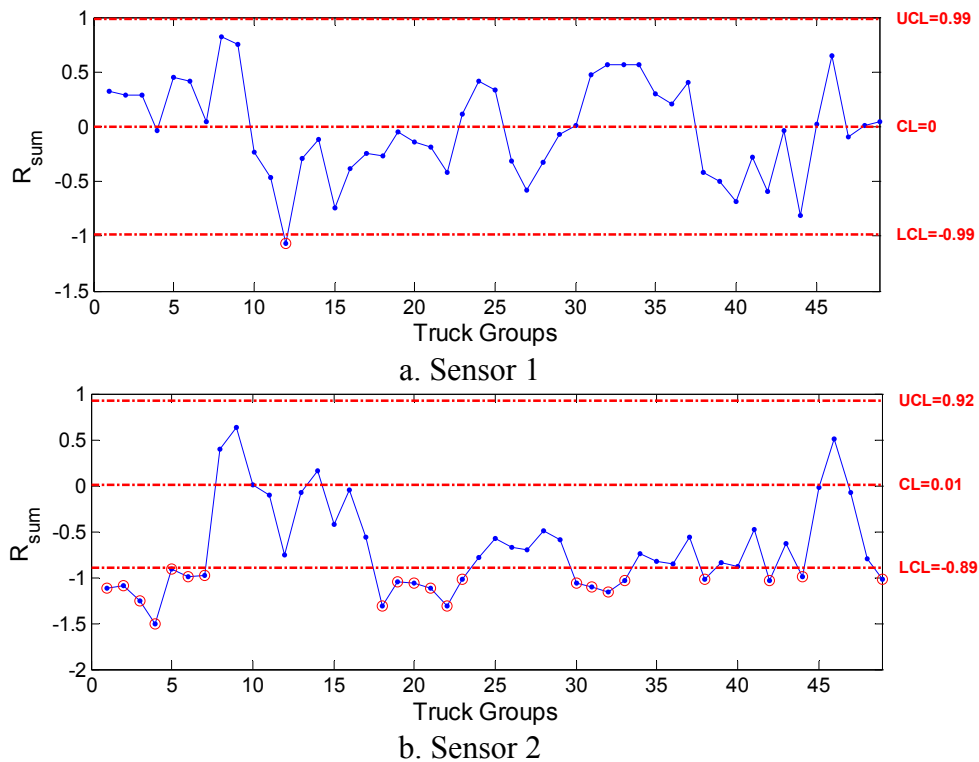
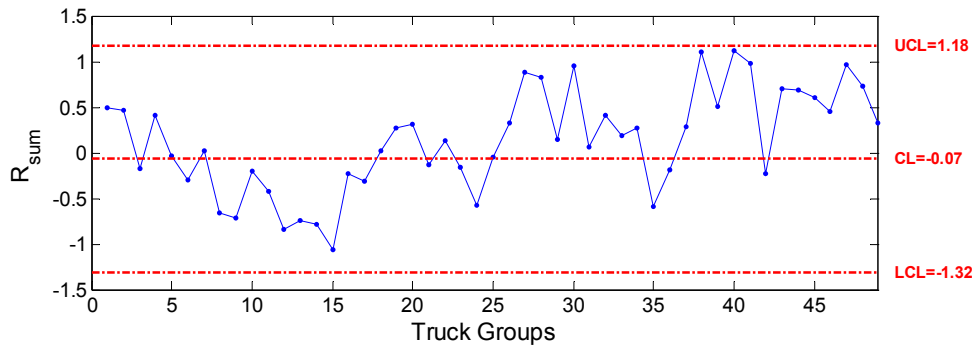
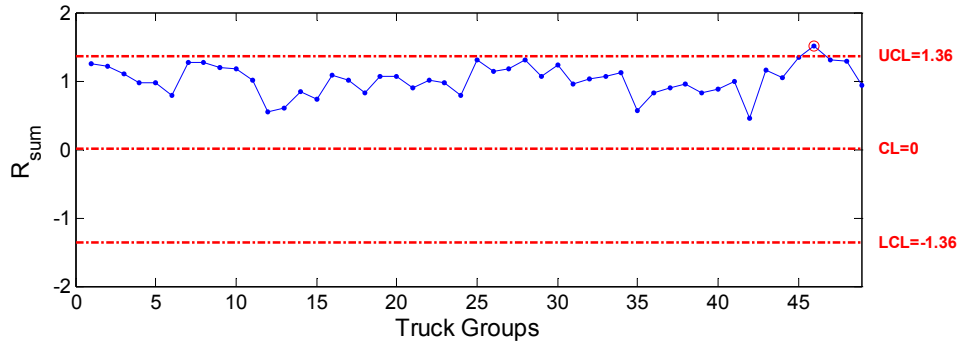


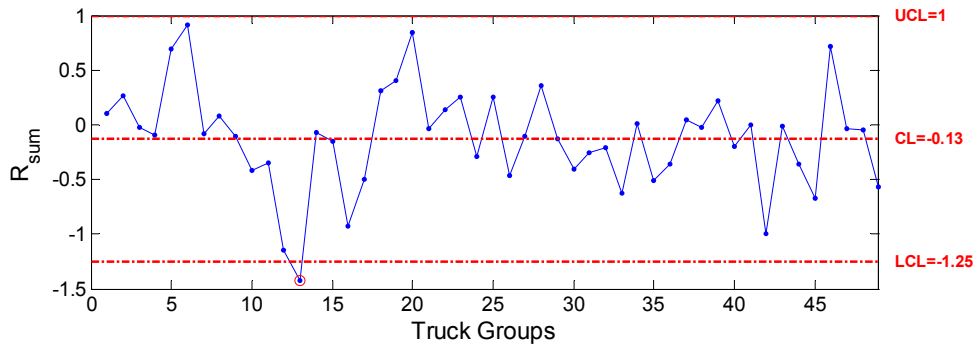
Figure 4.12 Post-Corrosion Sacrificial Specimen 2 Control Charts



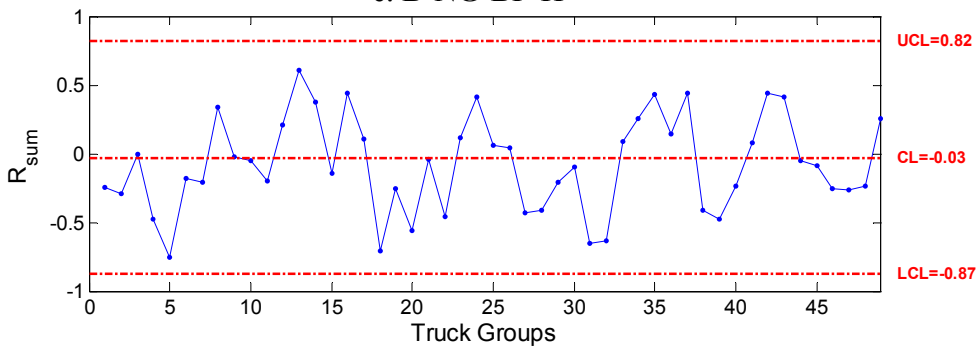
c. Sensor 3



d. Sensor 4



e. B-NG-BF-H



f. D-SG-BF-H

Figure 4.12 continued Post-Corrosion Sacrificial Specimen 2 Control Charts

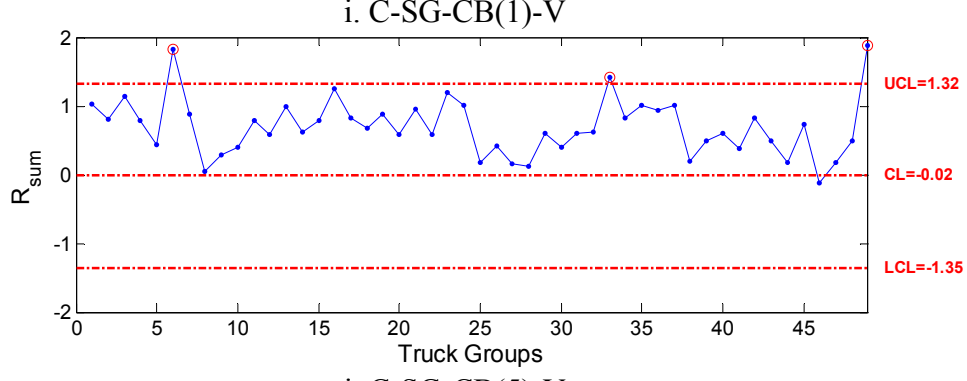
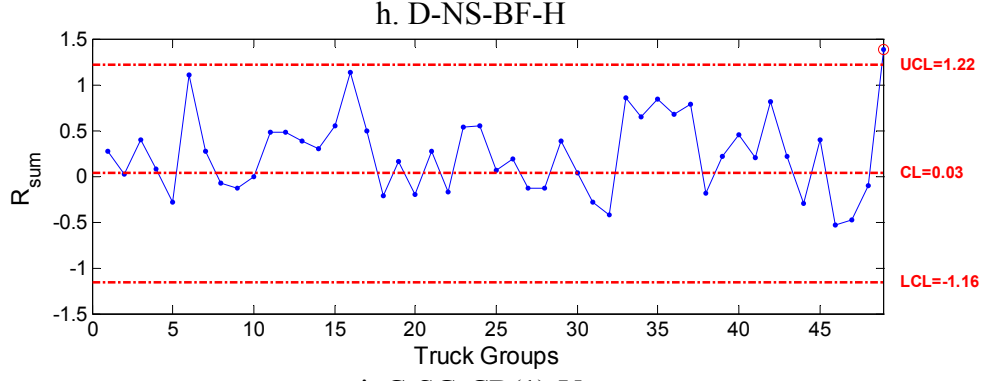
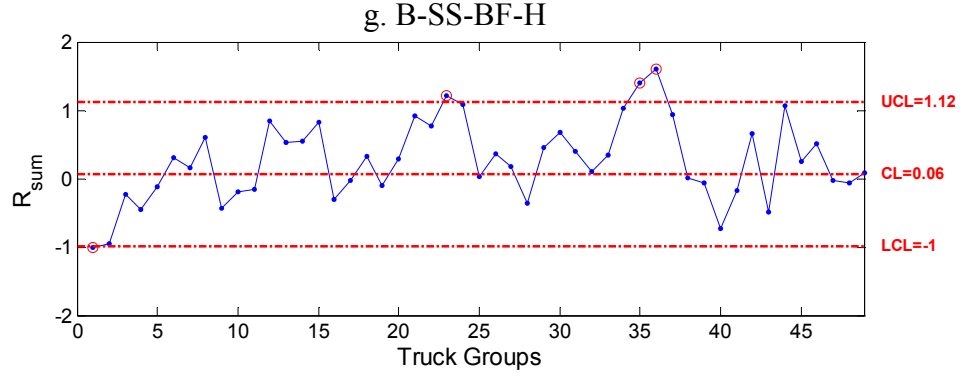
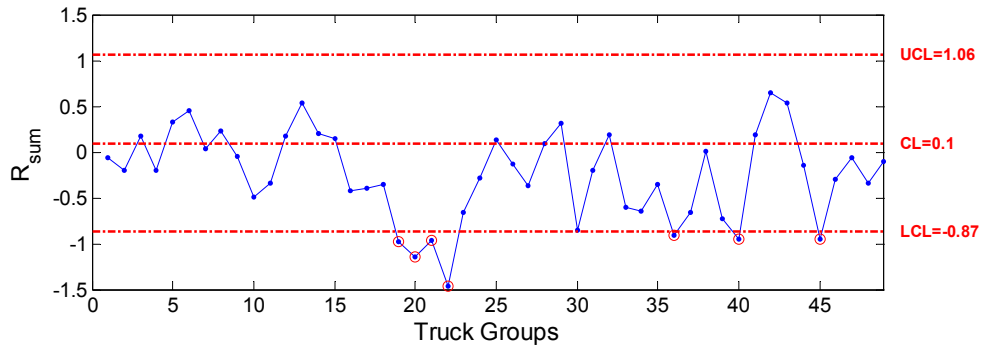


Figure 4.12 continued Post-Corrosion Sacrificial Specimen 2 Control Charts

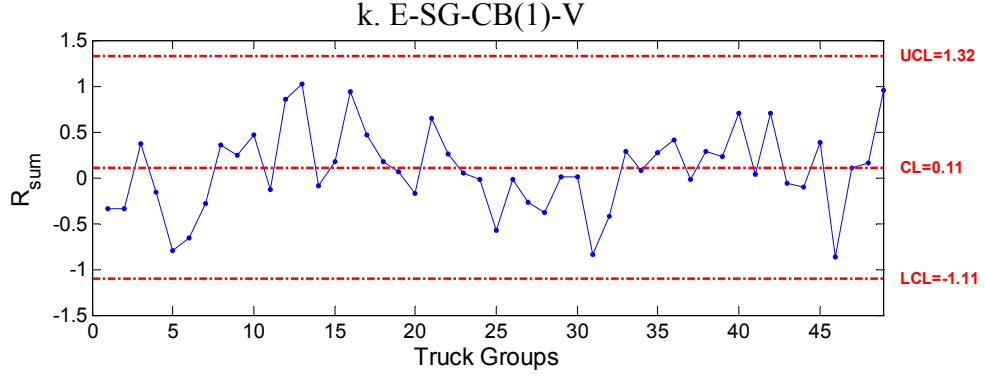
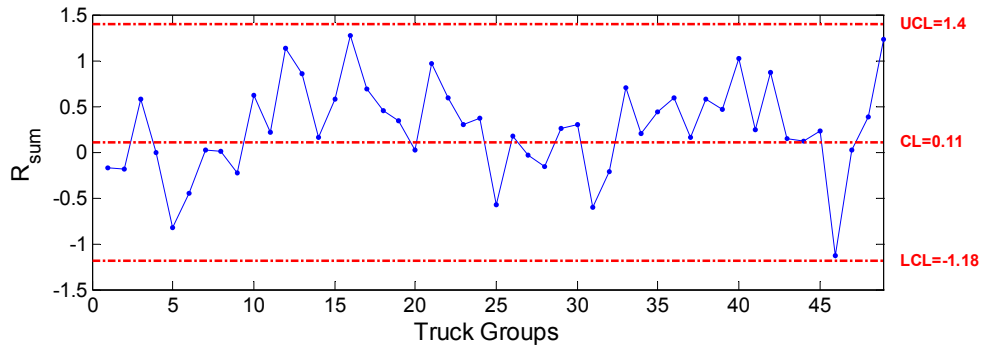


Figure 4.12 continued Post-Corrosion Sacrificial Specimen 2 Control Charts

5 ALGORITHM EVALUATION AND RECOMMENDED IMPROVEMENTS

Due to the relatively high false-positive rate observed in this work, an evaluation of the components of the current methodology and methods for improving the approach were investigated. In this chapter an evaluation of the current methodology, including the evaluation of the linear regression and of the statistical parameters, is described and recommended methodology modifications are presented.

5.1 Evaluation of Current Methodology

In this section, an evaluation of the current method is completed through the assessment of the underlying sub-algorithms. This assessment involves an investigation into the appropriateness of assumptions made, coupled with a discussion on issues resulting from the use of linear prediction models and the applied matrix simplification method.

5.1.1 Linear Prediction Model

In the current methodology, a traditional linear regression model is used to establish the relationship between sensor pairs. A traditional linear regression model minimizes the square of the vertical distance between the best-fit line and the data points, as shown in Figure 5.1 by the *vertical* lines, which are referred to as a residual herein.

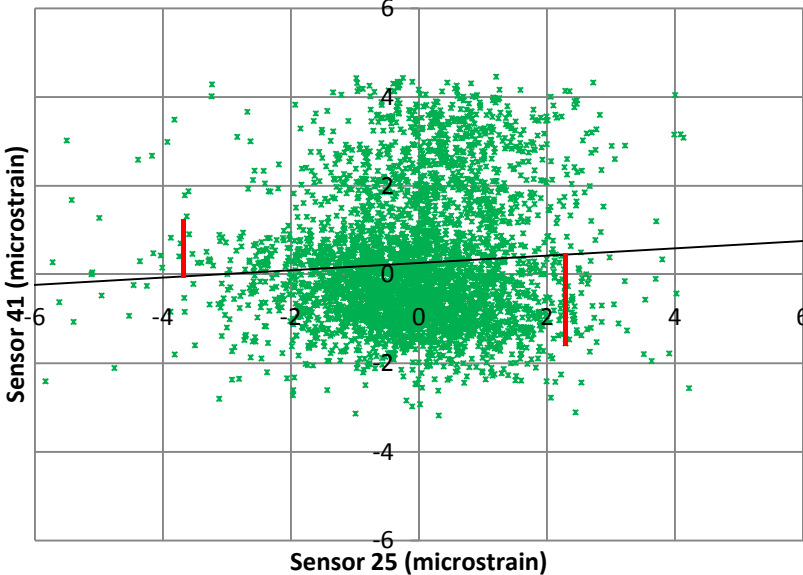


Figure 5.1 Sample Linear Regression

The linear regression, also called the least square regression, specifically minimizes the value, which is called the sum of the squares:

$$\sum (y_i - \hat{y}_i)^2 \quad (5.1)$$

where \hat{y}_i is the predicted value of the response obtained from the linear prediction equation (Dallal 2000). In this work, the linear prediction models are then used to calculate residuals for damage detection as previously discussed. The required assumption in the use of this type of linear regression is that one “input” needs to be known to predict the “output.” With the type of data input into the overall damage-detection algorithm, there are no predictors and response variables. Rather, each variable is independent. Therefore, it appears that such a linear regression may not be appropriate.

5.1.2 Normalcy of Residual and R-Sum Data

In the current damage-detection approach, the strain residuals and the R-sum values are assumed to be taken from a normal distribution, an example of which is shown in Figure 5.2. A normal distribution is defined by the function:

$$f(x) = \frac{1}{\sqrt{2\pi}\sigma} e^{-\frac{(x-\mu)^2}{2\sigma^2}} \quad (5.2)$$

where x and μ are the mean and standard deviation of the sample, respectively. The assumption of normally-distributed data is critical to how the control charts are constructed. Specifically, the control limits were set to achieve a specific false-positive rate, based on known characteristics of normal distributions related to the mean and multiples of the standard deviations.

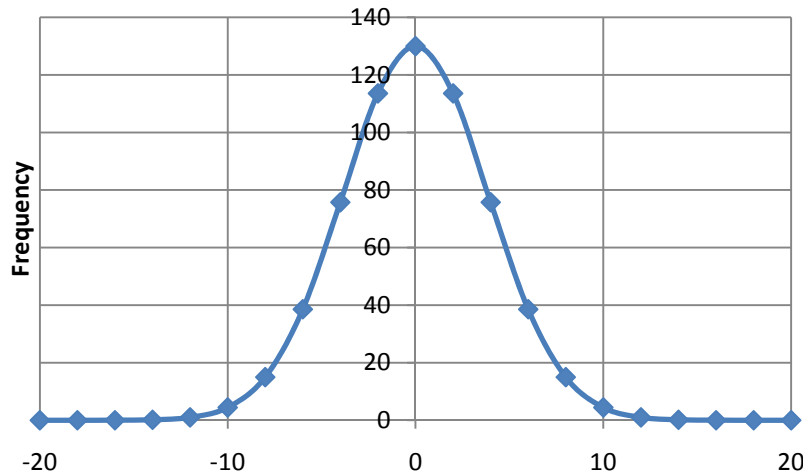


Figure 5.2 Sample Normal Distribution

To determine if a sample (e.g., strain residuals, R-sum values, etc.) is taken from a population that is considered normally distributed, the chi-squared test for goodness of fit may be used. This test helps to determine at what significance level, α , the data constitute a sample from a population with a distribution $f(x)$ for a sample that falls into r categories (Crow, Davis and Maxfield 1960). The comparison of observed frequencies, n_i , in each category can be compared to the expected frequencies, e_i , through:

$$\chi^2 = \sum_{i=1}^r \frac{(n_i - e_i)^2}{e_i} \quad (5.3)$$

A significance level for χ^2 is then calculated as:

$$P(\chi^2) = \int_{\chi^2}^{\infty} \frac{1}{\left(\frac{f-2}{2}\right)! 2^{f/2}} (\chi^2)^{(f-2)/2} e^{-\chi^2/2} d(\chi^2) \quad (5.4)$$

where $f = r - 1 - g$ degrees of freedom and g is the number of quantities necessary to complete the specification (Crow, Davis and Maxfield 1960). If the calculated significance level is below the user-set target significance value, the null hypothesis that the sample is from a population with a distribution of $f(x)$ should be rejected. In the case of the damage-detection algorithm, $f(x)$ is set to be a normal distribution.

In Figure 5.3 an actual distribution is graphically compared to a theoretical normal distribution. Through the χ^2 Test, the calculated significance level is 0.98, which for this project supports the null hypothesis that the actual data are obtained from a population that is normally distributed. It can be seen that even though the actual distribution does not exactly match the theoretical distribution, the actual data supports the null hypothesis.

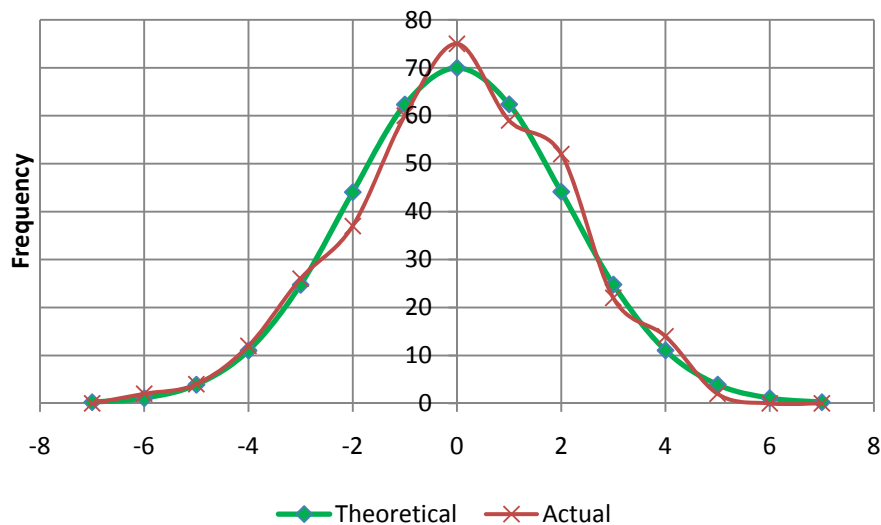


Figure 5.3 Sample Distribution Comparison with 0.98 Significance Level

In Figure 5.4, another actual distribution is compared to a theoretical normal distribution, but with a significance level of 0.0.

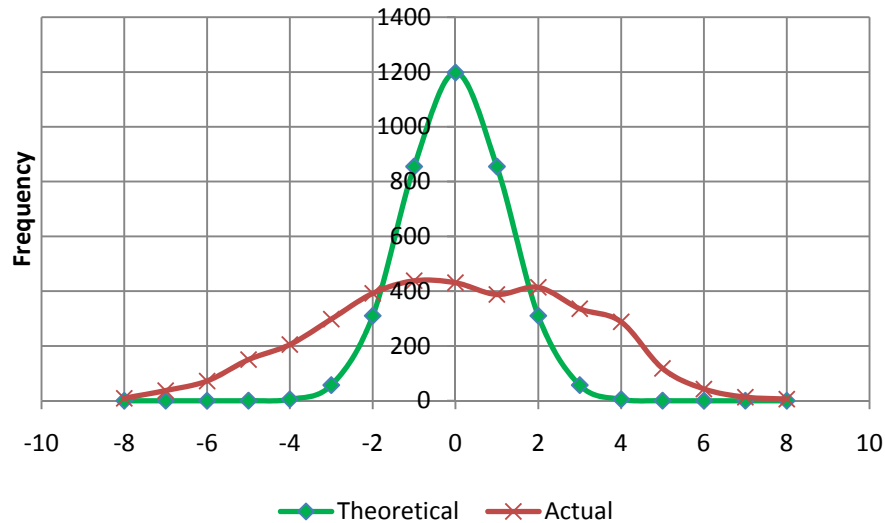


Figure 5.4 Sample Distribution Comparison with 0.0 Significance Level

5.1.2.1 Normalcy of Residual Data

In the damage-detection approach evaluated herein, residual data are assumed to be normally distributed in order to calculate the control limits based on a set false-positive rate. In this work, residual values calculated from training and the first damage level obtained from all the sensors on the US 30 Bridge were evaluated for normal distribution using the χ^2 Test as previously described.

Through analysis, it was determined that a large percentage of the residual data were above the 0.85 significance level and for this work were considered to be a sample from a normally-distributed population. Because of the large percentage of calculated significance levels above 0.85, all of the residual data sets were taken to be a sample of a population with a normal distribution, confirming the initial assumption.

5.1.2.2 Normalcy of R-Sum data

The residual data after the column- and row-summation procedure were also tested to determine whether or not these data sets were taken from a population that is normally distributed. Through analysis, it was determined that a large percentage of this data were well below the 0.85 significance level and the original null hypothesis was rejected. The construction of the control charts was based on the assumption that all data used came from a population with a normal distribution; this represents a potential problem in the approach.

5.1.3 Quantification of Results

The current developed damage detection did not include an automated approach for quantification of damage-detection results. As such, numerous techniques were evaluated, including further use of the χ^2 Test and the Student's T-test, for their abilities to quantify the damage-detection results.

First, the damaged data distribution was compared to the training data distribution for each sensor using a procedure similar to the one outlined previously. It was postulated, if the null hypothesis (the damaged data were a sample of the population of training data) was rejected, damage would be detected. This method proved inaccurate and the Student's T-test was then investigated.

The Student's T-test is used to compare the means of two different data sets. A null hypothesis is set and, based on the calculated significance level, can either be accepted or rejected (Crow, Davis and Maxfield 1960). After further investigation of the T-test and applying the test to numerous sensor pairs, it was concluded that the T-test was too sensitive (to slight changes in the data sets from training data to damaged data). Therefore, no recommendations on incorporating a quantification process into the current procedure can be made.

5.2 Recommended Methodology Changes

Due to the relatively high false-positive rate and the apparent violation of several key assumptions, potential improvements to the current methodology were developed and evaluated. This section summarizes the recommended changes to the current methodology.

5.2.1 Orthogonal Regression and Orthogonal Residual

An alternative linear regression technique that doesn't require one variable to be a predictor and one to be a response is recommended. The recommended regression approach is called an orthogonal regression and an example is shown in Figure 5.5. The differences between the linear regression and the orthogonal regression shown in Figure 5.1 and Figure 5.5, respectively, can immediately be noticed in the slope of each of the lines.

An orthogonal regression is appropriate when there is no natural distinction between predictor and response variables (MathWorks 2010). As it turns out, by using orthogonal regression, the residual matrix becomes symmetric, because the two equations for one sensor pair are inversely related and therefore the same residuals are calculated. This, albeit unintended, attribute reduces the computation time associated with the damage-detection approach.

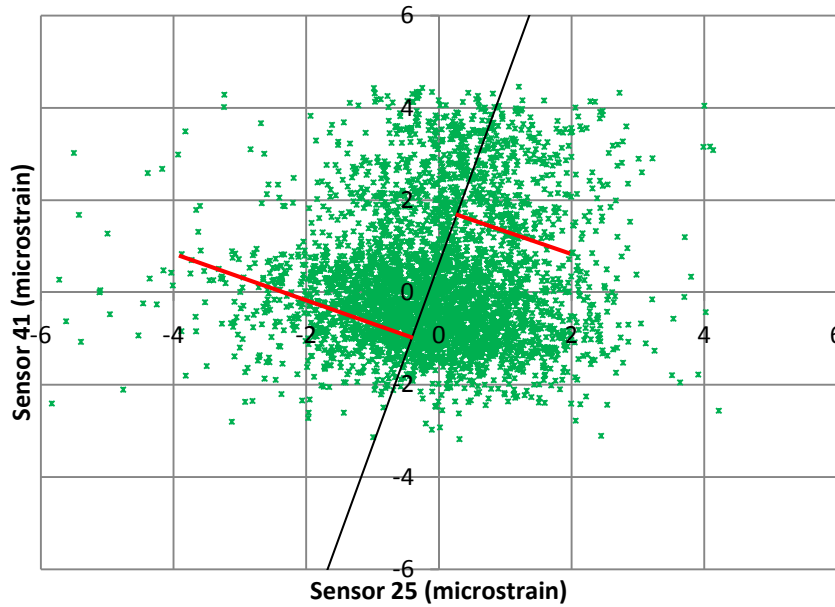


Figure 5.5 Sample Orthogonal Regression

Whereas traditional regression seeks to minimize the error in the response variable prediction, the orthogonal regression minimizes the perpendicular distance of each x, y pair from the line called the orthogonal residuals and shown in Figure 5.5. According to Carroll and Ruppert in “The Use and Misuse of Orthogonal Regression Estimation in Linear Errors-In-Variables Models,” the orthogonal regression is derived from a “pure” measurement perspective. As with any linear regression, y and x are linearly related through:

$$y = \beta_0 + \beta_1 X \quad (5.5)$$

Through Equation (5.5), it can be found that y and X are exactly linearly related. For an orthogonal regression, y and X are corrupted by measurement and it can be observed that:

$$Y = y + \varepsilon \quad (5.6)$$

$$W = X + U \quad (5.7)$$

where ε and U are independent mean zero random variables with variances σ_ε^2 and σ_u^2 , respectively (Carroll and Ruppert 1996). After combining Equation (5.5) and Equation (5.6), a new equation results:

$$Y = \beta_0 + \beta_1 X + \varepsilon \quad (5.8)$$

To obtain an orthogonal regression, the perpendicular distance from the data points to the regression must be minimized, that is by minimizing:

$$\sum_{i=1}^n \left\{ \frac{(Y_i - \beta_0 - \beta_1 x_i)^2}{\eta} + (W_i - x_i)^2 \right\} \quad (5.9)$$

Specifically, $\beta_0, \beta_1, x_1, \dots, x_n$ and where:

$$\eta = \frac{\text{Var}(Y|X)}{\text{Var}(W|X)}$$

For example, let s_x^2, s_y^2 , and s_{yx} be the sample variance of the Xs, the sample variance of the Ys, and the sample covariance between the two, respectively (Carroll and Ruppert 1996). Then, the estimation of the slope of the orthogonal regression is:

$$\hat{\beta}_1(OR) = \frac{s_x^2 - \eta s_y^2 + \left\{ (s_x^2 - \eta s_y^2)^2 + 4\eta s_{yx}^2 \right\}^{1/2}}{2s_{yx}} \quad (5.10)$$

For the work completed in this project, commercial software was used to determine the orthogonal regression equations. The accuracy of the program was confirmed by comparing two orthogonal regressions created using the same two sensor data sets. Because the orthogonal regression minimizes the perpendicular distance from the data points to the regression, the two orthogonal regressions should remain the same, just inversed, regardless of which data set was chosen to represent the x-axis in the scatter-plot.

5.2.2 Damage-Detection Approach

After evaluating several potential approaches for assessing the presence of damage, it is recommended that the F-test be used. The F-test determines if a data set can be properly modeled with a simple (also known as a reduced) model, or if a more complex (also known as a full) model is required. For application to damage detection, the null hypothesis is: if there is no damage, then the response during and after training can be modeled with a reduced model because the during and after training responses would be the same. Therefore, when the full model is required, it is postulated that damage has occurred and the behavior has changed. In short, if the error using the full and reduced models is statistically the same, no damage has occurred. The full model was developed to be:

$$Y = k_1(\alpha_1 + \alpha_3 x) + k_2(\alpha_2 + \alpha_4 x) \quad (5.11)$$

where:

$$k_1 = \begin{cases} 1 & \text{for training data} \\ 0 & \text{for post training data} \end{cases}$$

and:

$$k_2 = \begin{cases} 0 & \text{for training data} \\ 1 & \text{for post training data} \end{cases}$$

In essence, the full model uses training and damaged data separately to create two lines (orthogonal regression lines in each case) that pass through both the training and post training data separately; although there are two lines, they are considered one model as shown with the dashed lines in Figure 5.6 and Figure 5.7. The reduced model, which must be a sub-model of the full model, is given by:

$$Y = \gamma_1 + \gamma_3 x \tag{5.12}$$

The reduced model is shown as the dot-dot-dashed lines in Figure 5.6 and Figure 5.7. It can be observed in Figure 5.6 that the reduced model is similar to the full model, leading to the conclusion that no damage has occurred at those two sensor locations. On the contrary, Figure 5.7 shows that the reduced model is drastically different from the full model. This would indicate that damage has been detected.

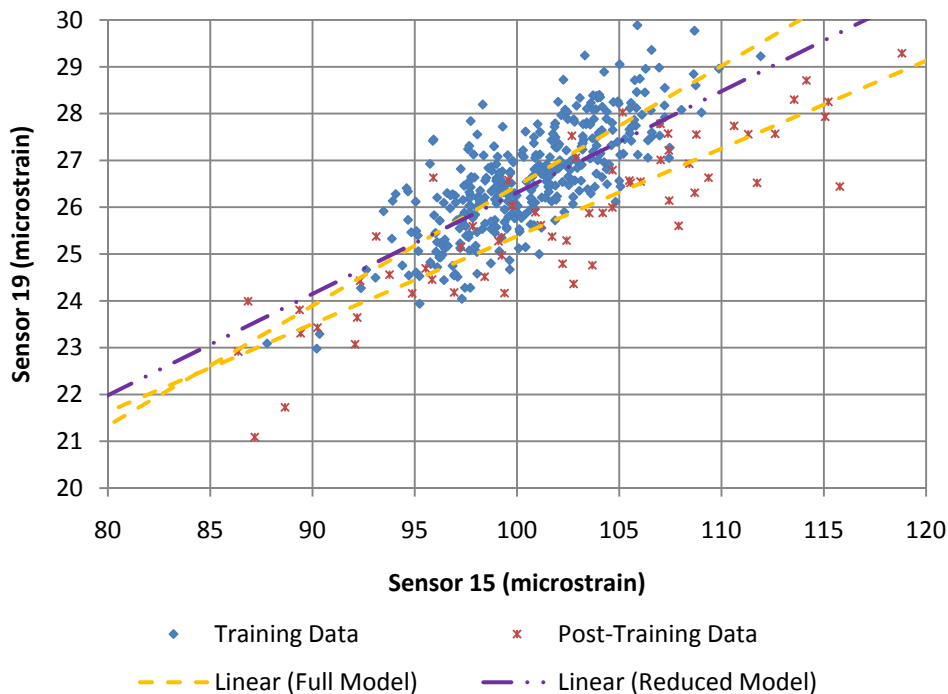


Figure 5.6 Sample Training Full and Reduced Model

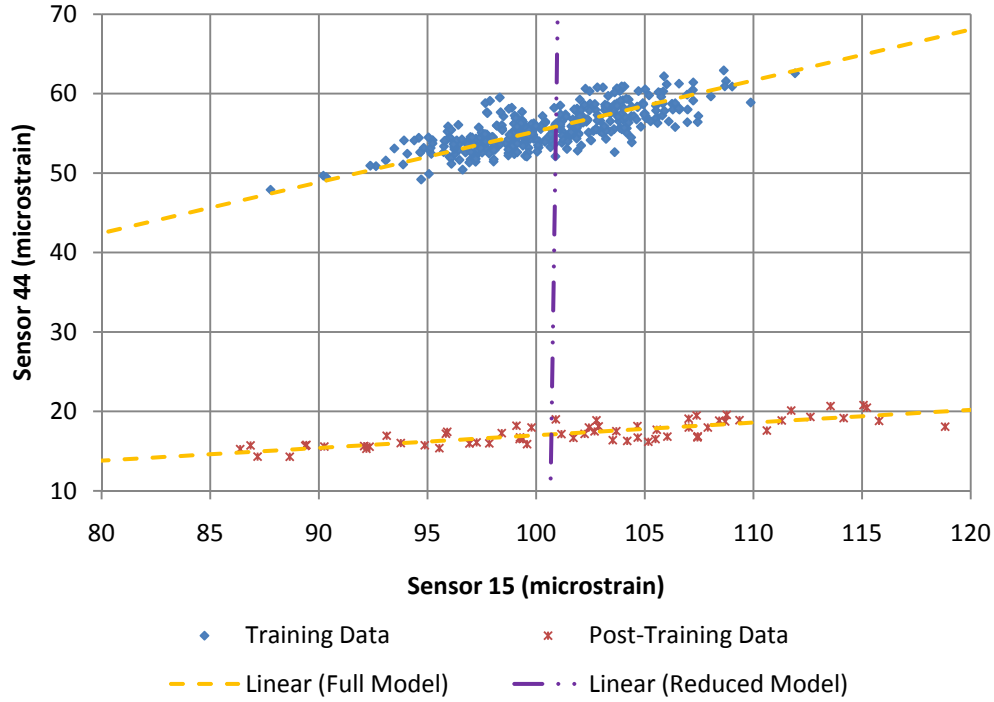


Figure 5.7 Sample Damaged Full and Reduced Model

To quantify these results, the F-test is completed with a null hypothesis that the reduced model is able to fit the data set as well as the full model. When the training and post training portions of the combined data set are different (as in Figure 5.7), the null hypothesis is rejected, which in turn may be an indication of damage. In general, the F statistic is defined as:

$$F = \frac{[RSS(reduced) - RSS(full)]/[df_{RSS(reduced)} - df_{RSS(full)}]}{RSS(full)/df_{RSS(full)}} \quad (5.13)$$

where RSS stands for residual sum of squares and df is the degrees of freedom associated with an RSS value (Caragea 2007). The alternative hypothesis states that the reduced model is too simple and that the more complex full model is more appropriate (Caragea 2007). F-values can be calculated and a significance level can be found using the F distribution. A significance level can then be set to either accept or reject the null hypothesis. A flow chart comparing the current method of damage detection to the proposed method is shown in Figure 5.8.

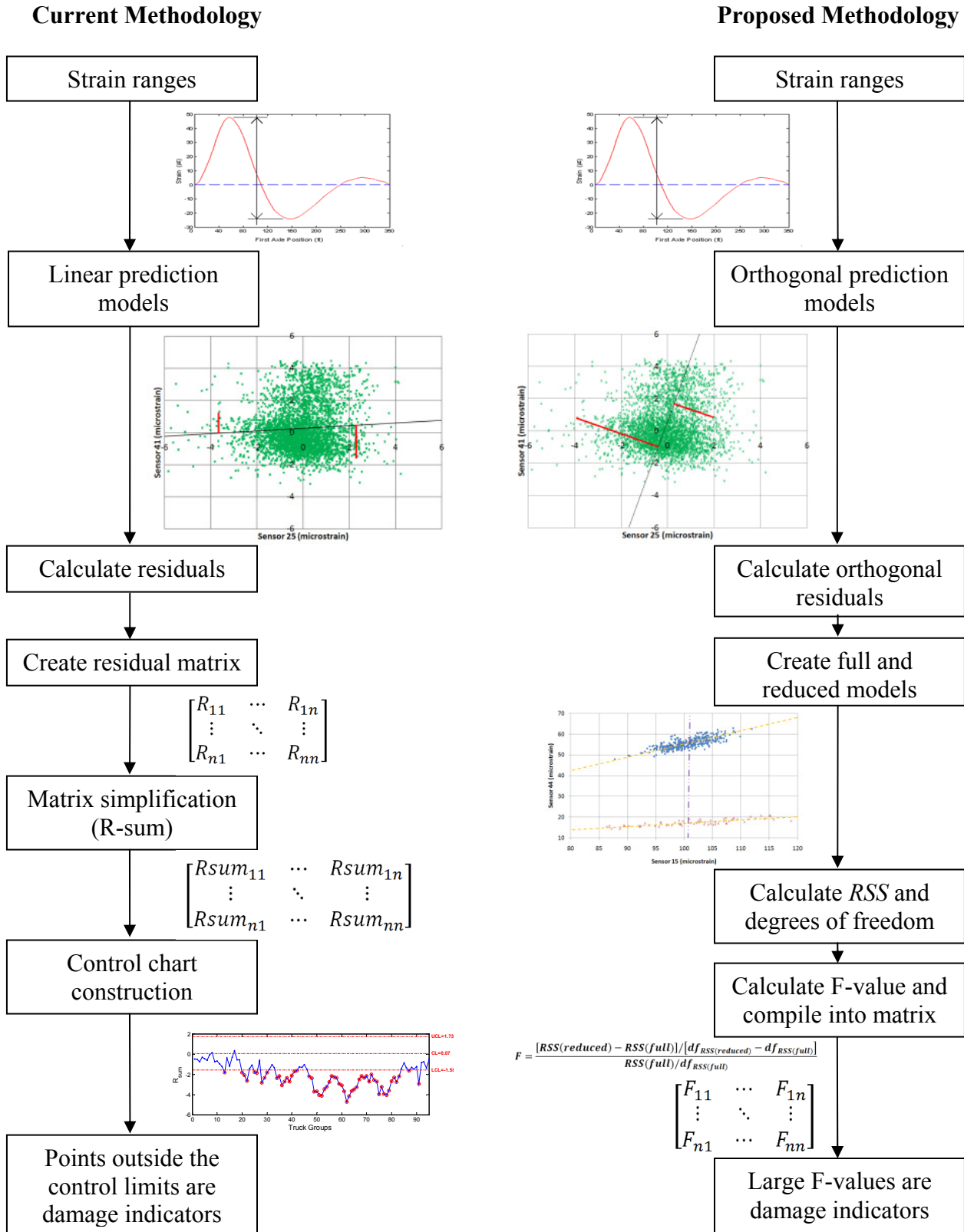


Figure 5.8 Flow Chart Comparison of the Two Damage-Detection Methods

5.2.3 Quantification of Results

To preliminarily evaluate the accuracy of the F-test, one of the previously-discussed damage cases was evaluated with F-test values computed for all sensor pairs (a total of 1,936 values). The damaged data for the 1.25 in. crack was used as the damaged data. Upon inspection of the F-test matrix the F-values for the sensors near the damage were larger than the F-values for sensors located farther away from the damage. To simplify this large matrix a column- and row-summation was again considered. It was found that only a column- *or* row-sum was needed, because the matrix is symmetric.

This simplification procedure had the same drawbacks as the previous control chart damage-detection method: the F-values of the sensors near the damage contribute a high percentage to the column- or row-summation procedure, possibly skewing the results for sensors located farther away from the damage.

One other possible method of matrix simplification is an exclusion method, where each sensor in a column- or row-sum will be evaluated to determine its contribution to the summation. Once the sensors that contribute the highest percentage to the sum have been identified, they will be excluded from the construction of the control charts or the recalculating of the column- or row-sum. This will allow the results for the sensors located farther away from the damage to be relatively free of the influence from the sensors located near to the damage.

6 SUMMARY, CONCLUSIONS, AND FUTURE WORK

In this chapter, a summary of the methods used and the results achieved in the experimental validation of the SHM damage-detection algorithm are presented. Conclusions are also given, along with recommendations for algorithm improvement.

6.1 Summary

In previous projects, an SHM system that can monitor bridges remotely and an autonomous damage-detection algorithm were developed and theoretically validated. As part of those efforts, numerous fiber-optic strain gauges were placed at different locations on the eastbound US 30 Bridge over the South Skunk River; this included the placement of sensors in the fatigue-sensitive areas.

The first-generation damage-detection system was created by Wipf, Phares, and Doornink using matched-event extrema to create a scatter plot. Limits were set by the user and points outside the limits were considered indications of detected damage. Damage was induced in a computer model of the US 30 Bridge and theoretical strains from the model were used to evaluate the damage-detection approach initially developed by Doornink and further refined by Lu. As part of the refinement, it was determined that additional strain gauges on the underside of the concrete deck were needed for truck characterization.

To validate the accuracy of the previously-developed detection system, multiple field tests were completed in this project. Located on the more than 50 fracture-critical bridges, similar to the US 30 Bridge over the South Skunk River, are multiple locations sensitive to fatigue damage, called the web-gap area. It was the desire to detect damage in these areas that was the precipitous for the development of the damage-detection system.

Because damage introduction into the US 30 Bridge was prohibited, a sacrificial specimen, which modeled the web-gap area in the US 30 Bridge, was designed. The plate thicknesses and welds of the sacrificial specimen were similar to those found on the US 30 Bridge. The flanges of the sacrificial specimen were mounted to a concrete abutment pedestal. Double curvature bending was induced in the sacrificial specimen by attaching a steel strut to the sacrificial specimen and a bridge stringer. In this way, the sacrificial specimen was exposed to ambient traffic loading.

To validate the accuracy of the damage-detection algorithm, damage in the form of cracks and loss of thickness were introduced into two sacrificial specimens. Cracking was induced by vibrating the sacrificial specimen with a rotary shaker. At resonance, the sacrificial specimen was subjected to a large number of cycles at high levels of strain, which produced cracks in a relatively short period of time. Multiple sacrificial specimens with different crack sizes were evaluated. Thickness loss was created by removing material with a hand-held rotary grinder.

Following training, sacrificial Specimen 1 was damaged with a large crack at the edge of the connection plate of both the top and bottom plates. Damage data were then collected and plotted on previously-constructed control charts. Every post-damage R-sum value for the three sensors closest to the damage was outside the control limits, indicating damage had been detected. Unfortunately, multiple R-sum values were outside the control limits for sensors not near the damage, giving false-positive readings. Upon further evaluation, it was concluded that these R-sum values were influenced by the large magnitude of the residuals from the sensors near the damage.

Sacrificial Specimen 2 was fabricated and tested similarly to Specimen 1. Specimen 2 was installed at the US 30 Bridge, training data were collected, control charts were constructed, and the sacrificial specimen was vibrated until a 1.25 in. long crack appeared in the top plate. Damage data were then collected and plotted on the control charts; this process was repeated with the crack further propagated to 1.50 in. and then 1.75 in. In all cases, all data points for the sensor closest to the damage were outside the control limits, indicating that damage had been detected. As with Specimen 1, multiple R-sum values for sensors far from the damage were outside the control limits, giving multiple false-positives.

After damaging Specimen 2 with the 1.75 in. long crack, new training data were collected and new control charts were constructed. To determine the detectability of corrosion, an area of the top plate was ground off to simulate thickness loss associated with the corrosion process. Damage data were collected and plotted on the control charts. The sensor closest to the section with the highest percentage of plate thickness ground off had numerous data points outside the control limits, indicating that thickness loss can be detected.

An evaluation of the components of the current methodology and methods for improving the approach were investigated. The linear prediction models and the normalcy of the residual and R-sum data were evaluated to determine if previously-made assumptions held true for collected data. It was determined that the R-sum data were not taken from a normally-distributed population and the control charts were constructed based on this false assumption. Therefore, a new method of damage quantification is introduced, which employs the F-Test and new prediction models, called orthogonal prediction models.

An orthogonal prediction model is an orthogonally fit line through the strain range data creating orthogonal residual, which are the perpendicular distance from the strain ranges to the prediction model. The F-Test uses a comparison of two different models and orthogonal residuals to calculate an F-value, which is then used for damage detection; the large F-values represent possible damage indicators. Through a similar matrix simplification method previously used, it was found that this damage quantification also produced a high false-positive rate. A new matrix simplification method that excludes the sensors closest to the damage from the control chart construction for the sensors farther away from the damage should be used.

6.2 Conclusions

Based on the work summarized herein, the following conclusions were made:

1. Damage can be autonomously detected by the damage-detection algorithm, as long as the damage is “close enough” to a sensor. It is not known how close is “close enough.”
2. There is a loose correlation between the level of damage and the distance between the mean training data and the post-damage data. Specifically, the mean of the data collected from a smaller amount of damage (i.e., a 2.0 in. crack) is closer to the mean of the training data than the data from a larger amount of damage (i.e., a 6.0 in. crack). A comparison of the means of the data collected from incremental amounts of damage proved inconclusive (See the Future Work section below).
3. The damage-detection algorithm has a relatively high false-positive detection rate. It was determined that the residual values for the sensors nearest to the damage influence the R-sum values for the other sensors during the simplification process.

6.3 Future Work

Additional work is required to create a turnkey system that is ready for full implementation:

1. Finalization of hardware and software components – The initial work on the US 30 Bridge used a monitoring system with fiber-optic sensors. Although these sensors have many desirable attributes, there have been instances where sensors have been damaged and the sensors have unexplainably stopped working. Therefore, it is recommended that the hardware system be reconfigured to use traditional sensors. Additionally, because there are multiple recommended changes to the algorithm, it is necessary to modify the existing and previously-developed software applications.
2. Integration of dynamic structural properties – The damage-detection system was originally configured to only use time-domain metrics. With an expressed interest by the Iowa DOT Office of Bridges and Structures in modal measurement approaches, it is recommended that work be conducted to identify frequency domain metrics that fit into the algorithm. Once identified, these metrics would be included in the hardware and software systems.
3. Determination of system Probability of Detection (POD) – This work has demonstrated that the system can autonomously detect damage. It is not known, however, what the probability of detecting different sizes of damage is. It is also not known, in terms of sensor placement, how “close” is “close enough.” Therefore, a POD study is recommended, so that the reliability of damage detection (including crack size, proximity to damage, false-positive rate, etc.) can be determined.

7 REFERENCES

Betz, B C, W J Staszewski, G Thursby, and B Culshaw. "Multi-Functional Fibre Bragg Grating Sensors for Fatigue Crack Detection in Metallic Structures." *Institution of Mechanical Engineers: Journal of Aerospace Engineering*. Professional Engineering Publishing Ltd., 2006. 453-461.

Caicedo, Juan M, and Shirley J Dyke. "Experimental Validation of Structural Health Monitoring for Flexible Bridge Structures." *Structural Control and Health Monitoring*, 2005: 425-443.

Caragea, Petruta C. *The F-Test as a Comparison of Full and Reduced Models*. Fall 2007. http://www.public.iastate.edu/~pcaragea/S401F07/Handouts/Full_vs_Reduced.pdf (accessed 11 7, 2010).

Carroll, R. J., and David Ruppert. "The Use and Misuse of Orthogonal Regression Estimation in Linear Errors-In-Variables Models." *The American Statistician*, 1996.

Chintalapudi, Krishna, et al. "Monitoring Civil Structures with a Wireless Sensor Network." *IEEE Internet Computing*, 2006: 26-34.

Crow, Edwin L., Frances A. Davis, and Margaret W. Maxfield. *Statistics Manual*. United Kingdom: Constable and Company, 1960.

Dallal, Gerard E. *Introduction to Simple Linear Regression*. 2000. <http://www.jerrydallal.com/LHSP/slr.htm> (accessed 11 3, 2010).

Doebbling, Scott W, Charles R Farrar, Michael B Prime, and Daniel W Shevitz. "Damage Identification and Health Monitoring of Structural and Mechanical Systems from Changes in their Vibration Characteristics: A Literature Review." 1996.

Doornink, J D. "Damage Detection in Bridges through Fiber Optic Structural Health Monitoring." *Proceedings of SPIE - The International Society for Optical Engineering*. Boston, Ma: SPIE, 2006.

Guan, Hong, Vistasp M Karbhari, and Charles S Sikorsky. "Long-Term Structural Health Monitoring System for a FRP Composite Highway Bridge Structure." *Journal of Intelligent Material Systems and Structures*, 2007: 809-823.

Hoult, Neil A, Paul R A Fidler, Ian J Wassell, Peter G Hill, and Campbell R Middleton. "Wireless Structural Health Monitoring at the Humber Bridge UK." *Proceedings of the Institute of Civil Engineers: Bridge Engineering*. Thomas Telford Services Ltd, 2008. 189-195.

Kim, Hansang, and Hani Melhem. "Damage Detection of Structures by Wavelet Analysis." *Engineering Structures*, 2004: 347-362.

Kim, Sukun, et al. "Health Monitoring of Civil Infrastructures Using Wireless Sensor Networks." *Proceedings of the Sixth International Symposium on Information Processing in Sensor Networks*. Cambridge, MA: Association for Computing Machinery, 2007. 254-263.

Lu, Ping. *A Statistical Based Damage Detection Approach for Highway Bridge Structural Health Monitoring*. Ames, Ia: Iowa State University, 2008.

MathWorks. *Fitting an Orthogonal Regression Using Principal Components Analysis*. 2010. <http://www.mathworks.com/products/statistics/demos.html?file=/products/demos/shipping/stats/orthoregdemo.html> (accessed 11 4, 2010).

Olund, Josh, and John DeWolf. "Passive Structural Health Monitoring of Connecticut's Bridge Infrastructure." *Journal of Infrastructure Systems*, 2007: 330-339.

Panigrahi, S K, S Chakraverty, and B K Mishra. "Vibration Based Damage Detection in a Uniform Strength Beam Using Genetic Algorithm." *Springer Online*, 2009.

Salah el Din, A. S., and J. M. Lovegrove. "A Gauge for Measuring Long-Term Cyclic Strains on Concrete Surfaces." *Magazine of Concrete Research*, 1981: 123-127.

Vis, James Martin. *Evaluation of a Structural Health Monitoring System for Steel Girder Bridges*. Creative Component Report, Ames, Iowa: Iowa State University, 2007.

Wang, Shanshan, Qingwen Ren, and Pizhong Qiao. "Structural Damage Detection Using Local Damage Factor." *Journal of Vibration and Control*, 2006: 955-973.

Wipf, Terry J., Brent M. Phares, and Justin D. Doornink. *Monitoring the Structural Condition of Fracture-Critical Bridges Using Fiber Optic Technology*. Ames, IA: Center for Transportation Research and Education: Iowa State University, 2007.

Yin, An, Bingwen Wang, Zhuo Liu, and Xiaoya Hu. "Design and Implementation of the Structure Health Monitoring System for Bridge Based on Wireless Sensor Network." *6th International Symposium on Neural Networks*. Wuhan, China: Springer Verlag, 2009. 915-922.

Yuan, Shenfang, Xiaosong Lai, Xia Zhao, Xin Xu, and Liang Zhang. "Distributed Structural Health Monitoring System Based On Smart Wireless Sensor and Multi-Agent Technology." *Smart Materials and Structures*, 2005: 1-8.

